Effects of Gasoline Composition on Compression Ignition in a Motored Engine

by

Kwang Hee Yoo

A dissertation submitted in partial fulfillment
of the requirements for the degree of
Doctor of Philosophy
(Mechanical Engineering)
in the University of Michigan
2020

Doctoral Committee:

Professor André L. Boehman, Chair
Associate Research Scientist John Hoard
Professor Venkat Raman
Professor Margaret Wooldridge

Kwang Hee Yoo
khyoo@umich.edu
ORCID iD: 0000-0001-7541-3553

Acknowledgments

First and foremost, I must thank my parents Soonam Yoo and Youngim Kim for their dedication over the years of my graduate studies. I would also like to thank my brother and sister and their families for their consistent support.

I would like to express my sincere gratitude to my advisor Prof. André Boehman for his guidance and encouragement. I also thank my thesis committee members, John Hoard, Prof. Venkat Raman, and Prof. Margaret Wooldridge for their valuable comments on my research.

I have many thanks to my former and current group members at Automotive Laboratory: Dr. Dongil Kang, Dr. Eduardo Barrientos, Dr. Vickey Kalaskar, Michael Mayo, Dr. Chenxi Sun, Dr. Vassilis Triantopoulos, Dr. Jeongyong Choi, Dr. Taehoon Han, Dr. Jonathan Martin, Justin Koczak, Shuqi Cheng, Taemin Kim, Andrew Di Mauro, Erick Garcia, Kaustav Bhadra, and Muhammad Abdullah. I appreciate their friendship and assistance.

This work was supported financially by Aramco Services Company, in support of the U.S.-China Clean Energy Research Center Truck Research Utilizing Collaborative Knowledge (CERC TRUCK) Consortium. Thanks to Dr. Alexander Voice, Dr. Xin He and Dr. Michael Traver of Aramco Services Company.

Lastly, I would like to give my special thanks to my beloved fiancé, Youjin Roh.

Table of Contents

List of Figures

List of Tables

Abstract

This study presents a fundamental investigation of gasoline autoignition behavior in a compression ignition engine, which is of great importance for next generation engine designs that employ low temperature combustion strategies. A total of eleven full boiling range gasolines with different octane number and sensitivity have been tested in a motored engine and a constant volume combustion chamber at various pressures, temperatures, and oxygen concentrations. For quantification of intermediate temperature heat release (ITHR) which occur at a temperature range of 950-1170 K, a new method was applied to the engine data by examining the maximum value of the second derivative of heat release rate.

First, influence of ITHR on autoignition reactivity of single-stage ignition fuels with varying octane sensitivity was investigated in a motored engine. Four full boiling range gasolines with research octane number (RON) of 92 and octane sensitivity range of 0.5 to 11.3 were tested through sweeps of intake temperature, intake oxygen mole fraction, and fuel loading. This study provided a new understanding of ITHR behavior depending on octane sensitivity and its effects on autoignition reactivity of single-stage ignition fuels under various engine operating conditions. Combustion phasing

comparisons of the test fuels showed that the S0.5, which is the lowest octane sensitivity fuel, became relatively more reactive as the intake temperature and the simulated exhaust gas recirculation (EGR) ratio decreased compared to the fuels with higher octane sensitivity. When low temperature heat release (LTHR) was not active, the amount of ITHR increased in the range of 2% to 7% of total heat release as the intake temperature and the intake oxygen mole fraction increased. These ITHR trends, depending on octane sensitivity, were almost identical with the trends of combustion phasing, showing that ITHR significantly affects fuel autoignition reactivity and determines octane sensitivity. In addition, the strong dependence of ITHR on equivalence ratio enhanced the ϕ-sensitivity. For the similar combustion phasing, the S11.3 and the S8.7 which were the higher octane sensitivity fuels exhibited faster rise rates of ITHR intensity than the S0.5 and the S4.8 respectively, leading to more advanced hot-ignition phasing with increasing equivalence ratio.

For two-stage ignition fuels, effects of RON, intake pressure, and intake oxygen mole fraction on low and intermediate temperature heat release were explored in the same motored engine. Three high reactivity gasoline-like fuels with RON range of 60 to 80 were investigated through compression ratio sweeps to characterize low and intermediate temperature oxidation behavior under various engine operating conditions. This study provided a new understanding of the correlation between LTHR and ITHR as well as the individual effects of pressure and oxygen mole fraction on ITHR. The engine experimental results showed that LTHR significantly enhanced ITHR, eventually advancing the autoignition timing. As the intake oxygen mole fraction decreased from 0.21 to 0.14, the LTHR and the ITHR of RON 60 were suppressed by 30% and 38%,

respectively. The intake boosting from atmospheric pressure to 1.4 bar absolute increased the LTHR by 49% even at a constant fuel loading. For all the test fuels, the average ITHR per crank angle also increased with the intake pressure, showing concise and strong intermediate temperature reaction. However, the magnitude of ITHR for the lower RON fuel, which exhibited a great amount of ITHR, became saturated as the intake pressure increased.

Effects of physical properties and chemical composition on autoignition behavior were also investigated in the motored engine and a constant volume combustion chamber. This study provided a fundamental investigation of autoignition behavior and physical and chemical ignition delay of FACE (fuels for advanced combustion engines) A, C, I, and J gasolines and three naphtha blends with RON range of 60 to 80 through sweeps of pressure, temperature, and oxygen concentration. With regard to physical property effects, higher aromatic content led to lower volatility and higher density, resulting in a slower liquid fuel evaporation process. The physical ignition delay was very sensitive to the ambient air temperature whereas the oxygen dilution rarely affected the physical ignition delay. With regard to chemical property effects at the same RON, the higher aromatic content fuels, the FACE J and RON 70 fuels, were more resistant to autoignition at boosted pressure and less sensitive to the oxygen dilution whereas the alkane-rich fuel, FACE I gasolines, was less sensitive to the temperature due to pronounced negative temperature coefficient (NTC) behavior. For the same RON and octane sensitivity, the fuel with higher amount of n-alkane, the FACE C gasoline, was less sensitive to the oxygen dilution than the FACE A gasoline. Both the FACE A and C gasolines showed similar ignition behavior during the ambient temperature sweep, but the gas-phase

ignition of FACE A gasoline was more delayed than the FACE C gasoline as the ambient oxygen concentration decreased due to more reduced LTHR intensity.

Chapter 1

Introduction

Internal combustion (IC) engines operating on petroleum-derived liquid fuels consume about 120 quadrillion Btu, which corresponds to 25% of the total global energy and these numbers are expected to increases especially in non-OECD countries [1, 2]. These IC engines produce around 23% and 14% of the world's carbon dioxide (CO_2) and greenhouse gas (GHG) emissions, respectively [2-4]. Thus, increasing fuel conversion efficiency and reducing emissions have been the primary goal of engine manufacturers and researchers for a number of years.

Also in recent years, there have been demands to replace vehicle IC engines with electric motors to reduce fuel consumption and vehicle GHG emissions. Many governments have announced the policy to ban vehicles powered by IC engines in the near future. It is also not clear whether they will forbid all IC engines or only ban IC engines without any electrical assistance, but this has led some people to believe that IC engines will be disappearing quickly [5].

Kalghatgi proposed several reasons why fully electric vehicles cannot replace IC engine vehicles in the near future [6]. First, battery electric vehicles (BEV) are not zero

emission vehicles. Electricity is currently generated from mostly non-renewable energy sources because solar is not available at night and wind and hydro power cannot change their output at will. Coal, which releases significant amounts of CO_2, sulfur dioxide (SO_2), nitrogen oxide (NOx), and particulate matter (PM), continues to be a major energy source especially in developing countries. Second, mining of metals needed for batteries causes serious environmental/human toxicity problems. Third, large investments in charging infrastructure, extra electricity generation, and grid management will be required for rapid growth in the number of BEVs. In addition, recycling large and heavy batteries, slow charging speed, and limited payload of heavy-duty vehicles will further hinder the deployment of BEVs. For these reasons, combustion engine vehicles will be the dominant transportation power source until these barriers are overcome. Many credible projections suggest that IC engines powered by petroleum will remain in most vehicles in 2050 as shown in Figure 1-1 [1, 2, 7, 8].

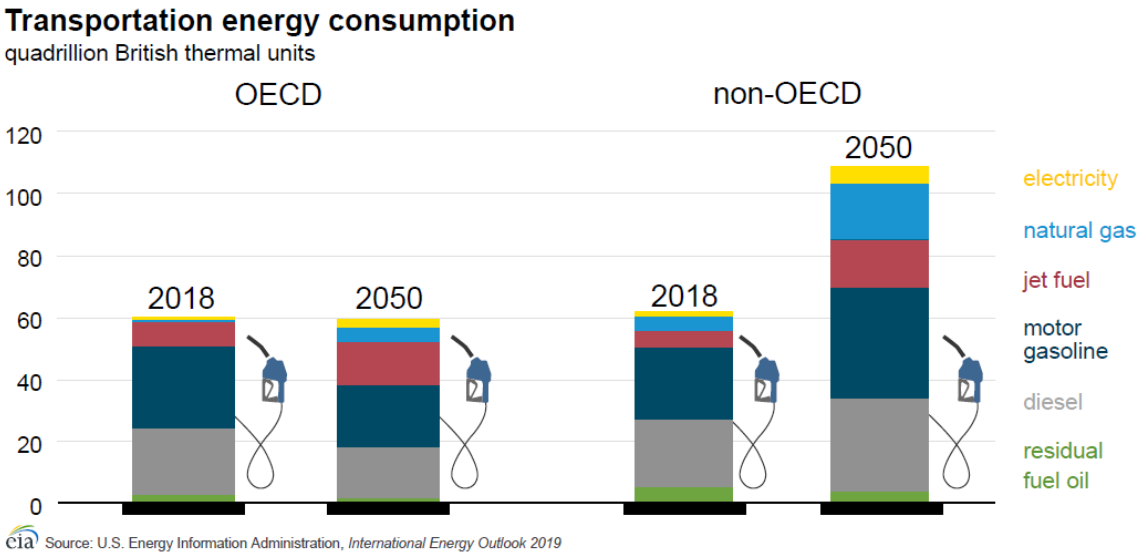

Figure 1-1 Transportation energy consumption projection [1]

Therefore, IC engines need to further improve with regard to combustion, after-treatment and control systems. Gasoline compression ignition (GCI) is a very promising and feasible concept to reduce fuel consumption and GHG and harmful emissions [9]. Compared to a diesel engine, a GCI engine produces lower PM and NOx emissions because the longer ignition delay of gasoline increases the portion of low temperature premixed combustion. Furthermore, well-to-wheels (WTW) GHG emissions from low octane fuel in a GCI engine are 22% and 9% lower than those of today's typical gasoline (spark ignition) and diesel (compression ignition) engines, respectively [10]. In addition, GCI engines require lower fuel injection pressure and a simpler after-treatment system than modern diesel engines. Despite of all these advantages, it is still challenging to bring GCI combustion to practical engine applications for several technical reasons, such as ignition and combustion phasing controls at cold start and transient conditions and excessive pressure rise rate at high load conditions. Thus, the goal of this work is to expand the fundamental understanding of autoignition and combustion behavior of gasolines with a range of reactivity to overcome the difficulties presented by using gasoline fuels in compression ignition engines. The following describes the structure and content of the dissertation.

Chapter 2 presents the experimental setup and the data analysis methods for a motored engine and a constant volume combustion chamber. A novel method for quantification of intermediate temperature heat release (ITHR) is described. In Chapter 3, the effects of intake temperature and oxygen mole fraction on ITHR were investigated using the motored engine under the conditions at which low temperature reactivity was not active. In addition, the dependence of ITHR behavior on octane sensitivity and its

influence on autoignition reactivity were explored. Lastly, the origin of equivalence (ϕ) sensitivity and its variation depending on octane sensitivity were identified. The first two parts of this chapter were accepted for presentation at *the 38th International Symposium on Combustion*, under the title of "Influence of Intermediate Temperature Heat Release on Autoignition Reactivity of Single-stage Ignition Fuels with Varying Octane Sensitivity". In Chapter 4, the correlations between LTHR and ITHR were explored through quantification of pre-ignition heat release for two-stage ignition fuels. Effects of intake pressure and oxygen mole fraction on LTHR and ITHR were investigated in the motored engine. Finally, in Chapter 5, the effects of fuel physical and chemical properties on autoignition behavior were studied in the motored engine and the constant volume spray combustion chamber. Liquid fuel jet evaporation as well as gas-phasing ignition of gasolines with varying RON and octane sensitivity were investigated.

Chapter 2

Experimental

2.1 Cooperative Fuel Research (CFR) Motored Engine

2.1.1 Motored Engine Setup

A cooperative fuel research (CFR) octane rating engine used in this study was originally modified for homogenous charge compression ignition (HCCI) combustion by Szybist et al. [11], and several alterations have been made by previous researchers to improve repeatability of experimental results and expand operable conditions [12-16]. Recent modification for a simulated exhaust gas recirculation (EGR) system has been made by the author to explore ignition and combustion characteristics at various intake oxygen mole fractions. Figure 2-1 shows the modified CFR engine setup schematically.

The engine was motored at constant speed of 600 or 900 rpm throughout this study. The compression ratio (CR) of engine can be adjusted from 4.0 to 15.7. Its original carbureted fueling system was replaced with a gasoline direct injection (GDI) fuel injector located far upstream of the intake valve to provide a premixed fuel-air mixture to the engine cylinder. The fuel pressure was maintained at 700 psi using an inert gas,

helium for this study. The intake system can deliver dry air up to 3 bar absolute pressure using building compressed air and multiple moisture, oil, and particle filters. The intake air and fuel flow rates were measured using a Delphi hot-wire mass airflow (MAF) sensor and a Max model 213 piston flow meter, respectively. To supply dry complete stoichiometric products (CSP) to the intake charge for the simulated exhaust gas recirculation (EGR), Brooks mass flow controllers (MFC) for nitrogen (N_2) and carbon dioxide (CO_2) were installed. For massive amount of CSP up to EGR ratio of 55% at boosted conditions, a 230 L ultra-high purity (UHP) grade liquid N_2 bottle and multiple highly pressurized gaseous N_2 and CO_2 bottles were attached to the intake system. A series of electric heaters followed by tape heaters can increase the charge temperature up to 280ºC under naturally aspirated as well as boosted conditions. To measure in-cylinder pressure data, a Kistler 6052B piezoelectric pressure transducer was installed in place of the standard knock meter on the octane rating engine. The signal from the transducer was amplified using a Kistler 5010 dual mode amplifier. This in-cylinder pressure data were recorded at a resolution of 0.1ºCA in conjunction with an Accu-Coder angular encoder. Cylinder wall temperature was obtained using a MEDTHERM coaxial thermocouple incorporated in place of the spark plug on the side wall of combustion chamber. For the steady state operation, water jacket temperatures for the engine cylinder and the GDI injector were maintained at 90±1ºC using 8 L, 1000 W and 6 L, 1100 W refrigerated/ heated coolant circulators with a series of radiators, respectively. Gaseous emissions were measured using California analytic instruments (CAI) analyzers including non-dispersive infrared (NDIR) analyzers for carbon monoxide (CO) and CO_2, and paramagnetic analyzer for oxygen (O_2). For measurement of unburned hydrocarbon such as

formaldehyde and acetaldehyde, AVL SESAM i60 FT, a Fourier transform infrared (FTIR) multi-component system, was used. The detail CFR engine specifications are presented in Table 2-1. All measurement error bars in this study indicate 95% confidential interval.

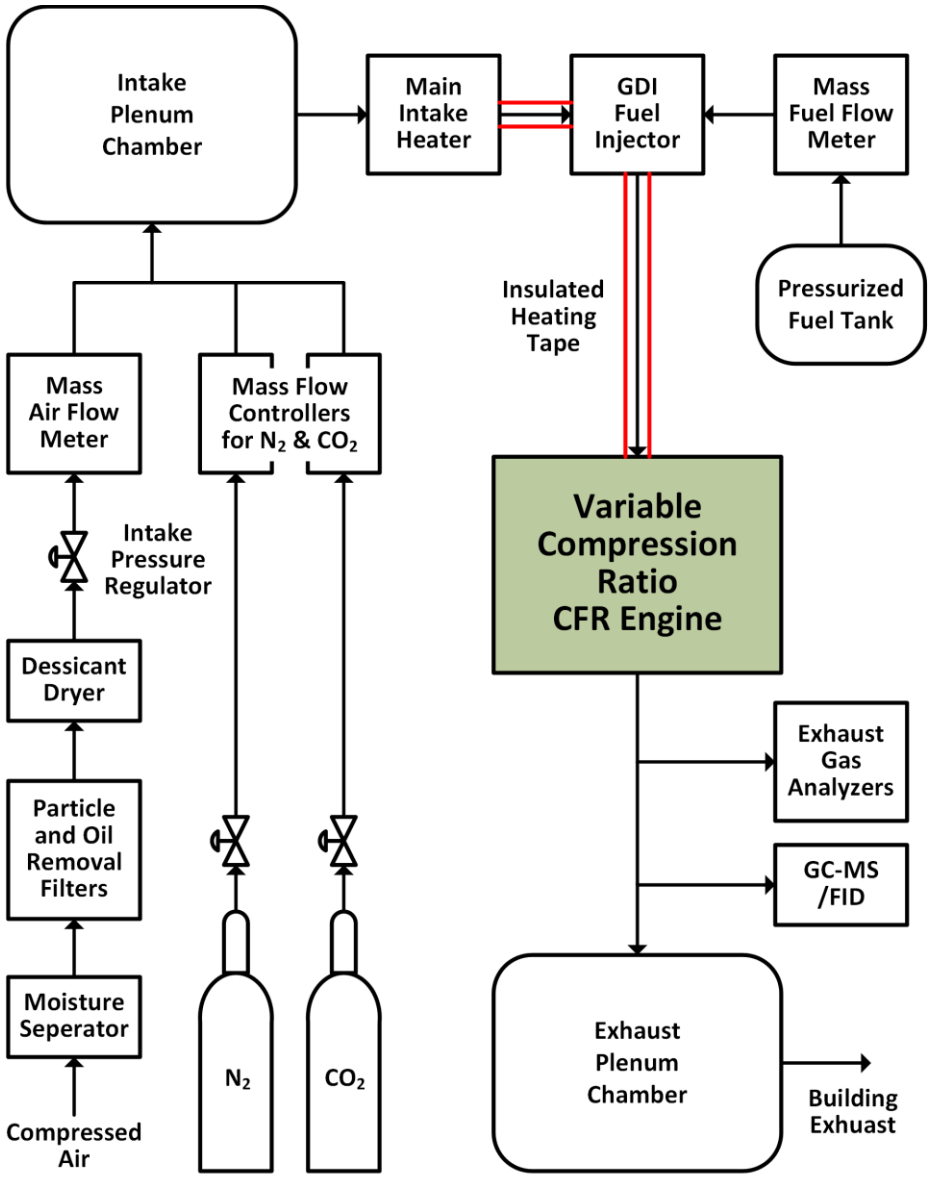

Figure 2-1 Schematic of CFR engine setup

Table 2-1 CFR engine specification

Parameter	Value
Number of cylinders	1
Engine speed (rpm)	600, 900
Bore (cm)	8.26
Stroke (cm)	11.43
Connecting rod (cm)	25.4
Displacement volume (cm^3)	611.7
Compression ratio	4.0 – 15.7
Number of overhead valves	2
Intake valve open (ºCA aTDC)	28
Intake valve close (ºCA aBDC)	14
Exhaust valve open (ºCA bBDC)	27
Exhaust valve close (ºCA aTDC)	0

2.1.2 In-cylinder Pressure Data Analysis

In-cylinder pressure data were measured at a resolution of 0.1ºCA using the piezoelectric pressure transducer as mentioned above. A custom LabVIEW based data acquisition program was used to acquire these pressure data for 70 consecutive cycles. Using these data, an ensemble-averaged pressure trace was computed, which is then smoothed using appropriate band-pass filters to remove only the high-frequency noise without altering its basic features. Apparent heat release rate (AHRR) without considering heat exchange to cylinder walls was calculated from the pressure trace using a zero-dimensional single-zone model as described by Heywood [17].

$$\frac{dQ_{net}}{dt} = \frac{dQ_{ch}}{dt} - \frac{dQ_{ht}}{dt} = p\frac{dV}{dt} + \frac{dU}{dt} \tag{2.1}$$

Changes in specific heat ratio with temperature and intake composition were also considered to calculate the AHRR using polynomial functions fitted from JANAF table thermodynamic data [17, 18]. The instantaneous bulk cylinder temperatures were computed using the ideal gas law in combination with the measured pressure. It is also note that residual gas significantly affects composition of the in-cylinder charge especially at low CRs. In this study, the residual gas fraction was estimated using a method proposed by Fox et al. [19]. The detail procedure of the in-cylinder combustion analysis is discussed in previous work conducted by Zhang [20].

The AHRR does not always precisely estimate the actual heat release rate (HRR) because of the heat loss to the walls. This is particularly important to quantify low

temperature heat release (LTHR) and intermediate temperature heat release (ITHR) which are small relative to high temperature heat release (HTHR). To obtain a better estimate of the start and end points of LTHR and ITHR, the HRR was computed using an ACE-HRA in-house code [21, 22] with a modified Woschni heat transfer model [23].

2.1.3 Quantification of LTHR and ITHR

In this study, start of combustion (SOC) was defined as when the HRR had reached 0.2 J/ºCA [24] to find the point where LTHR for two-stage combustion and ITHR for single-stage combustion started to increase, without the influence of noise. For two-stage combustion, end point of LTHR was set as the crank angle where the minimum value of the HRR between the peak of first stage combustion and the peak of second stage combustion.

For quantification of ITHR, the hot-ignition point where HTHR reactions start should be precisely determined because the variation of HRR near this point is considerable. The crank angle corresponding to 10% of the total cumulative heat release (CA10) has been widely used as a measure of the ignition timing for qualitative analysis of ITHR [25-32]. However, CA10 does not truly represent the hot-ignition point because the ITHR percentage of total heat release varies with fuel blends and engine operating conditions [33]. Yang et al. suggested that ITHR ends at several CA degrees (3~5º) before CA10 [34, 35]. Mehl et al. proposed a temperature range for ITHR of 850 K to 1000 K where low temperature reactions are no longer dominant [36]. However, the exact starting and ending temperatures for ITHR could not be estimated across different

fuel types and engine operating conditions [33, 37]. Vuilleumier et al. used a first-order derivative of the scaled HRR and an upper limit value of 0.004 ($1/deg^2$) to find the end of ITHR [33].

For more accurate quantification of the amount of heat released during the ITHR period, this study provides a new method to determine the hot-ignition point using the maximum value of the second derivative of HRR with respect to the crank angle. The maximum value of the second derivative of HRR coincides with the maximum curvature of HRR which indicates the point where the HRR changes the most. This method has been used to estimate the point where SI combustion converts to HCCI combustion in a spark assisted compression ignition (SACI) engine [38]. Katrašnik et al. also proposed this method to determine the SOC in diesel engines [39]. Following the idea presented above, the hot-ignition point where HTHR reactions start can be defined as Equation (2.2).

$$\theta_{HTHR\ Start} = \max\left(\frac{d^3Q}{d\theta^3}\right) \tag{2.2}$$

Figure 2-2 shows examples of how this method can be applied in the cases of single- and two-stage ignition. The second derivative HRR method can precisely find the ITHR/HTHR boundary where in-cylinder gas temperature suddenly increases, indicating the hot-ignition. Once the starting and ending points of each heat release are established, the HRR is integrated between these two points to quantify the amount of heat released during each hear release period.

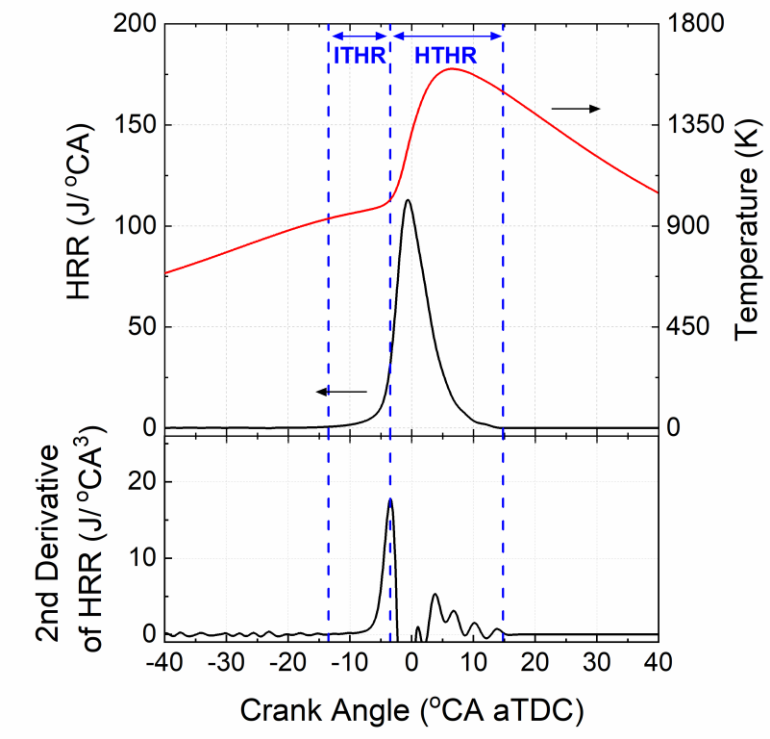

(a) Single-stage ignition

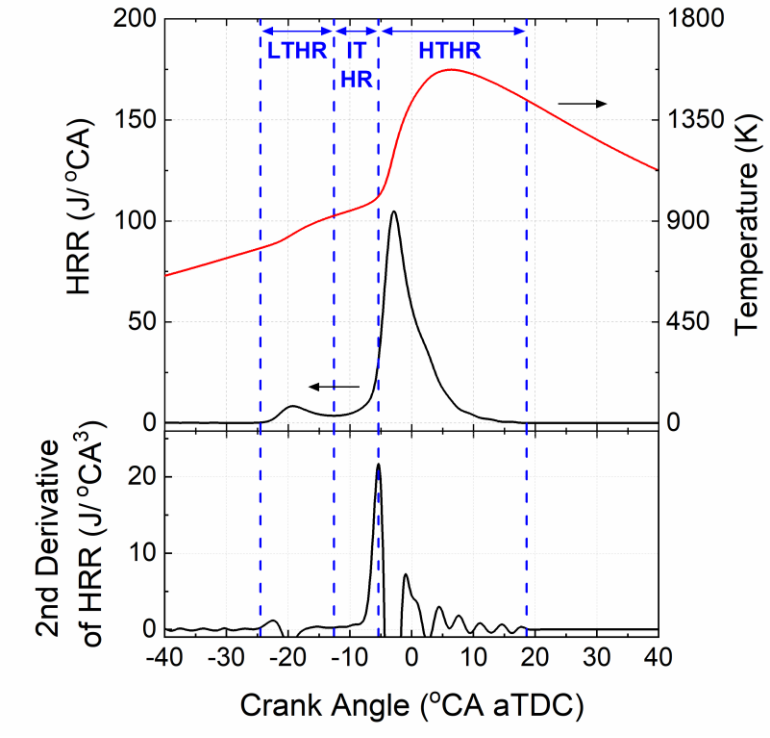

(b) Two-stage ignition

Figure 2-2 Example of SOC, LTHR/ITHR and ITHR/HTHR boundaries.

2.1.4 Critical Compression Ratio Criterion and Repeatability

The modified CFR engine is able to control the maximum pressure and temperature within the combustion chamber dynamically through a CR sweep without altering intake conditions. The CR starts at its lowest value of 4.0, where no or less reaction is expected. Then, the CR is increased in steps until autoignition occurs or the highest CR is reached. The amounts of CO and CO_2 are monitored during the CR sweep. For two-stage ignition, the CO emissions start to increase with low temperature oxidation and exponentially increase with main combustion event. Critical compression ratio (CCR) is defined at the CR where CO emissions start to decline from its maximum value, indicating the point where autoignition occurs, as presented in Figure 2-3. At this CCR, the CO_2 emissions simultaneously increase, meaning that more fuel molecules are completely oxidized. The higher CCR means more resistance of the fuel to autoignite, indicating lower reactivity compared to a fuel with lower CCR. This concept of CCR has been widely used by previous researchers to evaluate fuel autoignition reactivity [11, 14, 15, 40-53] .

Repeatability of the modified CFR engine was measured in terms of the CCR. Figure 2-4 shows the linear regression fit of two trials at each test condition which was randomly selected from overall test matrix. The regression result shows a very good fit. The maximum repeatability error and its standard deviation were 0.2 and 0.14 among 53 cases, respectively. The averaged repeatability error was only 0.04 which was lower than minimum CR increment in this study, indicating strong repeatability and reliability of the engine.

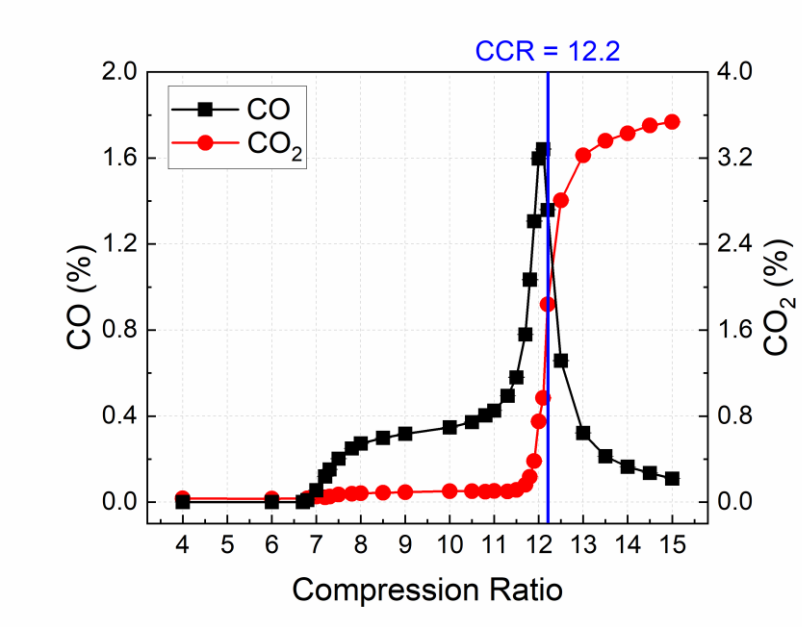

Figure 2-3 Critical compression ratio criterion

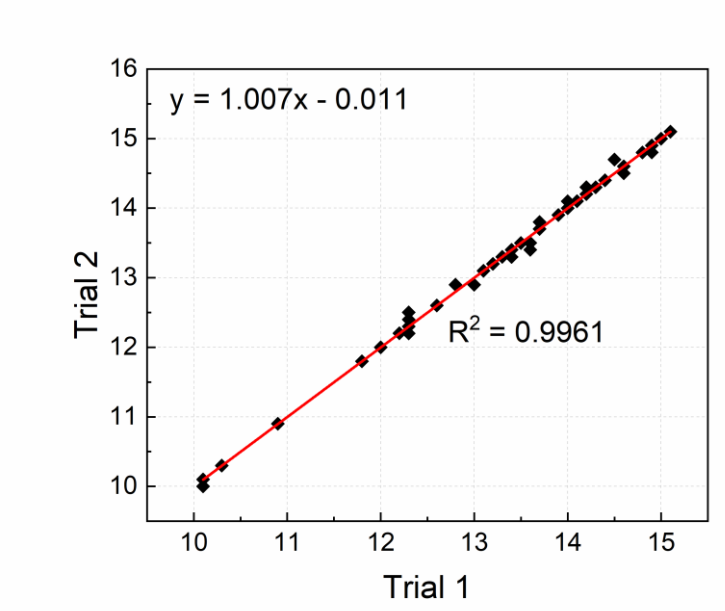

Figure 2-4 Repeatability of critical compression ratio

2.2 Cetane Ignition Delay (CID) 510 unit

2.2.1 Constant volume combustion chamber

The Cetane Ignition Delay (CID) 510 instrument manufactured by PAC L.P. is commercially available for measuring derived cetane number (DCN) of liquid fuels [54]. The CID unit equipped with a Bosch light-duty diesel injection can deliver the liquid fuel from 300 bar to 1500 bar in order to mimic a modern high-pressure common rail system. The entire system is controlled by an internal computer that has the capability to easily change operating conditions including chamber pressure, chamber temperature, fuel injection pressure, and fuel injection duration.

The constant volume combustion chamber within the CID unit was modified by Mayo et al. [55, 56] to provide optical access to the spray during fuel injection and ignition. Three ports were attached to the bottom of the combustion chamber for a high-speed camera system for physical spray characterization and a photomultiplier tube (PMT) system for chemiluminescence detection of excited chemical intermediate species. In this study, only the PMT system was utilized. For O_2 dilution, a gas mixer system developed by Polycontrols was installed to supply air with simulated EGR to the constant volume combustion chamber. The dry CSP for the simulated EGR was calculated using a method derived by Müller [57]. The detail modification of the constant volume combustion chamber can be found in previous work conducted by Mayo [55].

2.2.2 Chemiluminescence detection system (CDS)

A custom chemiluminescence detection system (CDS) was constructed by Mayo et al. [55, 56] to measure the physical and chemical ignition delay times through excited state chemical intermediates. An air-cooled, UV/Vis optical probe equipped with a 90º wide-angle, quartz observation lens was installed at the bottom of the combustion chamber. The photons emitted from excited state chemical intermediates pass through the optical probe and fiber to a collimating lens at the CDS as shown in Figure 2-5. The collimating lens aligns the light rays in parallel order, leading to homogenous beam of light. This light beam is segregated by two dichroic mirrors according to their cut-off wavelengths of 340 and 460 nm. The three resulting channels of light are individually filtered by wavelength of 307±5 nm, 430±5 nm, and 515±5 nm at each band-pass filter. The wavelengths of 307 nm, 430 nm, and 515 nm represent OH*, CH*, and C_2* photon emissions, respectively [58-60]. Excited formaldehyde (CH_2O*) chemiluminescence, which is characterized by a broadband emission spectrum, overlaps with the emission spectra of CH*, and C_2* which is high temperature radical species. Among these species, however, only formaldehyde is observed during low temperature oxidation [61, 62]. Each PMT module generates an amplified voltage (0-5 V) once the corresponding photons are present. A National Instrument high-speed data acquisition (DAQ) system simultaneously collect 40,000 to 100,000 samples at a rate of 1 MHz from each of the PMT signal channels.

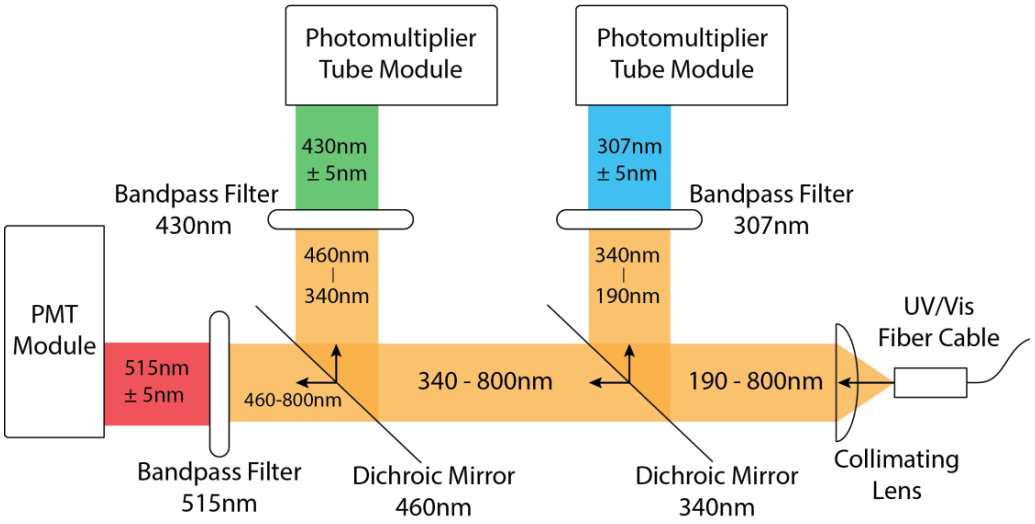

Figure 2-5 Schematic of light pathway in chemiluminescence detection system [55]

2.2.3 Ignition delay measurement from PMT data

The time value at the end of the physical and total ignition delay periods are measured through the PMT voltage signals captured by the CDS. An example of PMT data, AHRR, and bulk gas temperature during FACE I gasoline ignition under T_c = 600ºC, P_c = 20 bar, and X_{O_2} = 0.202 is shown in Figure 2-6. The physical ignition delay (τ_{phy}) is defined as the onset of low temperature combustion chemistry, where the excited formaldehyde chemiluminescence is first observed from the 430±5 nm PMT signal. The end of total ignition delay period (τ_{tot}) occurs when first significant OH* chemiluminescence is measured from the 307±5 nm PMT signal. A 2 kHz low-pass filter is applied to smooth the PMT signal for accurate calculation of ignition delay times. Figure 2-6 shows that the ignition delay times for low temperature combustion and main combustion events are precisely captured form the PMT data. The chemical ignition

delay time is calculated as the difference between the total and physical ignition delay times.

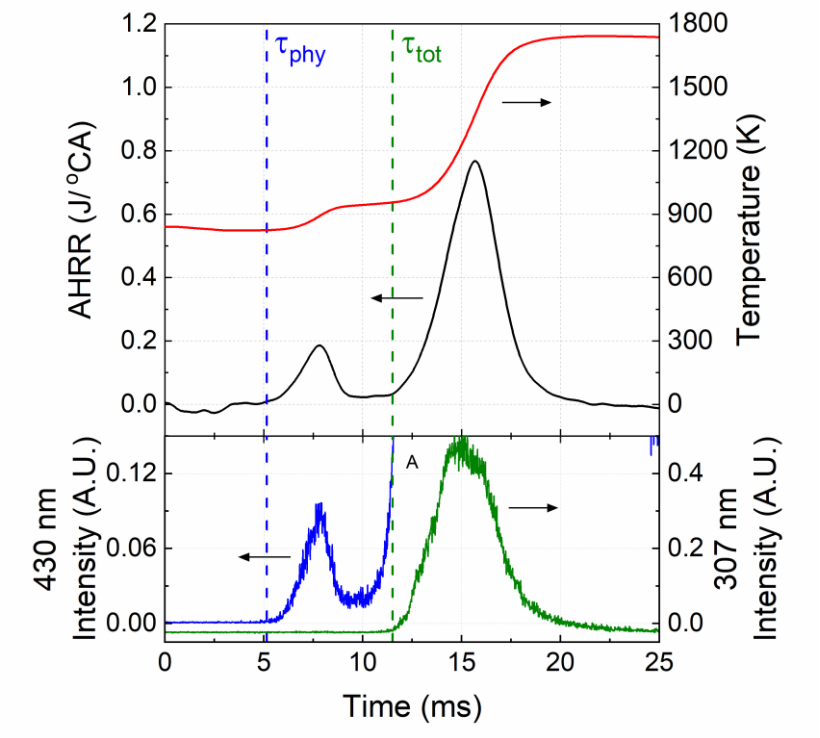

Figure 2-6 Example of physical, chemical, total ignition delay measurement.

2.2.3 Chamber Pressure Data Analysis

The pressure trace collected from a pressure transducer on the bottom of the chamber is smoothed using a 2.5 kHz low-pass filter to remove high frequency fluctuations created by large pressure-rise rates. As with the motored CFR engine, AHRR was calculated from the smoothed chamber pressure trace in the constant volume chamber, as shown in Equation (2.3).

$$\frac{dQ_{net}}{dt} = \frac{1}{\gamma - 1} V \frac{dP}{dt} \tag{2.3}$$

To consider the changes in specific heat ratio as the air mixture temperature varies, a correlation of specific heat ratio to temperature was applied as shown in Figure 2-7 [17]. The bulk temperature was calculated using the ideal gas law with constant volume of 0.473 L, air gas constant of 0.287 kJ/kg-K, total fuel-air mass, and smoothed pressure data.

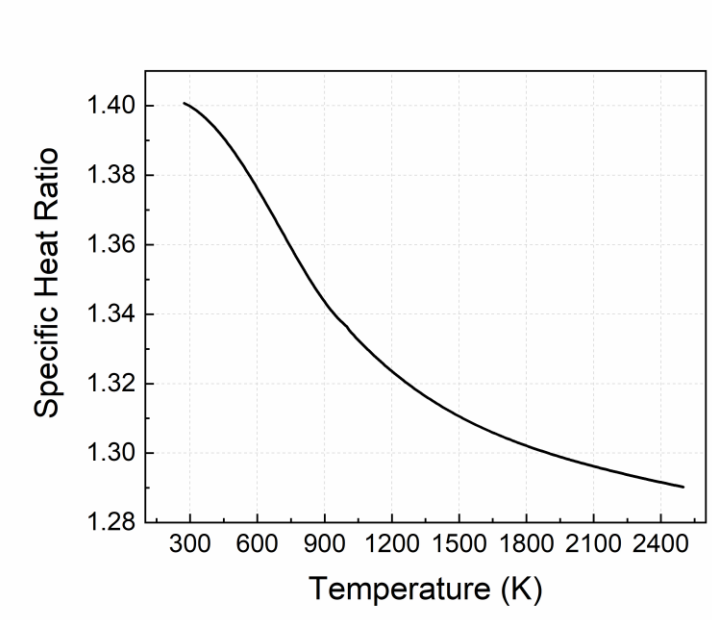

Figure 2-7 Specific heat ratio as a function of temperature.

Chapter 3

Influence of Intermediate Temperature Heat Release on Autoignition Reactivity of Single-stage Ignition Fuels with Varying Octane Sensitivity

3.1 Introduction

Octane sensitivity, defined as the difference between research octane number (RON) and motor octane number (MON), is a measure of how different a fuel's autoignition chemistry is compared to that of a primary reference fuel (PRF) which has zero sensitivity. The chemical origin of octane sensitivity has been investigated by several researchers. Leppard showed that lack of negative temperature coefficient (NTC) behavior of olefins and aromatics caused significant octane sensitivity [63]. Westbrook et al. also illustrated that suppressed low temperature reactivity by electron delocalization produced high octane sensitivity [64]. Interest in the octane sensitivity in internal combustion engines is increasing because of its relevance to knock resistance in spark ignition (SI) engines [65-69] and combustion behavior in advanced compression ignition (ACI) engines [70-73].

Intermediate temperature heat release (ITHR) is a result of slow exothermic reactions which occur at an intermediate temperature range of 950-1170 K before the hot-ignition (thermal runaway) point where high temperature heat release (HTHR) reactions raise the temperature rapidly [28, 74]. The chemical nature of ITHR is remarkably different from low temperature heat release (LTHR). The intermediate temperature oxidation chemistry was described in the following three reactions by Westbrook [75].

$$H\bullet + O_2 + M \rightarrow HO_2\bullet + M \quad (3.1)$$

$$HO_2\bullet + RH \rightarrow H_2O_2 + R\bullet \quad (3.2)$$

$$H_2O_2 + M \rightarrow HO\bullet + HO\bullet \quad (3.3)$$

where RH is an alkane, R• is an alkyl radical, and M is a third body. In this regime, hydrogen peroxide (H_2O_2) keeps accumulating via (3.1) and (3.2) until increasing temperature from compression and exothermic reactions reaches a threshold where it is rapidly dissociated into two hydroxyl radicals (•OH), providing chain branching. Mehl et al. also observed that the major contributions to the ITHR are reactions involving the formation of hydroperoxyl radicals ($HO_2\bullet$) and H_2O_2 and oxidation of formaldehyde (CH_2O) and methyl radicals ($\bullet CH_3$) [36]. These ITHR reactions are more enhanced when the LTHR is present, providing positive implications for late-cycle autoignition stability [27]. Dec and Yang also showed that intake boosting significantly intensified the ITHR using conventional gasoline whereas ethanol yielded no enhancement of the ITHR with increasing intake boost pressure [76]. For both single- and two-stage ignition fuels, the ITHR plays an important role not only in maintaining combustion stability at retarded

combustion phasing [27, 76] but also increasing equivalence ratio (ϕ) sensitivity which can enable partial fuel stratification for controlling the heat release rate (HRR) in ACI engines [30, 32, 34].

The fuel stratification is the most promising strategy to create a staged combustion event that reduces the maximum pressure rise rate (MPRR) and to control combustion phasing using multiple injection strategies in ACI engines. For effective fuel stratification, the hot-ignition phasing has to be significantly advanced with increasing equivalence ratio [77]. Previous studies found that two-stage ignition fuels showed high ϕ-sensitivity at both naturally aspirated and boosted conditions due to their strong ITHR, resulting in considerably lower MPRR than a fully premixed charge [34, 35]. Pintor et al. showed that ϕ-sensitivity was strongest for fuels capable of exhibiting NTC behavior through chemical kinetic simulations [32]. In contrast, single-stage ignition fuels exhibited that the hot-ignition timing was relatively insensitive to the local equivalence ratio at naturally aspirated conditions [25, 29]. However, Dec et al. observed that conventional gasoline, which typically showed single-stage ignition, became highly ϕ-sensitive with sufficient intake boost due to enhanced ITHR [30].

The objective of this study is to expand the understanding of the role of ITHR in autoignition reactivity and ϕ-sensitivity of single-stage ignition fuels with varying octane sensitivity through intake temperature, oxygen mole fraction, and fuel loading sweeps. The primary purposes are: 1) determining a precise method to quantify the ITHR, 2) understanding the effects of intake temperature and oxygen mole fraction on ITHR under the conditions at which low temperature reactivity is not active, 3) exploring how ITHR

varies depending on octane sensitivity and its influence on autoignition reactivity, 4) identifying the origin of ϕ-sensitivity and its variation depending on octane sensitivity.

3.2 Fuels and Operating Conditions

Four full boiling range gasolines with varying octane sensitivity at nearly identical RON were investigated, as presented in Table 3-1. In this paper, the test fuels are named for their octane sensitivity value (e.g., “S4.8” for a fuel with RON of 91.5 and octane sensitivity of 4.8). Heat of vaporization (HoV) was estimated from a detailed hydrocarbon analysis (DHA) using a method explained by Chupka et al. [78]. It should be noted that S11.3 had an increased HoV relative to the other fuels, as a result of its high ethanol content (11.5 vol%).

To describe fuel anti-knock and autoignition qualities, Kalghatgi proposed an octane index (OI), which is a linear function of RON and the octane sensitivity; OI = RON – KS [79, 80]. The K-value is a constant depending on engine design and operating parameters such as intake pressure and temperature, mixture strength, and EGR fraction which all can affect in-cylinder pressure and temperature history. Figure 3-1 shows the OI plotted against K-value for the tested fuels. In this study, the K-value was varied from about -0.85 to 3.79, showing that the reactivity trend was reversed as K-value increased.

Table 3-1 Properties of 92 RON gasolines.

Property		S0.5	S4.8	S8.7	S11.3
RON		91.0	91.5	92.0	93.0
MON		90.5	86.7	83.3	81.7
C/H/O (wt %)		84.0/16.0/0.0	85.1/14.9/0.0	87.3/12.7/0.0	82.4/13.3/4.3
Molecular weight		106.0	98.8	87.5	82.8
LHV (kJ/kg)		44627	44006	43634	41416
HoV at 25ºC (kJ/kg)		313.0	339.8	369.7	435.9
Composition (vol %)	Aromatics	1.4	15.8	29.3	25.9
	Olefins	0.1	3.9	10.7	21.4
	Naphthenes	0.0	9.1	9.0	12.3
	n-Paraffins	7.1	6.5	9.9	14.2
	i-Paraffins	90.7	64.0	38.5	12.9
	Oxygenates	0.0	0.0	0.0	11.5

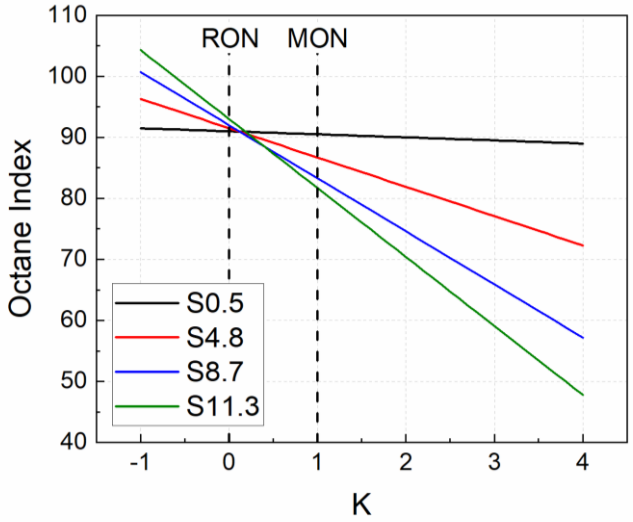

Figure 3-1 Octane Index as a function of K-value for 92 RON gasolines.

Table 3-2 Test conditions for single-stage ignition fuels.

Parameter	T_{int} sweep	EGR sweep	Φ sweep
Engine speed (rpm)		900	
Coolant temperature (ºC)		90±1	
Intake temperature (ºC)	CIT to CA50 limit	120, 160	80
Intake pressure (bar, abs)	1.4	1.4	1.4, 1.6, 1.8
Intake oxygen mole fraction	0.21, 0.175, 0.14	COF to 0.21	0.14, 0.12
Fuel loading (J/L/cycle)	635.3	635.3	CFL to MPRR limit

A modified CFR octane rating engine was used for homogeneous charge compression ignition (HCCI) combustion. For each fuel, intake temperature, intake oxygen mole fraction, and fuel loading sweeps were conducted at a fixed compression ratio of 15, as listed in Table 3-2. Critical intake temperature (CIT), critical oxygen mole fraction (COF), and critical fuel loading (CFL) are defined at the point where carbon monoxide (CO) emissions starts to decline from its maximum value, indicating the point where autoignition occurs. The engine operation limits for crank angle at 50% heat release (CA50) combustion phasing and MPRR were set to 10ºCA bTDC and 15 bar/ºCA, respectively. Charge-mass equivalence ratio (ϕ_m), defined as an equivalence ratio based on total charge mass instead of air, is used to compare data for operating conditions with different fuel and EGR levels [34]. For the intake temperature and oxygen mole fraction sweeps, the ϕ_m varied between 0.20 to 0.24 in order to maintain a constant fuel energy input. At all the conditions for ITHR quantification, the tested fuels showed no appreciable low temperature reactivity because of their low n-paraffins content [63], the high intake temperature and the low intake oxygen mole fraction [26, 27].

3.3 Results and Discussion

3.3.1 Intake temperature effect

Figure 3-2 shows the CA50 combustion phasing of each fuel as a function of intake temperature. For each intake temperature sweep at constant fuel loading, the combustion phasing was advanced from the CIT (the first hollow symbol) to the operation limit as the intake temperature was increased. The relative gross indicated mean effective pressure ($IMEP_g$) instability was consistently evaluated using corrected standard deviation (CSD) of $IMEP_g$ [81]. The hollow symbol was replaced with the solid symbol when CSD of $IMEP_g$ became lower than 5%.

At X_{O_2} = 0.21, the lowest octane sensitivity fuel, S0.5, shows the lowest intake temperature for autoignition and the most advanced combustion phasing below intake temperature of 120ºC. As intake temperature increases, however, the CA50 of S0.5 slowly advances and eventually becomes most retarded above intake temperature of 160ºC, showing the weakest intake temperature sensitivity. The lower octane sensitivity fuel is more reactive at lower intake temperature and less reactive at higher intake temperature compared to the higher octane sensitivity fuel. Kalghatgi et al. observed that the K-value increased as the compression temperature of the charge for a given pressure increased [80]. The OI of higher sensitivity fuel is then more reduced and thus the reversed reactivity between lower and higher sensitivity fuels can be observed, as shown in Figure 3-1.

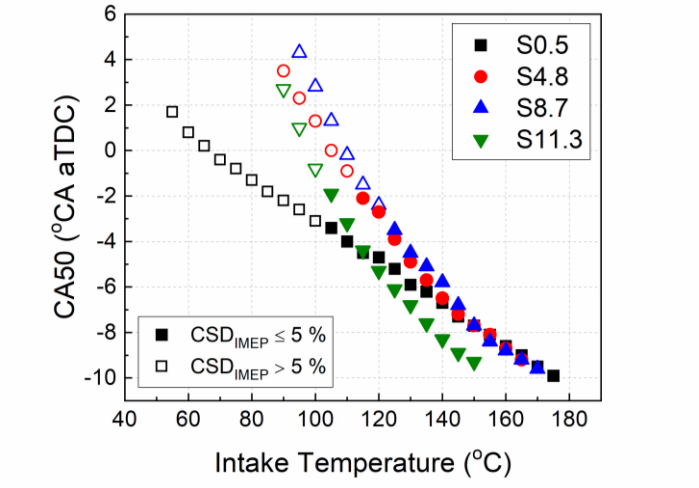

(a) X_{O_2} = 0.21

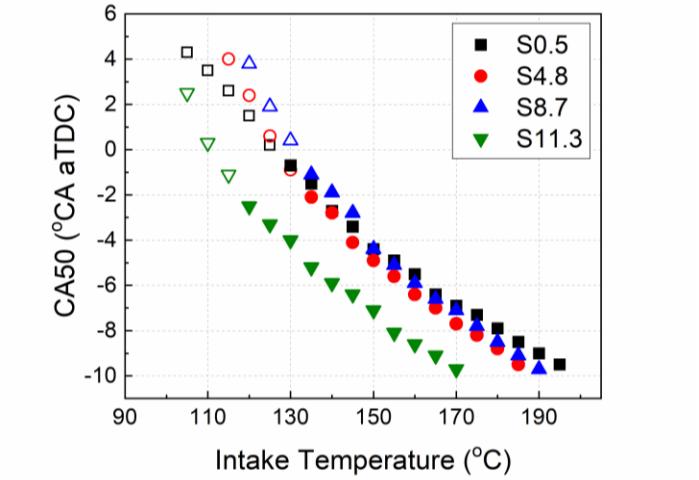

(b) X_{O_2} = 0.175

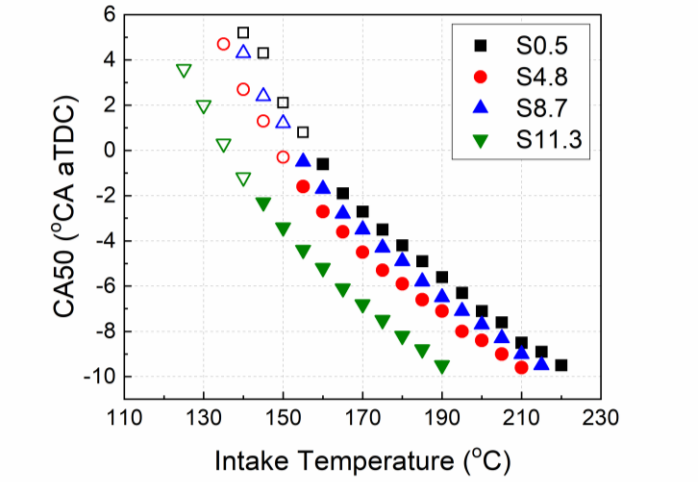

(c) X_{O_2} = 0.14

Figure 3-2 CA50 as a function of intake temperature at X_{O_2} = 0.21, 0.175, and 0.14.

In moving from X_{O_2} = 0.21 to 0.175 in Figure 3-2, the CIT of lower octane sensitivity fuel increases more than that of higher octane sensitivity fuel (S0.5: 50ºC, S4.8: 25ºC, S8.7: 25ºC, S11.3: 15ºC), meaning that autoignition reactivity difference between each fuel is diminished. Risberg et al. showed that the K-value slightly increased with cooled external EGR [82]. At our test condition, the K-value approaches from negative to zero due to the simulated EGR and this K-value further increases to positive with the intake temperature. At X_{O_2} = 0.175, the intake temperature sensitivity of S0.5 becomes much stronger than that at X_{O_2} = 0.21, but it is still weaker than that of higher octane sensitivity fuels.

The trends of reactivity variation from X_{O_2} = 0.21 to 0.175 are even steeper for X_{O_2} = 0.14, with the greater CIT and higher intake temperature sensitivity of S0.5. At this condition, S0.5 requires the highest CIT for autoignition and the highest intake temperature to maintain the same CA50 as the higher octane sensitivity fuels. The K-value is positive throughout the intake temperature sweep at X_{O_2} = 0.14.

For all the intake oxygen mole fractions, it is observed that CA50 of S11.3 which contains 11.5% ethanol does not correspond well to its OI. It shows much higher reactivity than other 92 RON fuels even at negative K-value. Liu et al. concluded that OI was not applicable for oxygenated fuels in HCCI combustion [83]. In addition, the evaporative charge cooling effect which can affect octane number determination was excluded in this study because the intake mixture temperature was controlled instead of the intake air temperature, which is set to 52ºC upstream of the carburetor in the RON test. Only the chemical octane effect contributed to the fuel reactivity, leading to more

advanced combustion phasing of S11.3 because it has the highest HoV, as indicated in Table 3-1.

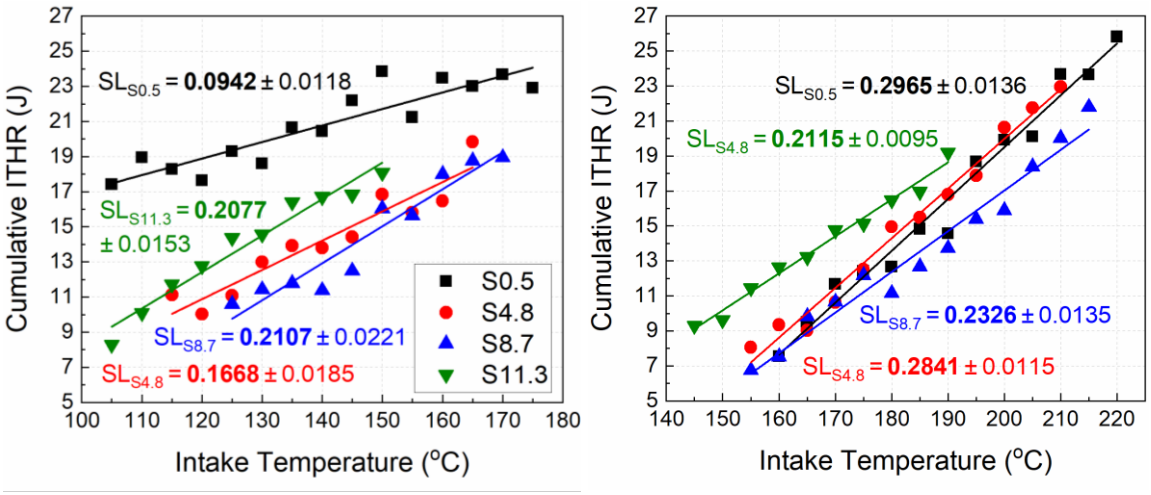

(a) X_{O_2} = 0.21 (b) X_{O_2} = 0.14

Figure 3-3 Cumulative ITHR as a function of intake temperature at X_{O_2} = 0.21 and 0.14.

To better understand the sources of these phenomenon at which LTHR is not shown, ITHR was quantified only for the cases where the CSD of $IMEP_g$ is lower than 5%. Figure 3-3 presents the correlation between ITHR and intake temperature via a linear regression for each fuel. While maintaining constant intake oxygen mole fraction and fuel loading, the figure shows that increasing intake temperature enhances the amount of ITHR in the range of 2% to 7% of total heat release. This ITHR trend with intake temperature is not matched with that of LTHR, which is another pre-ignition exothermic reaction sequence. The amount of LTHR decreases as intake temperature increases since the in-cylinder pressure in the window of 760 K to 880 K, where LTHR is most active, is lower at higher intake temperature compared to that at lower intake temperature [27].

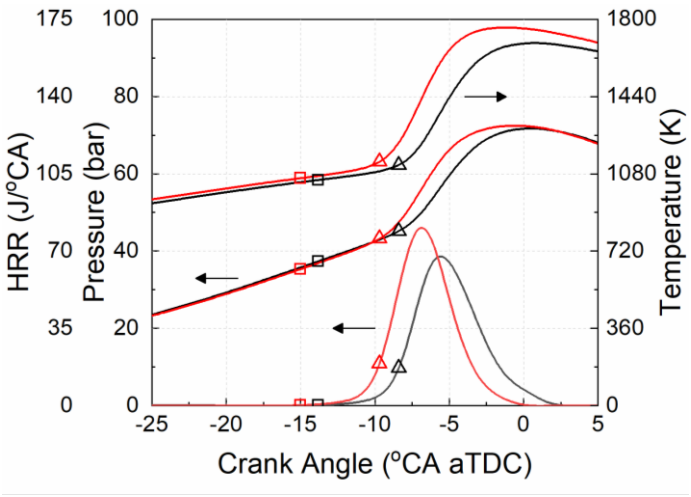

(a) HRR, P_{cyl}, T_{cyl}

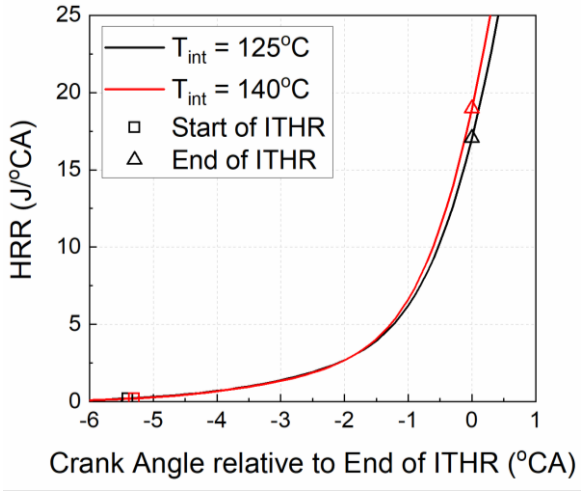

(b) Shifted HRR

Figure 3-4 Heat release rate, and in-cylinder pressure and temperature as a function of crank angle for S0.5 at T_{int} = 125 and 140ºC at X_{O2} = 0.21.

Figure 3-4 (a) shows the HRR, and in-cylinder pressure and temperature in the ITHR range for S0.5 at T_{int} = 125ºC and 140ºC. These HRR traces have been offset to align the hot-ignition point and are illustrated in Figure 3-4 (b). The increasing intake temperature advances the onset of ITHR, and then lower in-cylinder pressure and larger in-cylinder volume during the ITHR period can reduce molar concentration of the

reactants from (3.1) and (3.2). However, the exothermic reactions at higher intake temperature grow more rapidly due to the increased rate constant resulting from higher in-cylinder temperature, as shown in Figure 3-4. In addition, the hot-ignition requires much higher in-cylinder temperature to initiate HTHR at lower in-cylinder pressure. Thus, the ITHR duration is also extended as intake temperature rises for high octane sensitivity fuels, as demonstrated in Figure 3-5. These factors can contribute to increasing the total heat released during the ITHR period as intake temperature rises. More H_2O_2 accumulated from the exothermic reactions (3.1) and (3.2) produces more chain-branching OH radicals through (3.3) near the hot-ignition temperature, leading to faster consumption of fuel. This shows that ITHR can significantly affect combustion phasing as well as the onset of HTHR.

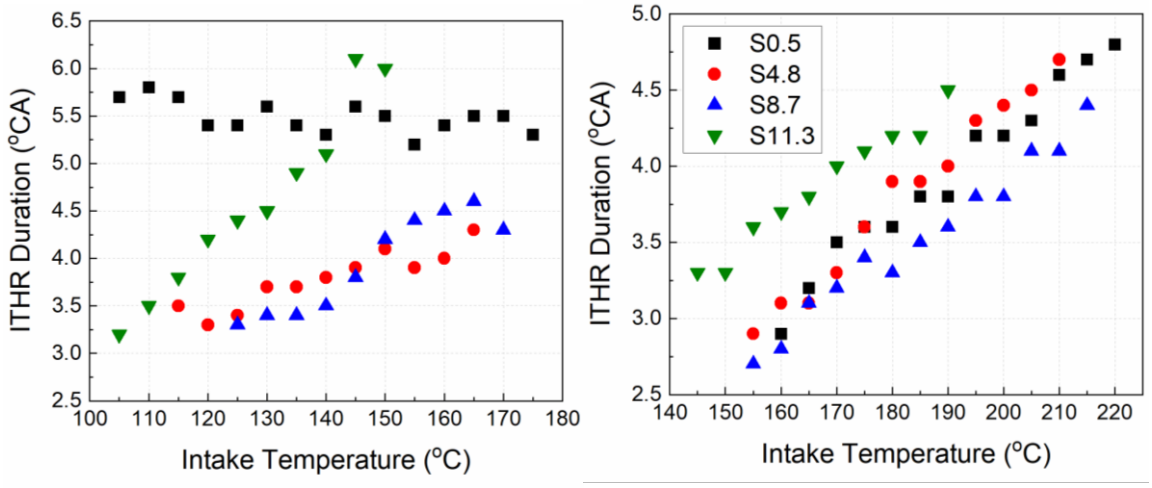

(a) X_{O_2} = 0.21 (b) X_{O_2} = 0.14

Figure 3-5 ITHR duration as a function of intake temperature at X_{O_2} = 0.21 and 0.14.

The observed increase of ITHR with intake temperature stands in contrast to previous experimental and numerical results which showed reduced ITHR with increasing intake temperature while adjusting the amount of EGR to hold the ignition timing constant [36, 76]. The different outcome is mainly due to the EGR addition with increasing intake temperature to maintain the combustion phasing. The effect of EGR on ITHR is discussed in the next section.

Figure 3-3 (a) also shows that there are distinct differences in how ITHR varies with octane sensitivity. As intake temperature increases, the ITHR of higher octane sensitivity fuel more steeply increases compared to that of lower octane sensitivity fuel. The possible reason is that olefins, alkylbenzenes, and alcohols contain weak C-H bonds resulting from electron delocalization due to the effects of the C=C double bond and O-H group [64], leading to more H atom abstractions which facilitates the reactions (3.1) and (3.2) [84], even though lower octane sensitivity fuel is composed of more H atoms per unit fuel energy. This result directly explains the difference in reactivity variation with octane sensitivity observed in Figure 3-2. The greater increase of ITHR with intake temperature causes more advanced combustion phasing. The same behavior also can be seen in Figure 3-3 (b) for X_{O_2} = 0.14. An increased ITHR slope of S0.5 leads to substantial CA50 advancement while there is no notable change in the slope of S11.3. The ITHR slope nearly coincides with the intake temperature sensitivity to combustion phasing. Thus, it appears that the autoignition reactivity variation depending on octane sensitivity of a single-stage fuel is mainly attributed to changing ITHR behavior. This observation is also confirmed in Figure 3-6, which shows that the ITHR phasing variation matches well with the change in CA50. These results clearly show that octane sensitivity

is determined not only by the low temperature reactivity but also the intermediate temperature reactivity.

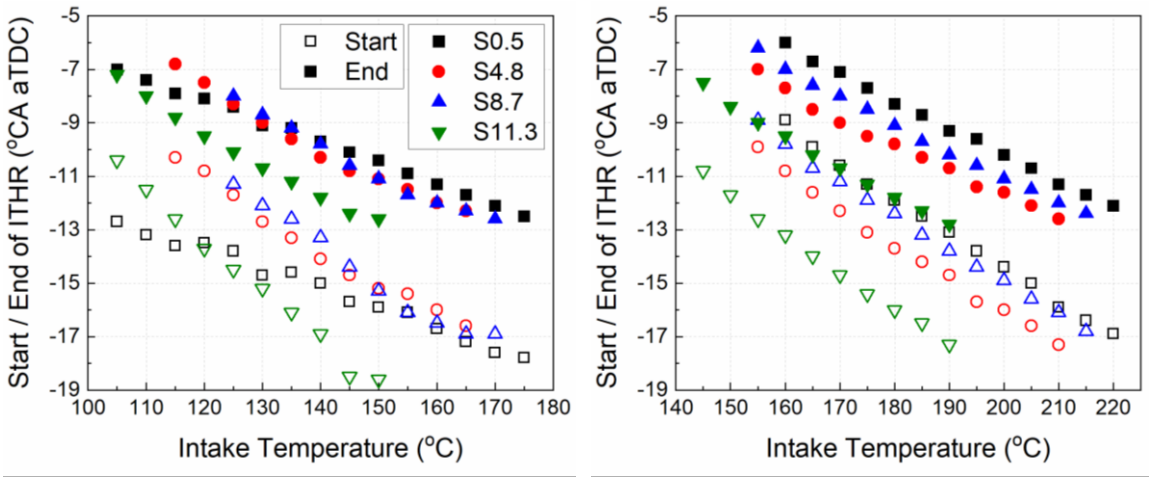

(a) X_{O_2} = 0.21 (b) X_{O_2} = 0.14

Figure 3-6 Start and end of ITHR as a function of intake temperature at X_{O_2} = 0.21 and 0.14.

3.3.2 EGR effect

The intake temperature sweep for different octane sensitivity fuels shows a significant variation in relative reactivity depending on intake oxygen mole fraction. To gain a deeper insight into the phenomena that leads to the octane sensitivity-specific difference in combustion phasing and ITHR, a simulated EGR sweep was performed at constant intake temperature, as shown in Figure 3-7 and Figure 3-8. As with Figure 3-2, the solid symbol was replaced with the hollow symbol when CSD of $IMEP_g$ became higher than 5%. In moving from T_{int} = 120ºC to 160ºC in Figure 3-7, the CA50 of higher octane sensitivity fuels is more advanced than that of S0.5 in the same manner as observed for the intake temperature sweep. At both temperature conditions, lower octane

sensitivity fuel shows a greater dependence of combustion behavior on the simulated EGR than higher octane sensitivity fuel. Sjöberg et al. also compared CA10 of iso-octane with S7.4 gasoline (90.8 RON) at various intake oxygen mole fraction conditions. A similar high dependence of autoignition timing on simulated and real EGR addition for the zero octane sensitivity iso-octane was observed even though these two fuels had different RON [26].

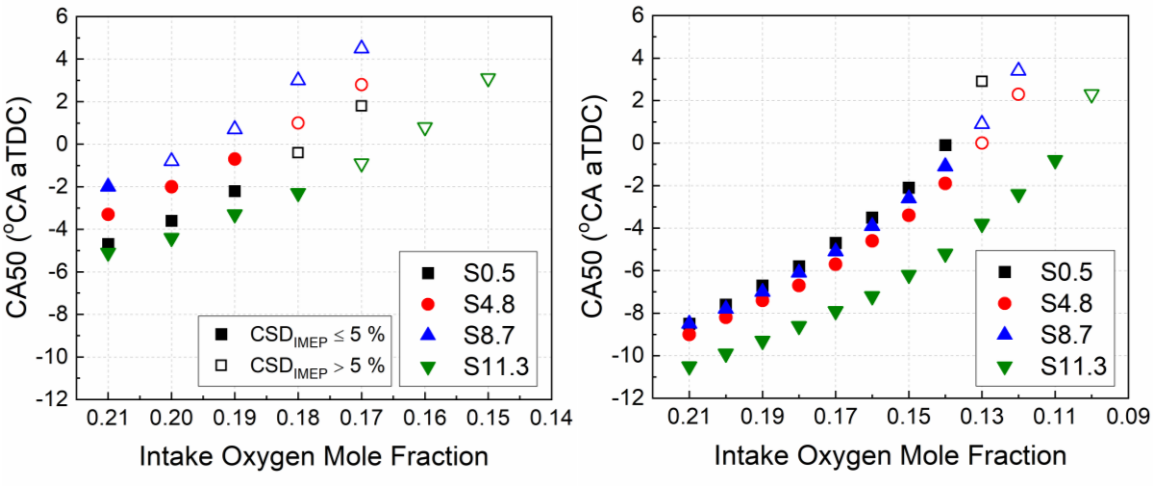

(a) T_{int} = 120ºC (b) T_{int} = 160ºC

Figure 3-7 CA50 as a function of intake oxygen mole fraction at T_{int} = 120 and 160ºC.

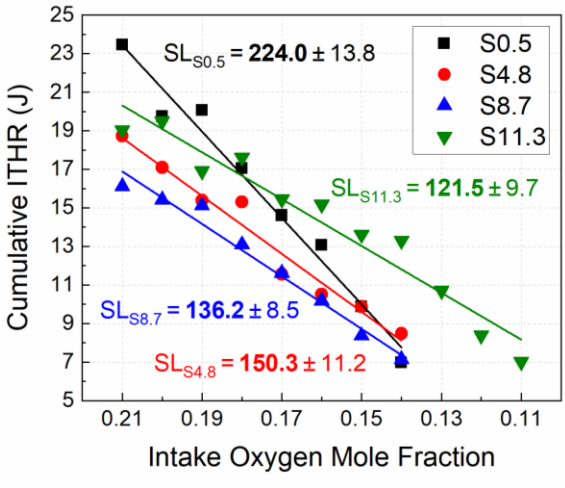

Figure 3-8 Cumulative ITHR as a function of intake oxygen mole fraction at T_{int} = 160ºC

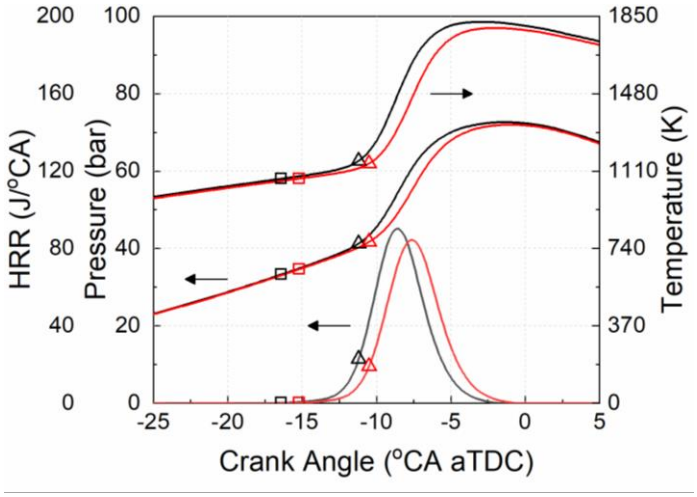

(a) HRR, P_{cyl}, T_{cyl}

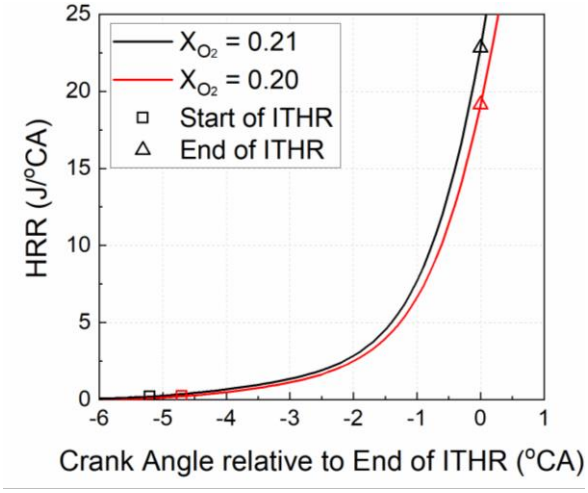

(b) Shifted HRR

Figure 3-9 Heat release rate, and in-cylinder pressure and temperature as a function of crank angle for S0.5 at X_{O_2} = 0.21 and 0.20 at T_{int} = 160°C.

Figure 3-9 shows the HRR and its shifted HRR, and in-cylinder pressure and temperature during the ITHR period for S0.5 at X_{O_2} = 0.21 and 0.20. The addition of CO_2 decreases the compressed gas temperature, retarding the onset of ITHR. Although the intermediate temperature reaction for X_{O_2} = 0.20 mainly occurs at higher in-cylinder pressure compared to X_{O_2} = 0.21, a lower oxygen molar concentration and a lower in-

cylinder temperature inhibit the intermediate temperature reaction. Furthermore, as can be seen in Figure 3-10, the hot-ignition at lower in-cylinder temperature shortens the ITHR duration as simulated EGR increases, eventually suppressing ITHR.

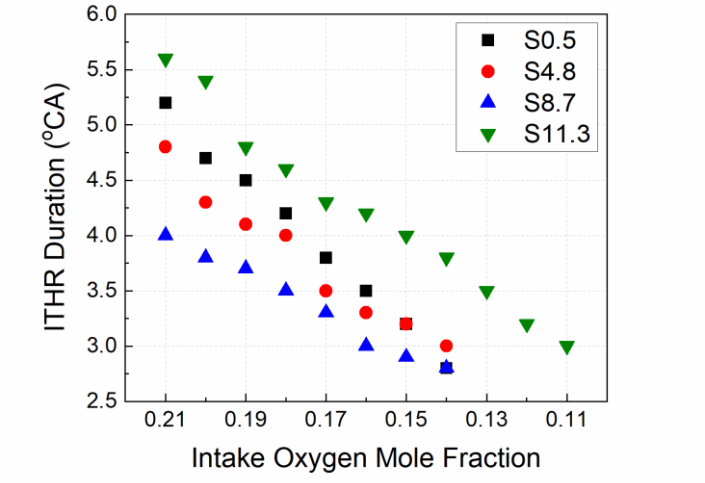

Figure 3-10 ITHR duration as a function of intake oxygen mole fraction at T_{int} = 160°C.

Figure 3-8 shows that the amount of ITHR for all the fuels is significantly reduced by the simulated EGR. Comparing the slopes of the regression lines from this figure, it can be concluded that the amount of ITHR for higher octane sensitivity fuel more steadily decreases than that of lower octane sensitivity fuel as oxygen mole fraction decreases. Then, the CA50 variation trend in Figure 3-7 can be explained by considering the changes of ITHR that occur with the addition of simulated EGR. The rapid decrease in the amount of ITHR for S0.5 reduces chain-branching radical production which can lead to hot-ignition, and eventually decreasing the relative reactivity of S0.5 among the 92 RON fuels. This ITHR and CA50 trend is consistent with the results from the intake

temperature sweep, showing that the ITHR plays a key role in determining autoignition reactivity of single-stage ignition fuels.

3.3.3 Fuel loading effect

In this section, fuel loading sweep was performed at various intake pressure and oxygen mole fraction conditions to better understand the causes of ϕ-sensitivity variation depending on octane sensitivity and explore the relationship between ϕ-sensitivity and ITHR. Figure 3-11 presents the CA50 combustion phasing of each fuel as a function of ϕ_m. As discussed in the previous section, it is clearly observed that the relative reactivity of lower octane sensitivity fuel decreases as simulated EGR ratio increases. Unlike EGR ratio, intake pressure boosting more advances the combustion phasing of lower octane sensitivity fuel than that of higher octane sensitivity fuel, showing higher reactivity increment of lower octane sensitivity fuel. Kalghatgi et al. and Risberg et al. observed that boost pressure had a much lower K-value than ambient intake pressure [80, 85]. The K-value from Figure 3-1 decreases as intake pressure increases, leading to more increased relative reactivity of lower octane sensitivity fuel.

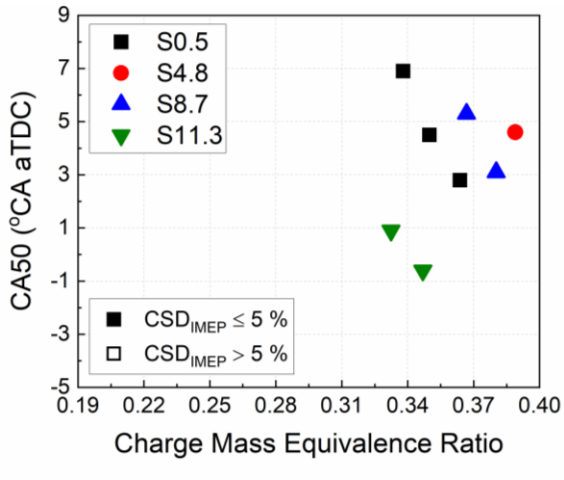

(a) P_{int} = 1.4 bar, X_{O_2} = 0.14

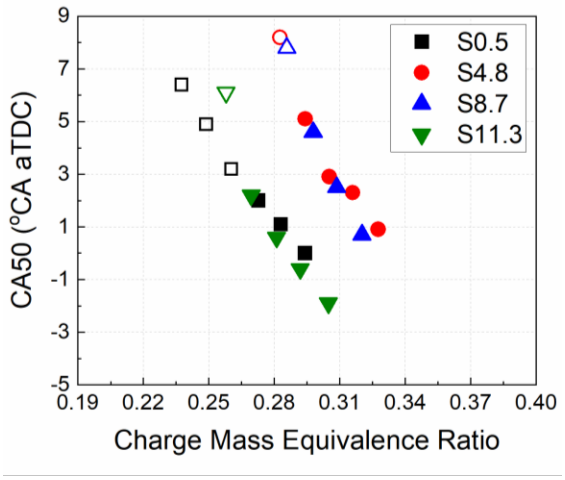

(b) P_{int} = 1.6 bar, X_{O_2} = 0.14

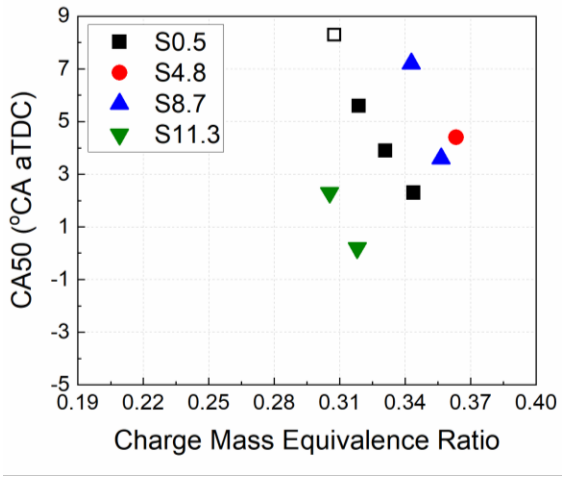

(c) P_{int} = 1.6 bar, X_{O_2} = 0.12

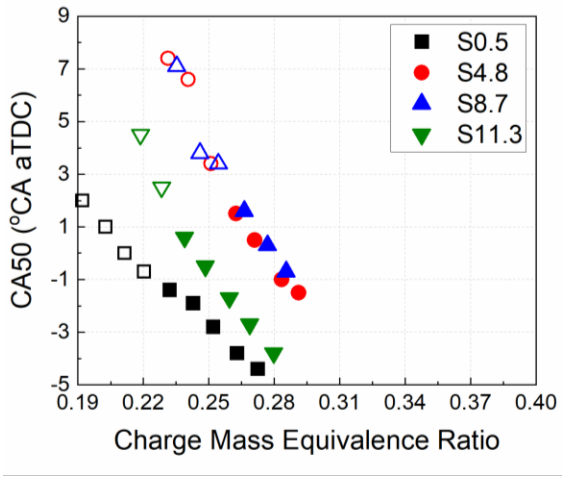

(d) P_{int} = 1.8 bar, X_{O_2} = 0.14

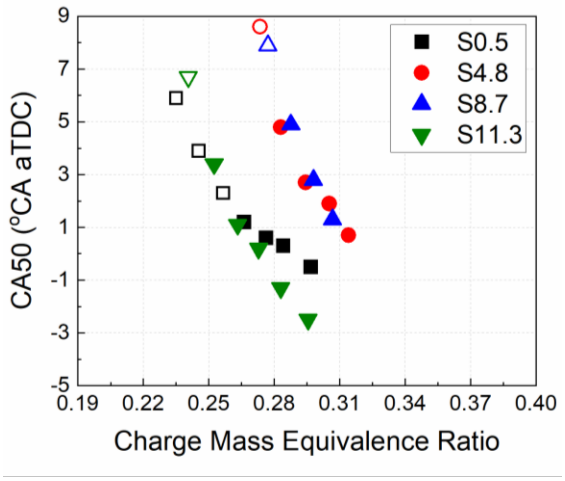

(e) P_{int} = 1.8 bar, X_{O_2} = 0.12

Figure 3-11 CA50 as a function of charge mass equivalence ratio at P_{int} = 1.4, 1.6, and 1.8 bar at X_{O_2} = 0.14 and 0.12

Figure 3-11 compares the combustion phasing advancement as fuel loading increases at each operating condition. It is interesting to note that the higher octane sensitivity fuels show slightly greater dependence of combustion phasing on equivalence ratio than the lower octane sensitivity fuels under the conditions at which they have similar combustion phasing, as shown in Figure 3-11 (b) and (e). Figure 3-12 presents the hot-ignition phasing, which is directly determined by autoignition chemistry, at these two operating conditions. The S11.3 and the S8.7 show more advancement of hot-ignition timing with increasing ϕ_m than the S0.5 and the S4.8 respectively, especially at high ϕ_m above around 0.29. Thus, the higher octane sensitivity fuels are more ϕ-sensitivity than the lower octane sensitivity fuels as a result of strong dependence of their pre-ignition reactions on the fuel concentration. Recent work by Cho et al. in partially premixed compression ignition (PPCI) indicates that the high octane sensitivity fuel is more reactive than the low octane sensitivity fuel, leading to more robust and stable PPCI combustion [71]. The strong ϕ-sensitivity of higher octane sensitivity fuels suggests that fuel stratification will be effective to produce a sequential autoignition event and eventually controlling HRR.

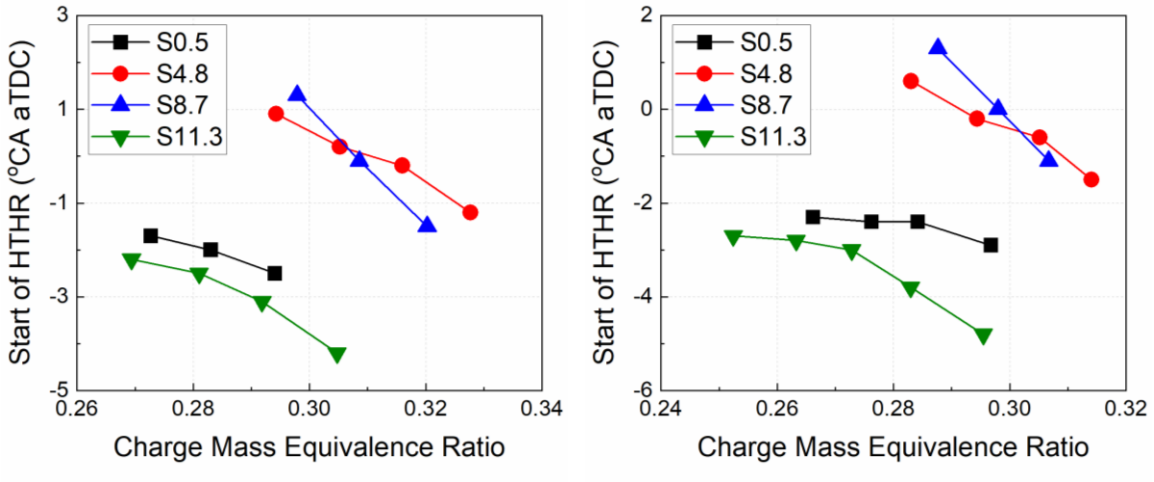

(a) P_{int} = 1.6 bar, X_{O_2} = 0.14 (b) P_{int} = 1.8 bar, X_{O_2} = 0.12

Figure 3-12 Start of HTHR as a function of charge mass equivalence ratio at similar CA50 phasing

To identify the causes of difference in ϕ-sensitivity for the fuels with varying octane sensitivity, ITHR intensity change with ϕ_m at each operating condition are presented in Figure 3-13. The ITHR intensity is defined as the contribution of ITHR to the total amount of heat released. This figure shows that the ITHR intensity for all the fuels is considerably enhanced by increasing ϕ_m up to around 0.29. Beyond this point, further increasing ϕ_m no longer increases the ITHR intensity, but instead maintains it or even decreases it at some cases. Figure 3-14 shows the normalized HRR by total cumulative heat release, in-cylinder pressure and temperature in the ITHR range for the fuel loading sweep of S11.3 at P_{int} = 1.6 bar and X_{O_2} = 0.14. The small bump of HRR at the end of combustion for high equivalence ratios is due to the pressure fluctuation after high and rapid HRR. As the ϕ_m increases from 0.269 to 0.292, the starting and ending points of ITHR advance due to the increased fuel concentration. The intermediate

temperature oxidation is also promoted by higher ϕ_m even though it starts from lower in-cylinder pressure and temperature. This greater amount of ITHR results in higher hot-ignition temperature as shown in Figure 3-14. At ϕ_m = 0.304, however, the hot-ignition temperature does not change with increasing ϕ_m anymore and level off at around 1058 K. This leads to the saturation of ITHR intensity and the further advancement of hot-ignition timing as illustrated in Figure 3-12 and Figure 3-13. This saturation behavior of ITHR and hot-ignition temperature can be also found in the other octane sensitivity fuels.

With this understanding, the ITHR intensity rise rate in Figure 3-13 can be used to provide a possible explanation for the difference in ϕ-sensitivity depending on octane sensitivity. The fuel with higher octane sensitivity shows a faster rise rate of the ITHR intensity and then reach to the saturation level at lower ϕ_m than the fuel with lower octane sensitivity. The rapid increment of ITHR can also contribute the advancement of hot-ignition timing at above the ϕ_m where the ITHR intensity starts to saturate. Thus, the strong dependence of ITHR of higher octane sensitivity fuel on equivalence ratio significantly enhances the ϕ-sensitivity.

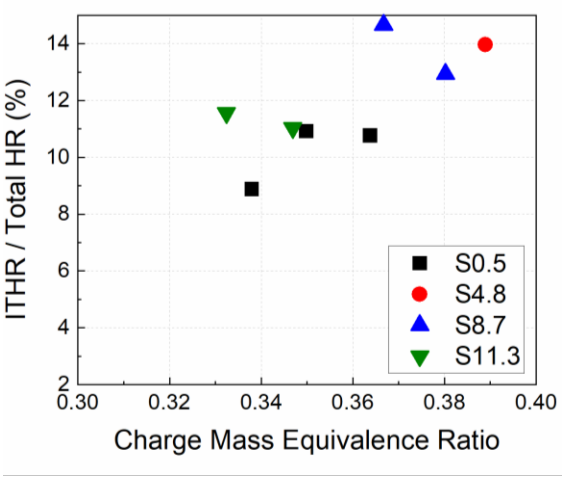

(a) P_{int} = 1.4 bar, X_{O_2} = 0.14

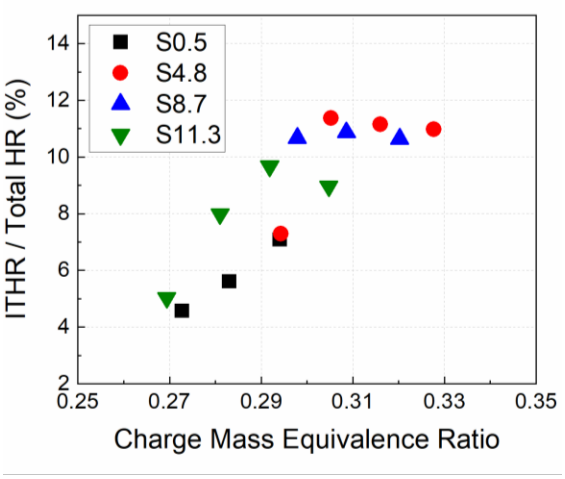

(b) P_{int} = 1.6 bar, X_{O_2} = 0.14

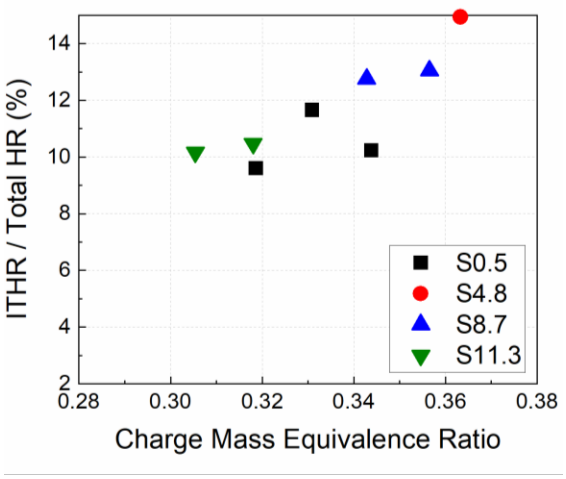

(c) P_{int} = 1.6 bar, X_{O_2} = 0.12

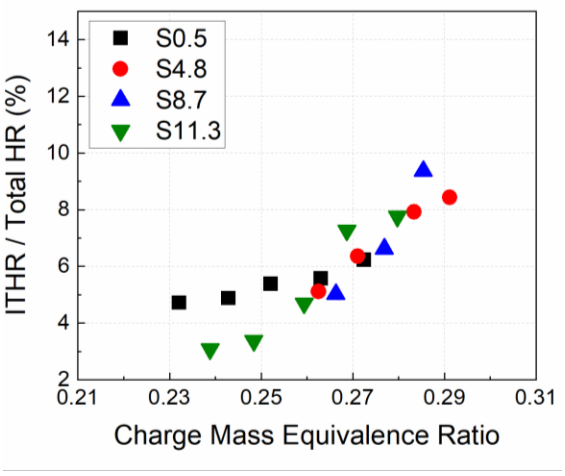

(d) P_{int} = 1.8 bar, X_{O_2} = 0.14

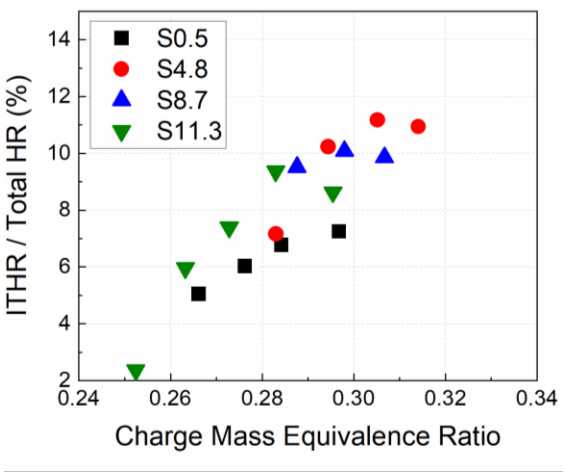

(e) P_{int} = 1.8 bar, X_{O_2} = 0.12

Figure 3-13 ITHR intensity as a function of charge-mass equivalence ratio at P_{int} = 1.4, 1.6, and 1.8 bar at X_{O_2} = 0.14 and 0.12

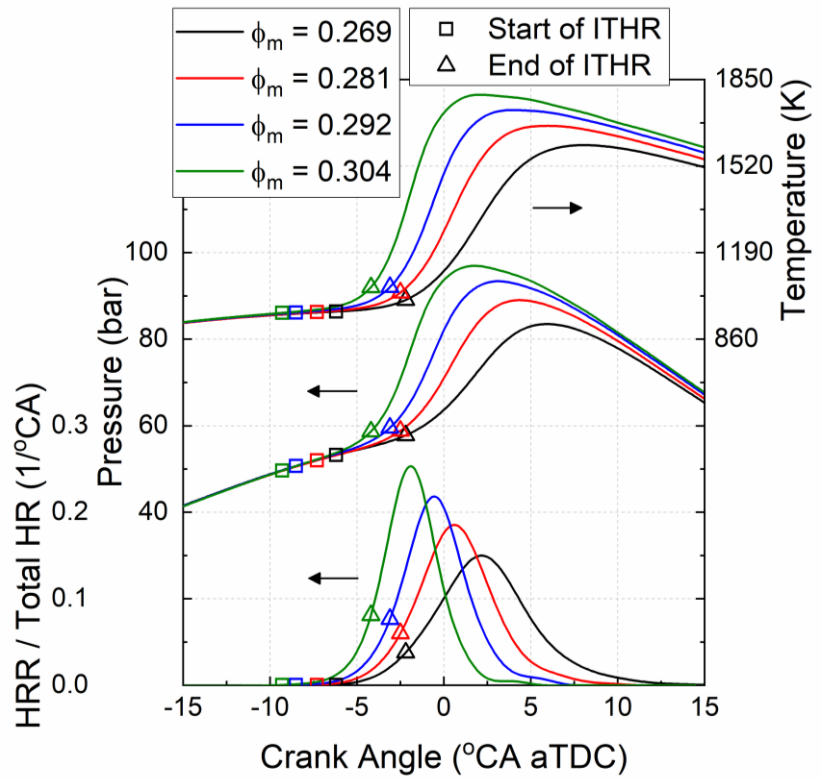

Figure 3-14 Normalized heat release rate, in-cylinder pressure and temperature as a function of crank angle for S11.3 at P_{int} = 1.6 bar and X_{O2} = 0.14

As described in previous researches [25, 29, 30, 34, 35, 77], fuel-chemistry effect should be isolated from thermal and residual-gas effects on ignition timing for accurate ϕ-sensitivity test. However, the tested engine for current study is not equipped with in-cylinder fuel injection system for an alternative firing method explained in [25]. For minimizing the effects of wall temperature and residuals, the coolant outlet temperature was stabilized at 90±1ºC during the fired conditions. Moreover, the exhaust back pressure was maintained lower than ambient pressure and the EVC timing was set to 0ºCA aTDC with negative valve overlap to reduce trapped burn gas and eliminate exhaust backflow. Although these methods cannot be fully isolate the fuel-chemistry effect, they can

minimize the in-cylinder temperature variation prior to autoignition as shown in Figure 3-14.

3.4 Conclusions

Four full boiling range gasolines with RON of 92 but different octane sensitivity from 0.5 to 11.3 have been investigated in an HCCI engine under the conditions at which low temperature reactivity is not active through sweeps of intake temperature, intake oxygen mole fraction, and fuel loading. This study provides a new understanding of ITHR behavior and its effects on autoignition reactivity of single-stage ignition fuels under various engine operating conditions. Significant findings are as follows:

- The maximum of second derivative of HRR method was firstly applied for quantification of ITHR. This novel method accurately predicted the hot-ignition point where HRR changes the most and in-cylinder temperature suddenly increases.
- The relative reactivity of investigated fuels with the absence of LTHR varies as the intake temperature and the intake oxygen mole fraction change. The S0.5 is the most reactive at T_{int} = 55ºC and X_{O2} = 0.21 and is the least reactive at T_{int} = 220ºC and X_{O2} = 0.14. This indicates that the relative reactivity of lower octane sensitivity fuel increases at lower intake temperature and lower EGR ratio conditions, whereas the relative reactivity of higher octane sensitivity fuel increases at higher intake temperature and higher EGR ratio conditions. In other words, the fuel with lower octane sensitivity is less sensitive to intake temperature

and more sensitive to simulated EGR, while the fuel with higher octane sensitivity exhibits an opposite trend.

- The amount of ITHR for the test fuels increases in the range of 2% to 7% of total heat release as the intake temperature and the intake oxygen mole fraction increase mainly due to increased in-cylinder temperature within the ITHR range and longer ITHR duration.
- The ITHR trends, along with the intake temperature and the intake oxygen mole fraction, nearly coincide with the autoignition reactivity variation trends depending on octane sensitivity. This indicates that ITHR plays a significant role in determining fuel octane sensitivity as well as autoignition reactivity.
- The strong dependence of ITHR on equivalence ratio considerably enhances the ϕ-sensitivity. For the similar combustion phasing, the S11.3 and the S8.7 which are the higher octane sensitivity fuels exhibit faster rise rates of ITHR intensity than the S0.5 and the S4.8 respectively, leading to more advanced hot-ignition phasing with increasing equivalence ratio.

Chapter 4

Effects of Octane Number, Pressure, and EGR on Low and Intermediate Temperature Heat Release of Two-stage Ignition Fuels

4.1 Introduction

Strategies to enable advanced, low temperature combustion in compression ignition engines have been widely studied in recent years because of high fuel conversion efficiencies and very low nitrogen oxide (NOx) and particulate matter (PM) emissions [86-88]. Higher reactivity gasoline fuels are appropriate to obtain autoignition at low load and attenuate maximum pressure rise rate (MPRR) at high load in advanced compression ignition (ACI) engines. Yang et al. found that the MPRR can be substantially reduced with partial fuel stratification using high reactivity two-stage ignition fuels which show strong equivalence ratio (ϕ) sensitivity. Several researchers have shown possible improvements in efficiency and emissions from the use of naphtha fuels with octane number range of 60 under partially premixed compression ignition (PPCI) operating conditions [89-92]. Manente et al. achieved a gross indicated efficiency of roughly 53.5% throughout full load range PPCI operation using a 70 RON gasoline, but showed high MPRR (>15 bar/ºCA) at high load [93, 94]. Hildingsson et al. suggested that the most

suitable fuel should have a research octane number (RON) range of 75 to 85 based on the results in a single cylinder engine [95]. Kolodziej et al. and Cho et al. concluded that RON 80 gasoline exhibited better performance and emissions behavior among fuels with RON range of 60 to 92 under PPCI operating conditions [96, 97].

These lower RON fuels mostly demonstrate a two-stage ignition behavior, with a low temperature heat release (LTHR) event followed by the main combustion. The LTHR, also known as cool flames, is mainly attributed to n-paraffins [11, 24, 45, 98-100] and its behavior is considerably affected by engine operating conditions. Increasing engine speed has the effect of reducing the amount of LTHR since the LTHR rate is constant on a time basis [101-104]. The low temperature reactivity is also enhanced at higher intake pressure and lower intake temperature because the charge passes through the active LTHR range (760 - 880 K) at higher pressure [27, 103]. In addition, the LTHR is significantly suppressed by lower oxygen concentration [26, 103]

Intermediate temperature heat release (ITHR), which occurs at temperatures above LTHR and below hot ignition, plays an important role in determining the autoignition timing as well as increasing the ϕ-sensitivity. This ITHR also can be influenced by engine operating parameters. Yang et al. found that increasing engine speed did not modify the ITHR behavior of a two-stage ignition fuel, while maintaining CA50 and ringing intensity by reducing the EGR ratio and the equivalence ratio [34]. Yang et al. also observed that the ITHR was nearly identical with increasing intake pressure, while varying the EGR ratio to keep CA10 constant [35]. However, it could be observed that the intake oxygen mole fraction and the equivalence ratio remarkably increase or decrease the amount of ITHR from Chapter 3. For high reactivity two-stage

ignition fuels, the correlation between LTHR and ITHR as well as the individual effects of pressure and oxygen mole fraction on ITHR are still unclear.

The objective of this study is to expand the understanding of the low and intermediate temperature oxidation behavior through compression ratio (CR) sweep at various engine operating conditions. The primary purposes are: 1) evaluating a newly developed method to quantify the pre-ignition heat release for two-stage ignition fuels, 2) exploring the impact of fuel composition on pre-ignition behavior and reactivity, 3) understanding the effects of intake oxygen mole fraction and pressure on LTHR and ITHR.

4.2 Fuels and Operating Conditions

Three full boiling range naphtha fuels with relatively low octane number were investigated in this study, as presented in Table 4-1. Naphtha, which covers a range of light petroleum distillates from 30ºC to 200ºC, is a typical feedstock for conventional gasoline. However, it requires much less refinery processing compared to high octane conventional gasoline or high cetane diesel fuels. Thus, it can significantly reduce energy consumption and greenhouse gas emissions during its production [105]. In addition, naphtha will be readily available and also could be in surplus as the demand moves to heavier fuels which is used for commercial transport [106]. The high reactivity fuels tested in this study were formulated in order to match the target octane numbers; RON 60, RON 70, RON 80, and their octane sensitivity.

Table 4-1 Properties of RON 60, 70, and 80 fuels.

Property		RON 60	RON 70	RON 80
RON		61.0	70.0	80.0
MON		58.0	67.0	76.9
S (RON-MON)		3.0	3.0	3.1
C/H/O (wt %)		84.8/15.2/0.0	85.4/14.6/0.0	85.8/14.2/0.0
Molecular weight		94.6	91.6	89.1
Density at 15.56℃ (g/mL)		0.7083	0.7172	0.7241
LHV (kJ/kg)		43215	43623	43581
HoV at 25ºC (kJ/kg)		359.1	361.4	367.6
Composition (vol %)	Aromatics	9.9	14.7	20.3
	Olefins	1.1	3.5	5.9
	Naphthenes	16.5	15.1	13.4
	n-Paraffins	33.0	26.8	20.0
	i-Paraffins	38.1	38.5	38.1
	Oxygenates	0.0	0.0	0.0

The octane index (OI) [107] can be also applied to compare the reactivity variation depending on engine operating conditions, as shown in Figure 4-1. Due to the nearly identical octane sensitivity of the test fuels, the reactivity order would not be changed by operating parameters including the current test conditions.

A modified CFR octane rating engine was used for homogeneous charge compression ignition (HCCI) combustion. The engine was motored at a constant speed of 900 rpm throughout this study. For each fuel, the CR was swept from 4.0 to 15.0 to explore not only pre-ignition characteristics but also post-ignition behavior under the test conditions listed in Table 4-2. Three intake pressure and three intake oxygen mole fraction conditions were chosen to investigate the effects of intake boosting and EGR ratio.

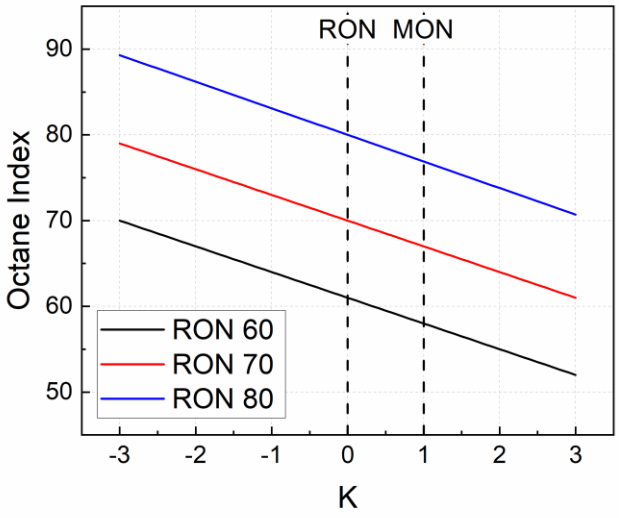

Figure 4-1 Octane Index as a function of K-value for RON 60, 70, and 80 fuels.

Table 4-2 Test conditions for two-stage ignition fuels.

Parameter	Value
Engine speed (rpm)	900
Coolant temperature (ºC)	90±1
Intake temperature (ºC)	40
Intake pressure (bar, abs)	1.0, 1.2, 1.4
Intake oxygen mole fraction	0.210, 0.175, 0.140
Fuel loading (J/L/cycle)	635.3

4.3 Results and Discussion

4.3.1 RON effect

Carbon monoxide (CO) is known as a representative stable intermediate species and a good indicator of the extent of autoignition chemistry. The CO is formed by the conversion of aldehydes and their acetyl radicals in both low and high temperature hydrocarbon oxidation regimes [108]. The subsequent oxidation of CO to carbon dioxide (CO_2) through reaction (4.1) is mostly retarded until the high temperature reaction produces high levels of OH radical [109]. For this reason, many researchers have characterized the reaction process and investigated global oxidation reactivity and negative temperature coefficient (NTC) behavior by tracking CO emissions during CR sweep [11-15, 40-53, 63, 100, 110-115]. In addition, small aldehydes (formaldehydes and

acetaldehyde), which are known as key species in the low temperature oxidation region [11], were measured for this study.

$$HO\bullet + CO \rightarrow H\bullet + CO_2 \quad (4.1)$$

Figure 4-2 presents the entire reaction processes for the three different RON fuels with similar sensitivity at P_{int} = 1.0 bar and X_{O2} = 0.21. Figure 4-3 shows their apparent heat release rate (AHRR) profiles at selected CRs. Kang et al. observed three distinct autoignition characteristics, including low temperature oxidation, NTC, and high temperature oxidation, by monitoring CO emissions as CR increases [14]. In this study, intermediate temperature oxidation was additionally included in the combustion event. Thus, the autoignition process can be classified into four regimes by tracking the aldehydes, CO and CO_2 emissions and the calculated maximum in-cylinder gas temperature.

At CRs below 6.8, no distinct autoignition chemistry was detectable under the current experimental condition due to low in-cylinder temperature (< 700 K). At CR of 7, LTHR initially appears only for the RON 60 fuel which is most reactive among the tested fuel. The formation of CO, formaldehyde, and acetaldehyde also starts with the onset of LTHR. The fuel with lower RON produces LTHR at lower in-cylinder temperature (RON 60: 710 K, RON 70: 714 K, RON 80: 726 K) mainly due to higher mass percentage of n-paraffin content which act as radical providers through hydrogen abstraction at low temperature. As the in-cylinder temperature increases with the CR, the magnitude of LTHR increases, resulting in high concentrations of CO, formaldehyde, and acetaldehyde.

The LTHR has been found to produce considerable amounts of formaldehyde and acetaldehyde [11, 28, 116]. At CR of 8.5, it is clearly observed that low temperature reactivity is higher for the fuels composed of more n-paraffins.

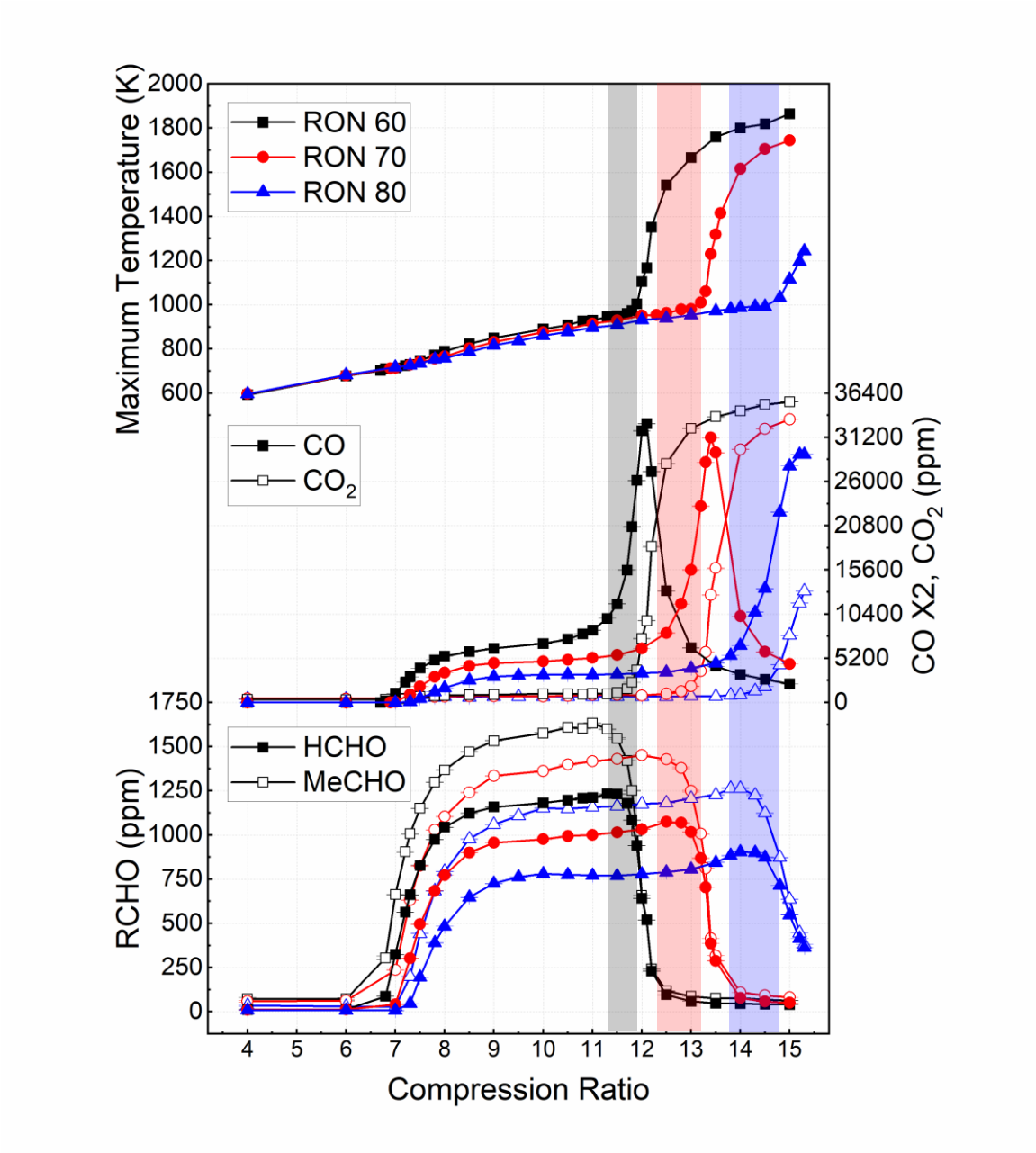

Figure 4-2 Maximum in-cylinder bulk temperature, carbon monoxide, carbon dioxide, formaldehyde, and acetaldehyde emissions as a function of CR at P_{int} = 1.0 bar and X_{O2} = 0.21. The shading represents the range of CR where ITHR is dominant for each fuel.

As the in-cylinder temperature increases over this CR, the formation of alkylperoxy radical in reaction $R\bullet + O_2 \rightarrow ROO\bullet$ is no longer favored, resulting in the NTC behavior. In the NTC regime, overall reaction rate decreases as in-cylinder temperature increases, causing the concentration of CO and aldehydes to level out. Lower RON fuels produce less pronounced NTC regions due to the relatively more LTHR, which can increase the in-cylinder temperature and produce high concentrations of intermediates and radicals prior to the NTC region. This leads to the beginning of intermediate temperature reaction at lower CR.

At CR of 11.7 from Figure 4-3, the RON 60 fuel shows a small but distinct second peak heat release event which indicates ITHR. Lilik also observed a significant second heat release resulted from ITHR through equivalence ratio sweeps of high ignition quality fuels [117]. From Figure 4-2, the shaded areas between the onset of the second heat release and the hot-ignition temperature represent the range of CR at which intermediate temperature oxidation is dominant for each fuel. During this ITHR range, formaldehyde reaches its maximum value and then decreases steeply near the hot-ignition temperature. Hwang et al. found, through a combination of chemiluminescence spectroscopy and chemical kinetic analysis, that formaldehyde is still formed during the ITHR phase as well as the LTHR phase [28]. As the maximum in-cylinder temperature reaches the hot-ignition temperature during the ITHR period, CO is rapidly produced from the aldehydes by removing hydrogen atoms consecutively. Mehl et al. concluded that oxidation of formaldehyde through CH_2O abstraction followed by $HCO\bullet + O_2 \rightarrow CO + HO_2$ was one of major contribution to the ITHR through detailed chemical kinetic modeling simulations. It is also noteworthy that the oxidation of CO to CO_2 starts to

increase during the ITHR range, indicating that the intermediate temperature oxidation produces significant OH radicals through reaction (3.3).

As with the low temperature oxidation, the intermediate temperature oxidation begins at lower CR and lower in-cylinder temperature for the higher reactivity fuel (RON 60: 945 K, RON 70: 955 K, RON 80: 981 K) even though the clearance volume is larger at lower CR. This is mainly due to the greater amount of intermediate species and radicals produced by LTHR. Furthermore, a higher concentration of intermediates and radicals enhances the intermediate temperature oxidation, causing more rapid temperature rise to the hot-ignition temperature during ITHR regime. This indicates that the amount of LTHR can significantly affect the ITHR behavior and eventually influence the onset of HTHR.

At CR of 13.0, the reactivity difference is clearly observed in that the RON 60 fuel is ignited at a CCR of 12.2 and reveals strong HTHR whereas the RON 70 and 80 fuels exhibit ITHR and NTC behavior, respectively. The hot-ignition temperature for lower RON fuel is also lower than that for higher RON fuel (RON 60: 1003 K, RON 70: 1010 K, RON 80: 1032 K). This shows that the greater magnitude of LTHR leads to stronger ITHR, inducing autoignition at lower in-cylinder temperature.

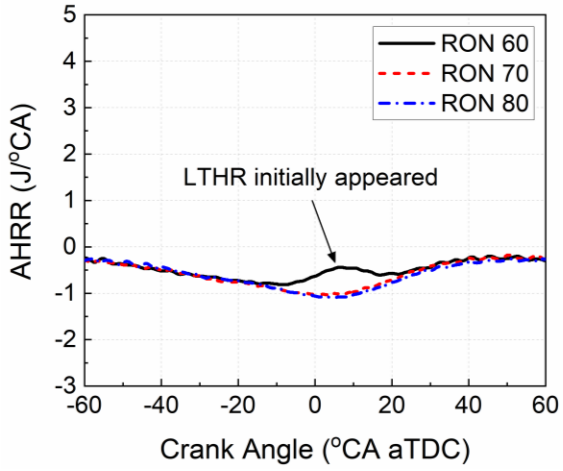

(a) CR = 7.0

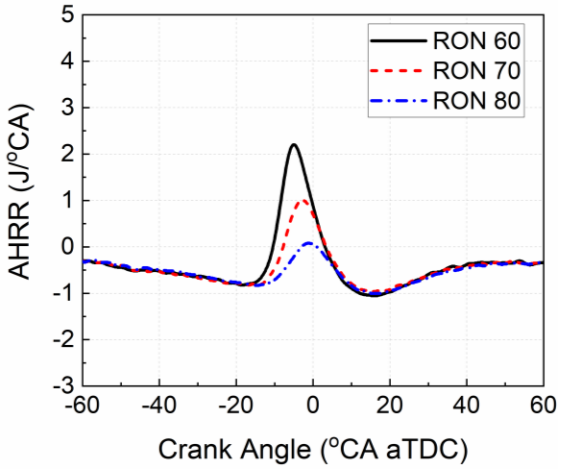

(b) CR = 8.5

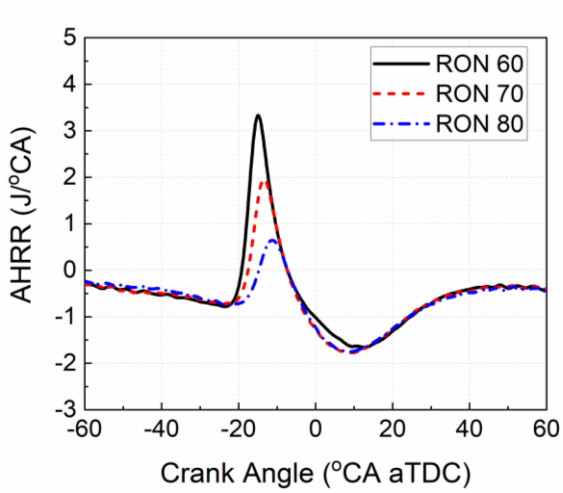

(c) CR = 11.0

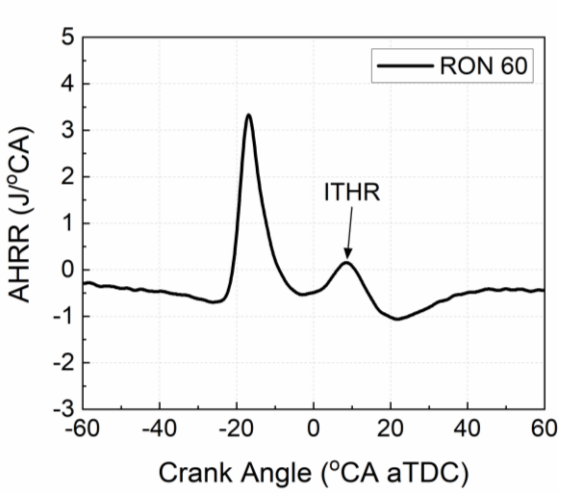

(d) CR = 11.7

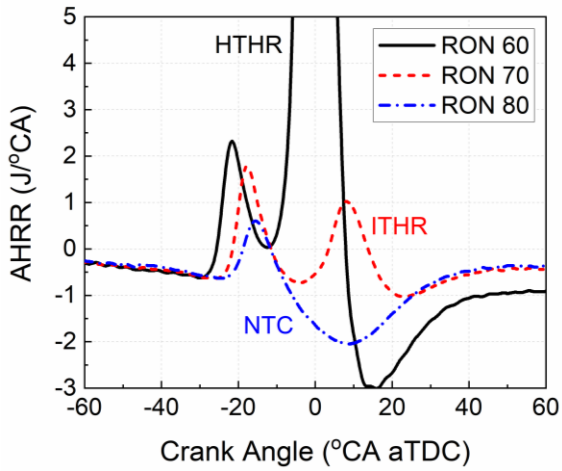

(e) CR = 13.0

Figure 4-3 Apparent heat release rate as a function of crank angle at P_{int} = 1.0 bar and X_{O2} = 0.21.

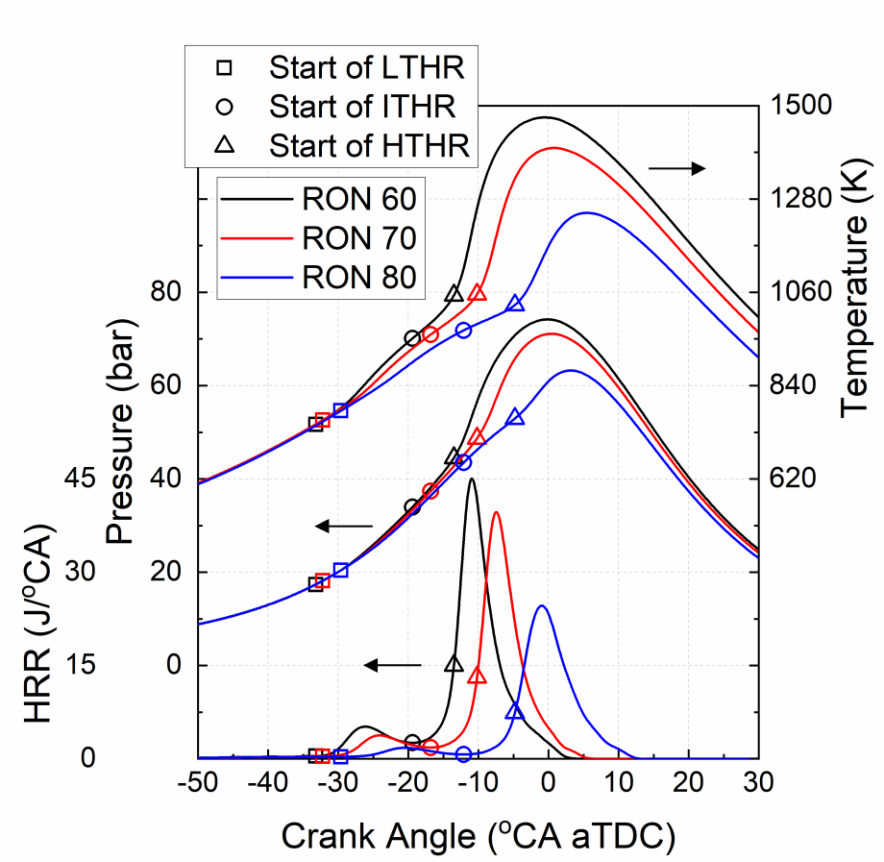

Figure 4-4 Heat release rate, and in-cylinder pressure and temperature as a function of crank angle at P_{int} = 1.4 bar, X_{O2} = 0.21, and CR of 15.

To gain a deeper insight into pre-ignition behavior depending on RON for two-stage ignition fuels, the HRR, in-cylinder pressure and temperature in the LTHR and ITHR ranges at P_{int} = 1.4 bar, X_{O2} = 0.21, and CR of 15 are presented in Figure 4-4. Table 4-3 also shows the difference between the low and intermediate temperature oxidation of various RON gasoline-like fuels through an examination of the cumulative heat release in each region. As observed in Figures 4-2 and 4-3, the lower RON fuel have earlier phasing than the higher RON fuel, which is due to the difference in pre-ignition heat release. The lower RON fuel produces more LTHR than the higher RON fuels even though it passes

through the lower temperature and pressure window at an earlier crank angle. The higher amount of LTHR strongly accelerates the temperature rise rate, leading to earlier onset of ITHR. More importantly, the stronger LTHR results in more enhancement of ITHR. It has been shown that increasing the ITHR can not only improve combustion stability at retarded combustion phasing [27] but also increase ϕ-sensitivity to reduce the maximum heat release rate and control the combustion phasing using the fuel-injection strategy in ACI engines [30, 34, 35].

Table 4-3 Key phasing parameters of HRR traces at P_{int} = 1.4 bar, X_{O2} = 0.21, and CR of 15.

	RON 60	RON 70	RON 80
LTHR start (ºCA aTDC)	-33.2	-32.2	-29.6
ITHR start (ºCA aTDC)	-19.4	-16.8	-12.1
HTHR start (ºCA aTDC)	-13.5	-10.2	-4.8
Cumulative LTHR (J)	42.28	32.97	17.96
Cumulative ITHR (J)	30.93	27.59	15.78
Cumulative HTHR (J)	255.81	227.99	185.01
Average LTHR (J/ºCA)	3.06	2.14	1.03
Average ITHR (J/ºCA)	5.24	4.18	2.16

4.3.2 EGR effect

This section discusses the low and intermediate temperature oxidation behavior under various intake oxygen mole fractions. Figure 4-5 shows the maximum in-cylinder temperature and engine-out emissions as a function of CR for RON 60 fuel at three different intake oxygen mole fraction conditions. The addition of CO_2 remarkably reduces in-cylinder gas temperature due to its high specific heat capacity, leading to the onset of low temperature oxidation at higher CR. Moreover, the AHRR profiles illustrated in Figure 4-6 shows that the LTHR is suppressed as the simulated EGR ratio increases. This is because the lower oxygen concentration significantly inhibits the heat release during the LTHR period [26, 103, 118] even though the lower charge temperature causes more LTHR [27]. The suppressed LTHR less produces formaldehyde, acetaldehyde, and CO emissions as shown in Figure 4-5. This lower concentration of intermediates, combined with the lower in-cylinder temperature, retards the intermediate temperature reaction. From Chapter 3, it has been observed that the amount of ITHR for single-stage ignition fuels decreases with increasing the simulated EGR ratio due to a lower oxygen molar concentration and a lower in-cylinder temperature. This finding is also consistent with the results for two-stage ignition fuels in Figure 4-5 since the intermediate temperature oxidation begins at lower in-cylinder temperature for lower intake oxygen mole fraction. In addition, the reduced intermediates and radicals from LTHR further slows down the development of ITHR as the CR increases. These significantly inhibit the autoignition of two-stage ignition fuels as observed from HRR profiles in Figure 4-6 (b).

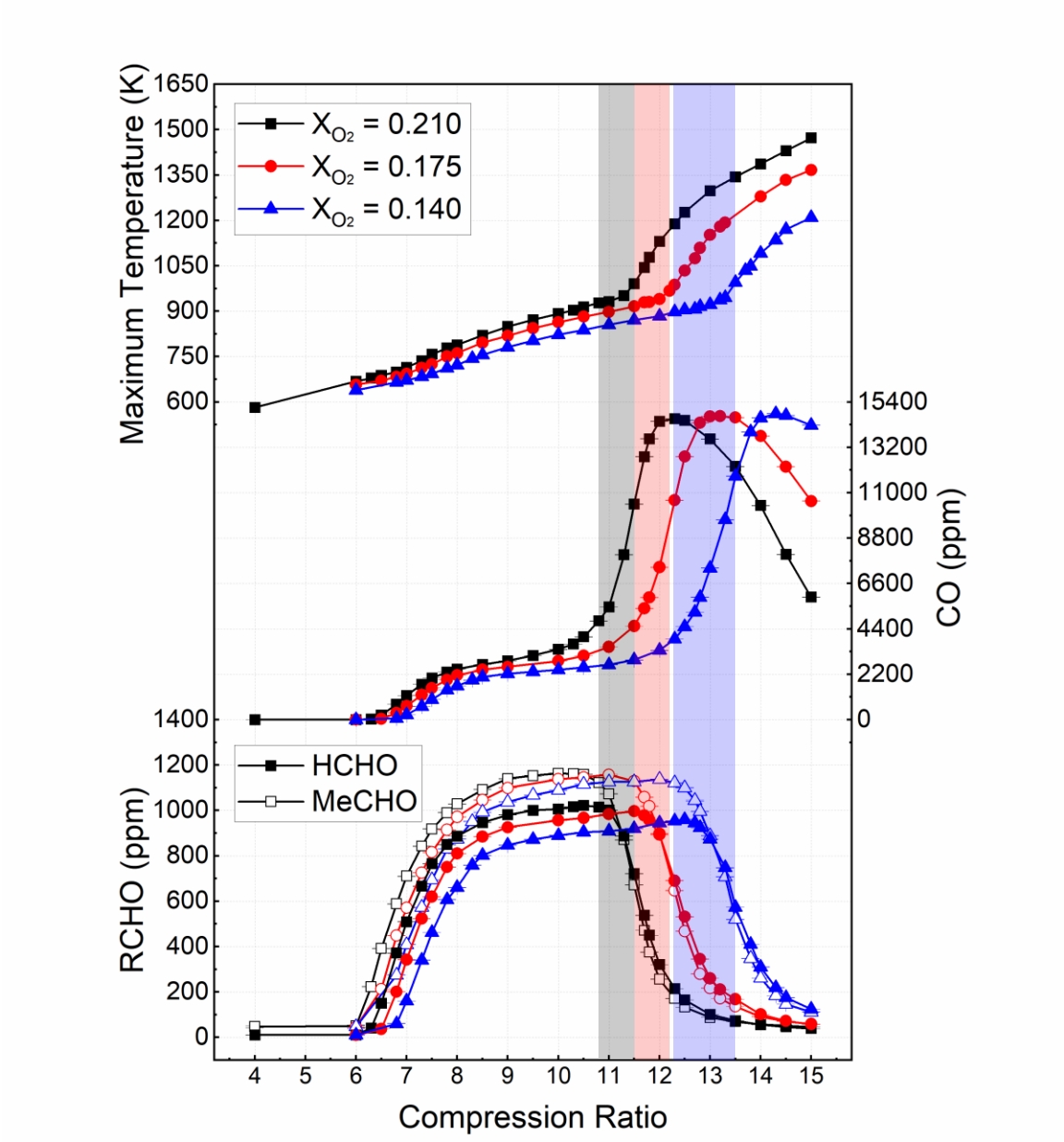

Figure 4-5 Maximum in-cylinder bulk temperature, carbon monoxide, formaldehyde, and acetaldehyde emissions as a function of CR for RON 60 fuel at P_{int} = 1.4 bar. The shading represents the range of CR where ITHR is dominant for each fuel.

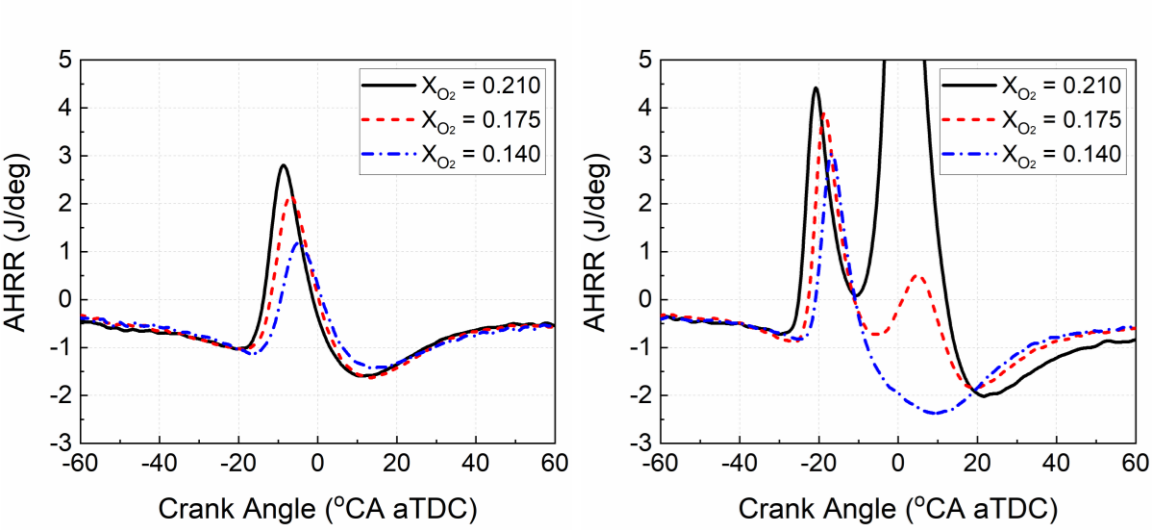

(a) CR = 8.5 (b) CR = 12.0

Figure 4-6 Apparent heat release rate as a function of crank angle for RON 60 fuel at P_{int} = 1.4 bar.

Figure 4-7 presents the variation of HRR, in-cylinder pressure and temperature depending on intake oxygen mole fraction at P_{int} = 1.4 bar and CR of 15. Table 4-4 provides their quantitative values for key phasing and heat release events. At lower intake oxygen mole fraction, the charge passes through much higher pressure window during LTHR period and its low temperature reaction starts at a similar in-cylinder temperature around 745 K. However, the amount of heat released during this period is lower than that at higher intake oxygen mole fraction due to the reduced oxygen concentration. This lower LTHR not only retards the onset of ITHR, but also decreases the magnitude of ITHR, as listed in Table 4-4. Unlike the LTHR, the ITHR for lower intake oxygen mole fraction starts at even lower in-cylinder temperature (X_{O2} = 0.21: 951 K, X_{O2} = 0.175: 946 K, X_{O2} = 0.14: 922 K). In addition, as observed in Figure 4-5, the lower concentration of intermediate products from the first heat release event further decreases the amount of

heat released during the ITHR period. The reduced ITHR decreases the temperature rise rate, eventually leading to the retarded hot ignition at lower temperature and higher pressure for the lower intake oxygen mole fraction.

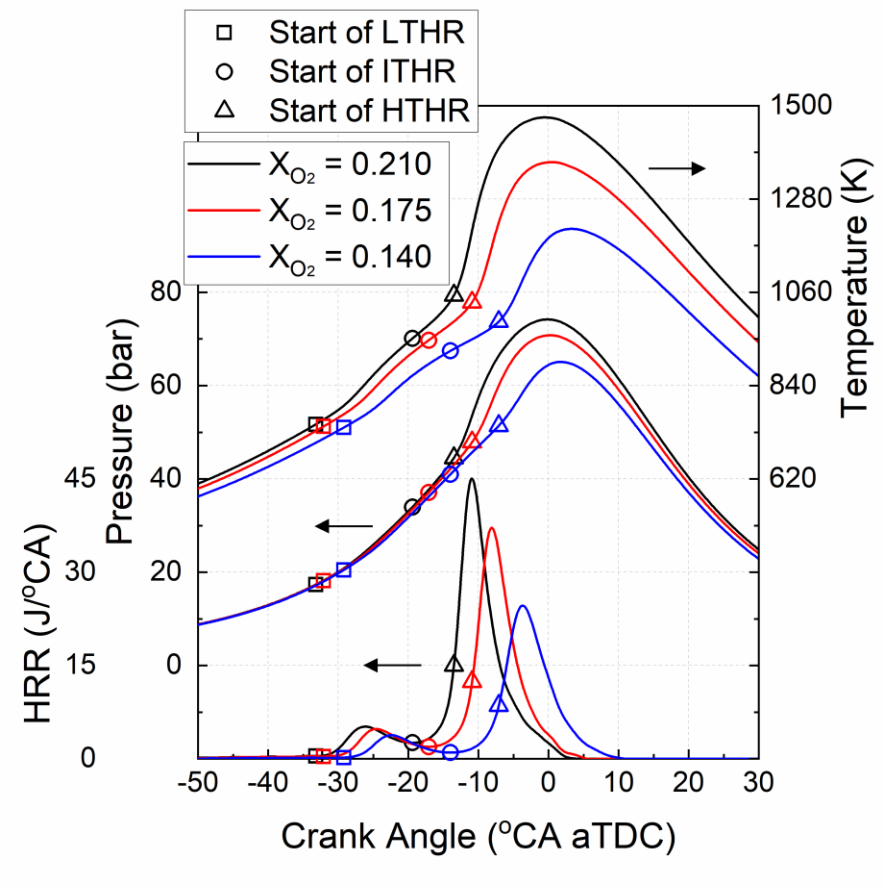

Figure 4-7 Heat release rate, and in-cylinder pressure and temperature as a function of crank angle for RON 60 fuel at P_{int} = 1.4 bar and CR of 15.

Table 4-4 Key phasing parameters of HRR traces for RON 60 fuel at P_{int} = 1.4 bar and CR of 15.

	0.210	0.175	0.140
LTHR start (ºCA aTDC)	-33.2	-32.1	-29.2
ITHR start (ºCA aTDC)	-19.4	-17.1	-14.0
HTHR start (ºCA aTDC)	-13.5	-10.9	-7.1
Cumulative LTHR (J)	42.28	38.79	29.78
Cumulative ITHR (J)	30.93	26.41	19.16
Cumulative HTHR (J)	255.81	216.85	173.40
Average LTHR (J/ºCA)	3.06	2.59	1.96
Average ITHR (J/ºCA)	5.24	4.26	2.78

4.3.3 Intake pressure effect

Figure 4-8 shows the maximum in-cylinder temperature and engine-out emissions as a function of CR for RON 60 fuel at three different intake pressure. Increasing intake pressure does not significantly change the maximum in-cylinder temperature during the pre-ignition period because the charge air mass also increases with the intake pressure. The equivalence ratio with fixed fuel loading decreases from 0.29 to 0.20 as the intake pressure increases from 1.0 bar to 1.4 bar at CR of 15. The fuel mole fraction at P_{int} = 1.4 bar is 0.68 times lower than that at P_{int} = 1.0 bar, but the ratios of volumetric exhaust formaldehyde and acetaldehyde emissions at P_{int} = 1.4 bar to those at P_{int} = 1.0 bar are much higher than the ratio of fuel mole fraction. Furthermore, the volumetric CO emissions at P_{int} = 1.4 bar even close to that at P_{int} = 1.0 bar during LTHR and NTC periods. This indicates that more intermediate species per unit fuel mass were produced during these periods at higher intake pressure. It has been shown that the intake boosting increases the reactivity in the low temperature regime at constant equivalence ratio [15, 103, 119]. At constant fuel flow rate, Figure 4-9 shows that the low temperature reaction still becomes enhanced as the intake pressure increases mainly due to the increased oxygen molar concentration. This increased LTHR with the intake pressure also advances the onset of ITHR, as observed in Figure 4-9 (b). At higher intake pressure, the high temperature oxidation also begins at lower CR, but the CO emissions is slowly converted to CO_2 beyond CCR due to its lower combustion temperature.

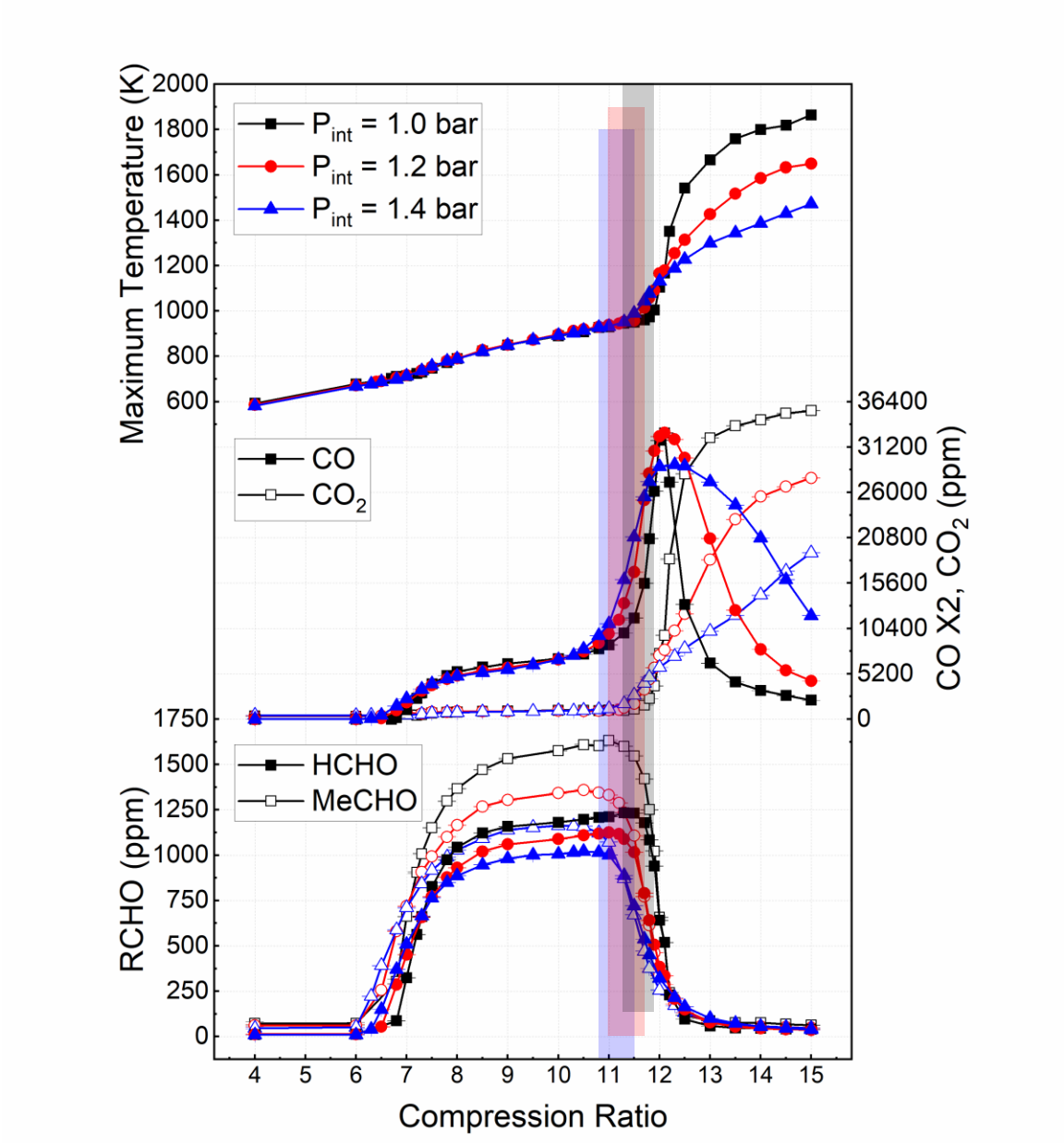

Figure 4-8 Maximum in-cylinder bulk temperature, carbon monoxide, formaldehyde, and acetaldehyde emissions as a function of CR for RON 60 fuel at X_{O2} = 0.21. The shading represents the range of CR where ITHR is dominant for each fuel.

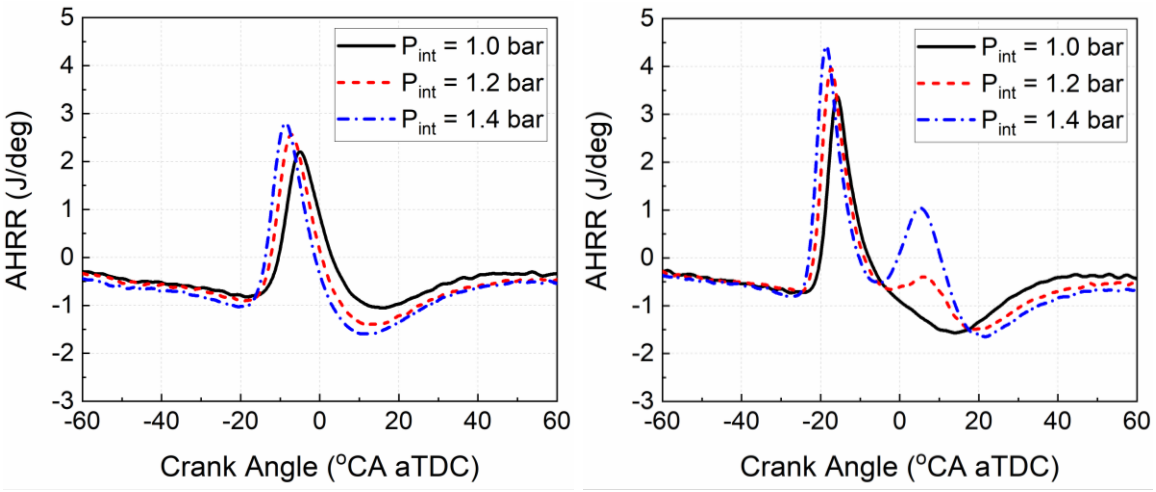

(a) CR = 8.5 (b) CR = 11.3

Figure 4-9 Apparent heat release rate as a function of crank angle for RON 60 fuel at X_{O_2} = 0.21.

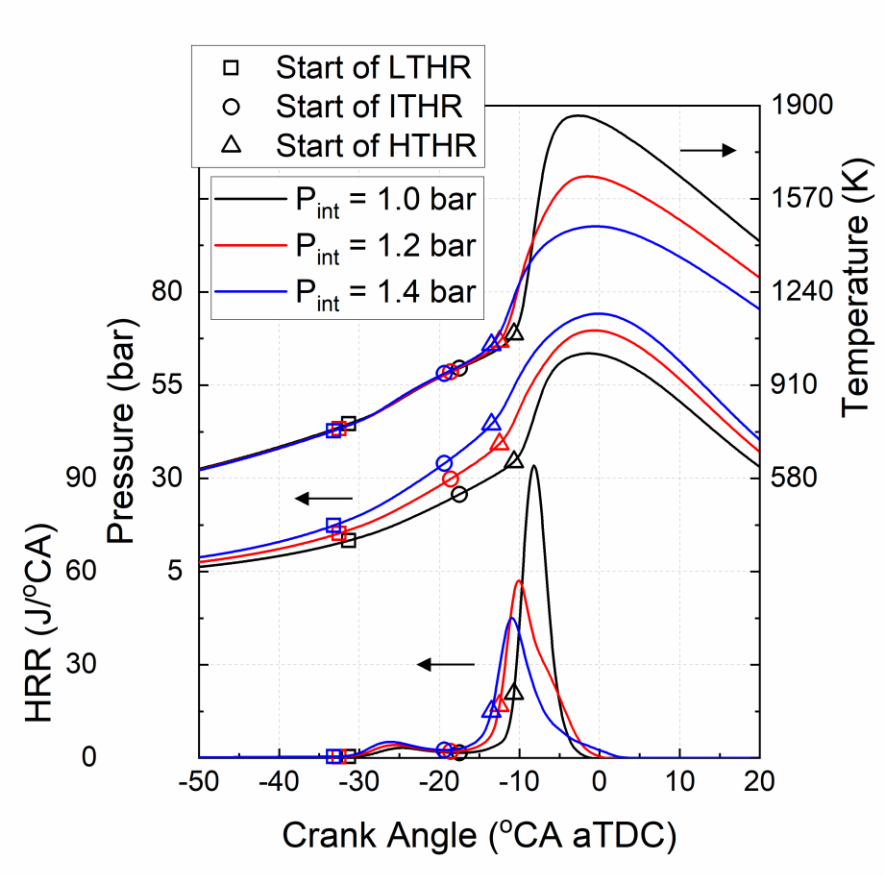

Figure 4-10 Heat release rate, and in-cylinder pressure and temperature as a function of crank angle for RON 60 fuel at X_{O_2} = 0.21 and CR of 15.

For quantitative analysis of pre-ignition behavior, the boundary points and the cumulative heat release of each region at CR of 15 are presented in Figure 4-10 and Table 4-5. The phasing of each heat release is slightly advanced as intake pressure increases due to the promotion of low temperature reaction. In Figures 3-13 (b) and (d) from Chapter 3, it was observed that intake boosting can increase the ITHR intensity as well as the ITHR magnitude itself, while keeping the equivalence ratio constant. However, the amount of ITHR does not noticeably change with increasing intake pressure at constant fuel loading. Instead, the ITHR duration becomes shorter as intake pressure increases, resulting in more intense intermediate temperature reaction prior to hot ignition. This eventually leads to the early onset of HTHR.

Table 4-5 Key phasing parameters of HRR traces for RON 60 fuel at X_{O2} = 0.21 and CR of 15.

	1.0 bar	1.2 bar	1.4 bar
LTHR start (ºCA aTDC)	-31.3	-32.5	-33.2
ITHR start (ºCA aTDC)	-17.5	-18.6	-19.4
HTHR start (ºCA aTDC)	-10.7	-12.5	-13.5
Cumulative LTHR (J)	28.34	35.31	42.28
Cumulative ITHR (J)	30.48	29.88	30.93
Cumulative HTHR (J)	361.41	318.29	255.81
Average LTHR (J/ºCA)	2.05	2.54	3.06
Average ITHR (J/ºCA)	4.48	4.90	5.24

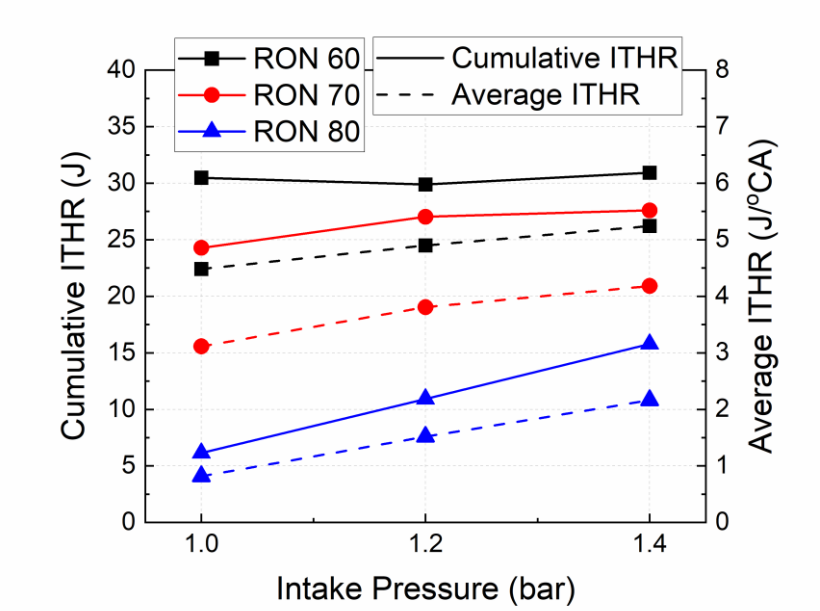

Figure 4-11 Cumulative and average ITHR as a function of intake pressure X_{O2} = 0.21 and CR of 15.

Figure 4-11 represents the cumulative ITHR and the average ITHR per unit crank angle as a function of intake pressure for the test fuels. As with the results in the previous section, the fuel with lower RON shows much higher average ITHR as well as higher cumulative ITHR. The RON increases from 60 to 80 decreases the amount of ITHR by 49% at P_{int} = 1 bar. However, the lower RON fuel reaches a saturated level of cumulative ITHR whereas the RON 80 fuel substantially increases the amount of ITHR by 157% with increasing the intake pressure from 1 bar to 1.4 bar. Although the cumulative ITHR for lower RON fuel almost stays unchanged at a high level, the ITHR duration still decreases as the intake pressure increases. This indicates that the HRR during the ITHR period becomes enhanced at higher intake pressure.

4.4 Conclusions

Three high reactivity gasoline-like fuels with different RON from 60 to 80 have been investigated in an HCCI engine through CR sweeps in order to characterize low and intermediate temperature oxidation behavior under various engine operating conditions. This study provides a new understanding of the correlation between LTHR and ITHR as well as the individual effects of pressure and oxygen mole fraction on ITHR. Significant findings are as follows:

- The maximum of second derivative of HRR method can precisely find the hot-ignition point from two-stage heat release profiles for quantification of ITHR.
- The amount of LTHR has a significant effect on ITHR behavior and eventually influences autoignition reactivity. The RON 60, which is the lowest RON fuel, produces the greatest amount of LTHR which can raise in-cylinder temperature and generate intermediates and radicals prior to NTC region. This results in more enhanced ITHR, inducing autoignition at advanced phasing compared to the higher RON fuels.
- Both the LTHR and the ITHR are suppressed by 30% and 38% respectively as the intake oxygen mole fraction decreases from 0.21 to 0.14. As with the single-stage ignition fuel, lower oxygen mole concentration and lower in-cylinder temperature reduce the magnitude of ITHR. In addition, the reduced intermediates and radicals from LTHR further attenuate the intermediate temperature reaction.
- The intake boosting from atmospheric pressure to 1.4 bar absolute increases the LTHR by 49% even at a constant fuel loading of 635.3 J/L/cycle. For all the test fuels, the average ITHR per crank angle also increases with the intake pressure,

showing concise and strong intermediate temperature reaction. However, the magnitude of ITHR for the lower RON fuel, which exhibits a great amount of ITHR, becomes saturated as the intake pressure increases.

Chapter 5

Effects of Physical Property and Chemical Composition on Autoignition of FACE Gasolines and Naphtha Blends

5.1 Introduction

Gasoline is a complex blend of several hundred hydrocarbon species including linear and branched paraffins, naphthenes, olefins, and aromatics in C_4 – C_{10} boiling range [120]. The gasoline has low chemical reactivity and high volatility which can enable low temperature combustion by achieving sufficient premixing time prior to autoignition. For these reasons, gasoline can be used for the application of advanced compression engine (ACI) concepts such as homogenous charge compression ignition (HCCI) [86, 121, 122], partially premixed compression ignition (PPCI) [9], and reactivity controlled compression ignition (RCCI) [123] to reduce emission without compromise on efficiency.

Gasoline compression ignition (GCI) has shown promising potential through both PPCI process and mixing controlled combustion (MCC) process using direct fuel injection system [124-131]. Under these combustion modes, the combustion phasing is controlled by injection strategy and engine operating conditions such as intake pressure,

intake temperature, and EGR ratio. Therefore, understanding both the physical and chemical ignition behavior of gasolines at various operating conditions is essential for optimizing their use in GCI engines. Badra et al. studied the effects of chemical and physical properties for different injection timing at part load using low octane gasoline fuels (RON = 60 – 65) [132]. The experimental and numerical results showed that the impacts of chemical and physical properties on combustion phasing and emissions were negligible. However, Naser et al. concluded that physical properties, such as volatility and surface tension, became increasingly dominant as injection timing is retarded from premixed conditions [133]. Zhang et al. investigated the fuel chemical and physical properties effects on GCI in a heavy-duty diesel engine through a computational study [134]. It was found that physical properties including heat of vaporization, density, vapor pressure, viscosity, and surface tension had little impact on ignition delay and combustion phasing at high in-cylinder temperature. For the chemical effect, higher RON primary reference fuels (PRF) showed a stronger dependency on temperature than lower RON fuels due to reduced NTC behavior. It was also observed that increasing octane sensitivity with constant RON resulted in shorter ignition delay at test conditions close to the MON test (T_{SOI} = 913 – 1000 K). Vallinayagam et al. tested RON 70 fuels with different octane sensitivity and physical properties at low load in a GCI engine [73]. It was found that the physical properties of the fuel with same RON and octane sensitivity rarely affected combustion phasing and ignition delay at test conditions where temperature at TDC was above 1000 K. The higher octane sensitivity gasoline exhibited more advanced combustion phasing and shorter ignition delay than the lower octane sensitivity fuel at this condition.

Several studies were implemented in the past to explore the effect of fuel physical and chemical properties on GCI at various operating conditions. However, there is still lack of fundamental investigation for engine experiment and ignition delay measurement especially at high load boosted conditions where low and intermediate temperature oxidation is important. In order to address this gap and expand the understanding of the physical and chemical effects on autoignition behavior in GCI engines, liquid fuel jet evaporation as well as gas-phasing ignition of gasolines with varying RON and octane sensitivity were investigated using a modified CFR variable compression ratio engine and a constant volume spray combustion chamber.

5.2 Fuels and Operating Conditions

FACE (fuels for advanced combustion engines) gasolines were designed to enable a detailed understanding of fuel composition effects in ACI engines by providing consistent well-characterized properties and compositions. They consist of a total of ten fuels and each represent four primary properties of fuels for ACI engines: RON; octane sensitivity; aromatic content; and n-paraffin content, as illustrated in Figure 5-1 [135]. These FACE gasolines have been widely studied for fuel effects on ignition behavior and surrogate validation in many types of combustion research devices such as shock tubes [136-139], rapid compression machines (RCM) [136, 138-142], jet-stirred reactors (JSR) [143-145], and motored engines [114, 115, 138, 141, 146, 147].

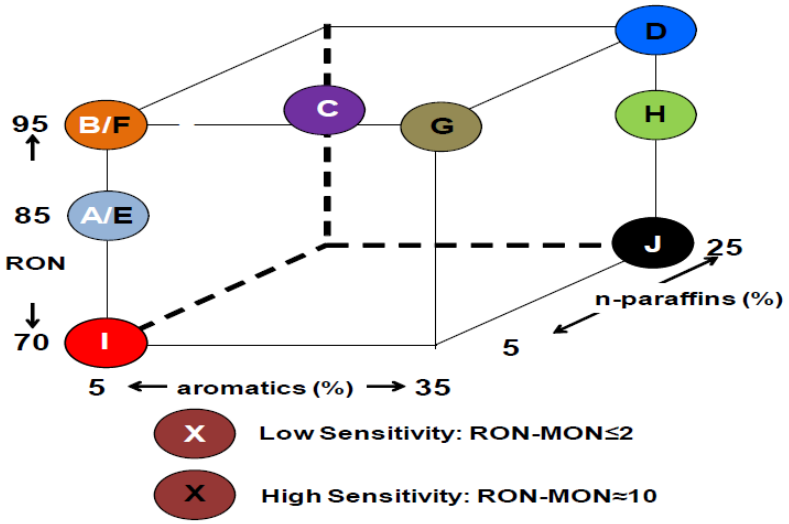

Figure 5-1 FACE gasoline matrix [135].

In this study, FACE A, C, I, and J gasolines and three naphtha blends tested from the previous chapter were investigated as presented in Table 5-1. Additional physical properties and detailed hydrocarbon analyses (DHA) for the FACE gasolines and naphtha blends are available in [135, 136, 145, 148] and Appendix A, respectively. The FACE A, C, and I gasolines are highly paraffinic while the FACE J gasolines and the naphtha blends contain considerable amounts of aromatics. As the mass percentage of aromatic content in the fuel increases, the liquid fuel density and the final boiling temperature increase while the heat of combustion decreases as can be observed in Table 5-1 and Figure 5-2. The gray area in the Figure 5-2 represents the distillation range of typical U.S. market gasolines [71]. Almost all fuels have higher T10 than the typical gasoline range, but the final boiling temperatures are lower than or in the typical range. Derived cetane number (DCN) of the test fuels were measured using the CID unit based on ASTM

D7668 method [54]. The measured DCNs of FACE gasolines in this study agree well with those measured by an ignition quality tester (IQT) [149].

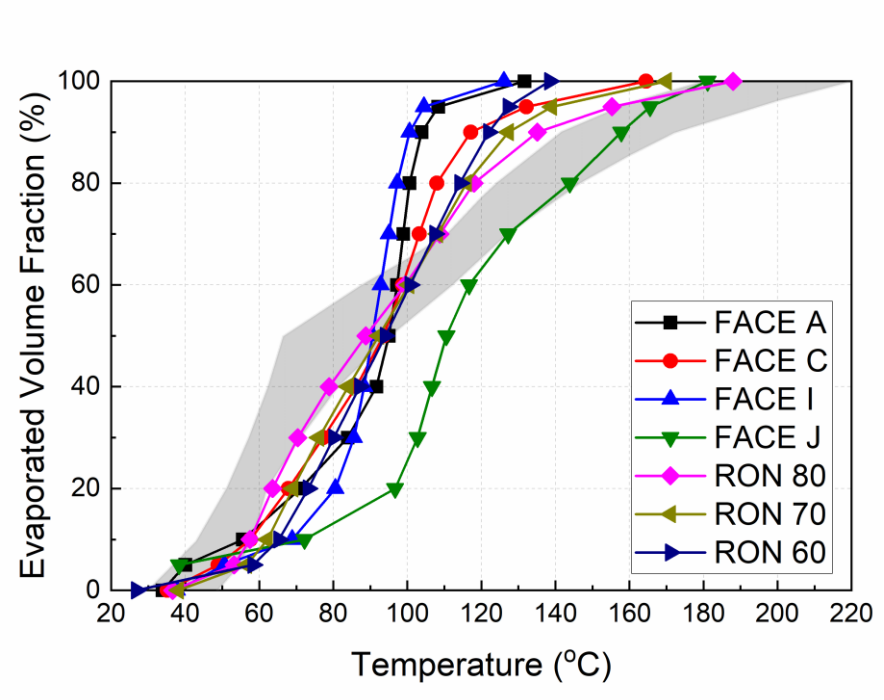

Figure 5-2 Distillation characteristics of FACE gasolines and naphtha blends.

The modified CFR engine was motored at a constant speed of 600 rpm throughout this study. For each fuel, the CR was swept from 3.9 to the ignition point to explore pre-ignition characteristics under both naturally aspirated and boosted conditions, as listed in Table 5-2. The constant volume combustion chamber offers a direct injection system to study the spray ignition behavior at various ambient air temperatures and oxygen mole fractions, as presented in Table 5-3.

Table 5-1 Fuel properties of FACE gasolines and naphtha blends.

Property		FACE A	FACE C	FACE I	FACE J	RON 80	RON 70	60 RON
RON		83.5	84.7	70.3	71.8	80.0	70.0	61.0
MON		83.6	83.6	69.6	68.8	76.9	67.0	58.0
S (RON-MON)		-0.1	1.1	0.7	3.0	3.1	3.0	3.0
DCN		26.2	25.6	30.0	26.5	23.3	27.8	32.7
C/H (wt %)		84.0/16.0	84.5/15.5	84.1/15.9	86.2/13.8	85.8/14.2	85.4/14.6	84.8/15.2
Density at 15.56℃ (g/mL)		0.685	0.691	0.697	0.742	0.724	0.717	0.708
LHV (kJ/kg)		44778	44792	44717	43568	43581	43623	43215
RVP (kPa)		55.8	51.0	51.7	51.7	49.6	44.8	44.0
Composition (vol %)	Aromatics	0.0	3.9	1.2	31.7	20.3	14.7	9.9
	Olefins	0.4	1.3	6.4	0.6	5.9	3.5	1.1
	Naphthenes	1.6	0.4	3.3	2.3	13.4	15.1	16.5
	n-Paraffins	11.7	24.4	14.4	31.6	20.0	26.8	33.0
	i-Paraffins	86.0	69.7	74.5	33.6	38.1	38.5	38.1
	Oxygenates	0.0	0.0	0.0	0.0	0.0	0.0	0.0

Table 5-2 Test conditions for CFR engine

Parameter	Value
Engine speed (rpm)	600
Coolant temperature (ºC)	90±1
Intake temperature (ºC)	190
Intake pressure (bar, abs)	1.0, 2.0, 3.0
Intake oxygen mole fraction	0.21
Equivalence ratio	0.25, 0.50

Table 5-3 Test conditions for CID 510

Parameter	Temperature sweep	EGR sweep
Injection pressure (bar, abs)	1000	
Injection time (ms)	2.5	
Initial chamber pressure (bar, abs)	20	
Initial chamber temperature (ºC)	540, 560, 580, 600, 620, 640	600
Simulated EGR ratio (%)	0	0, 15, 25, 40, 50, 55

5.3 Results and Discussion

This result section consists of two subsections based on fuel reactivity. The first section compares the experimental results of higher RON fuels including FACE A, C, and RON 80 fuels. The second section deals with lower RON fuels including FACE I, J, RON 70 and 60 fuels.

5.3.1 Higher RON fuels

To identify the impact of fuel chemical composition on gas-phase combustion behavior, the ignition characteristics of fuels with similar RON were explored through CR sweeps at various engine operating conditions. Figures 5-3, 5-4, and 5-5 present the comparisons of CO emissions, maximum in-cylinder temperature, and critical compression ratio (CCR) for FACE A, C, and RON 80 fuels at both naturally aspirated and boosted conditions. At P_{int} = 1 bar and ϕ = 0.25, the resultant CO emissions for the test fuels are relatively insignificant during pre-ignition, as compared to those at higher intake pressure or higher equivalence ratio. It is because the high intake temperature with low intake pressure and the low fuel concentration weaken the chain-branching reactions in the low temperature regime [27, 103].

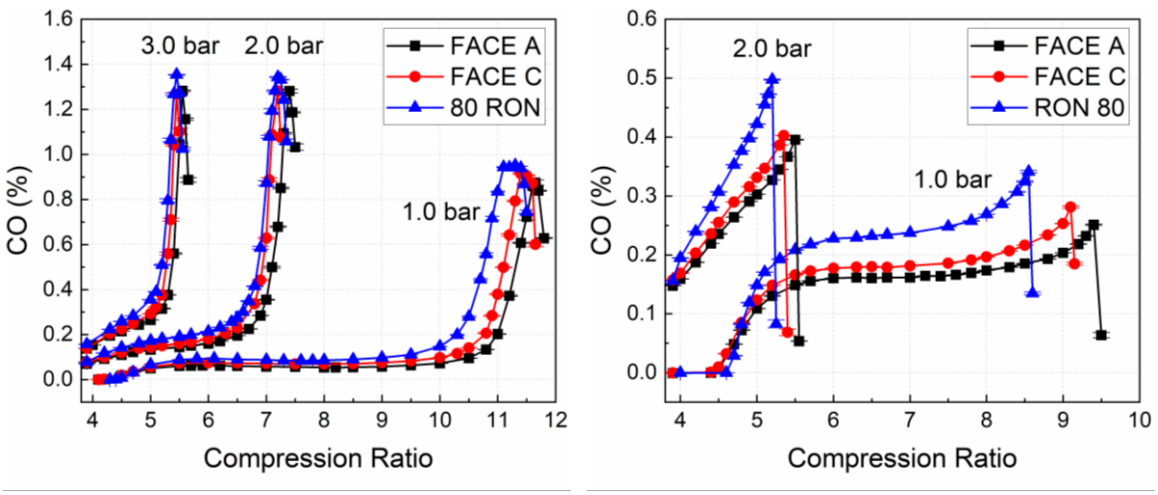

(a) ϕ = 0.25 (b) ϕ = 0.5

Figure 5-3 Carbon monoxide emissions as a function of CR for higher RON fuels at T_{int} = 190ºC and X_{O2} = 0.21.

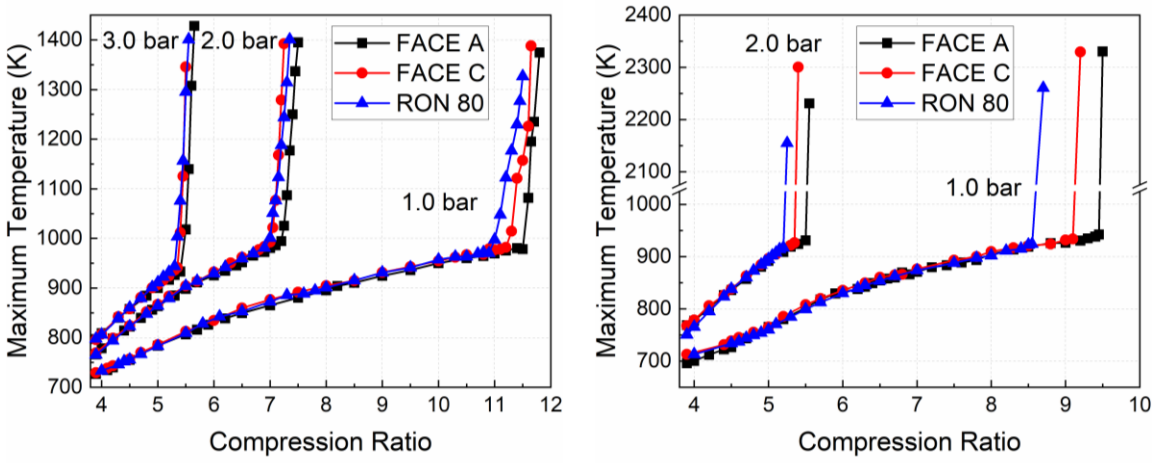

(a) ϕ = 0.25 (b) ϕ = 0.5

Figure 5-4 Maximum in-cylinder bulk temperature as a function of CR for higher RON fuels at T_{int} = 190ºC and X_{O2} = 0.21.

The RON 80 fuel, which has the lowest RON and MON among the higher RON fuels, produces slightly more CO emissions than the FACE gasolines at both equivalence ratios. The RON 80 fuel have a large fraction of aromatics, mostly toluene which acts as

a radical scavenger depressing the low temperature reaction [49, 150]. Furthermore, it also contains about 5% of cyclopentane which inhibits the LTHR [99]. However, its higher concentration of long chain n-alkanes, such as n-heptane and n-octane, and relatively lower amount of highly branched alkanes, such as 2,2,4-trimethylpentane and 2,3-dimethylpentane accelerate the low temperature reaction rate. The isomerization reaction rate of RO_2 radicals to QOOH radical species is fastest in long, linear alkane fuel molecules, and is slowest in highly branched fuel molecules due to less availability of secondary hydrogen atoms [75, 151]. The RON 80 fuel also exhibits less pronounced NTC behavior as observed in Figure 5-3. It reaches the hot-ignition temperature at lower CR which indicates the early onset of high temperature oxidation, eventually resulting in lower CCR as shown in Figure 5-5. For the FACE gasolines, both fuels show relatively similar ignition behavior throughout all test conditions. The FACE C gasoline exhibits marginally earlier hot-ignition timing and lower CCR even though it possesses higher RON compared to the FACE A gasoline.

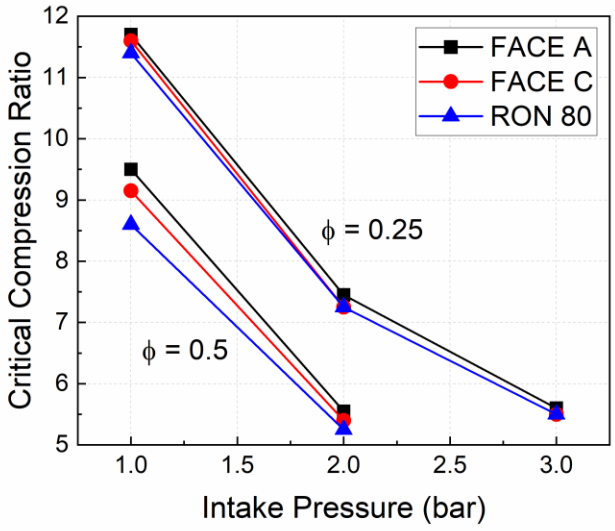

Figure 5-5 Critical compression ratio as a function of intake pressure for higher RON fuels at T_{int} = 190ºC and X_{O2} = 0.21.

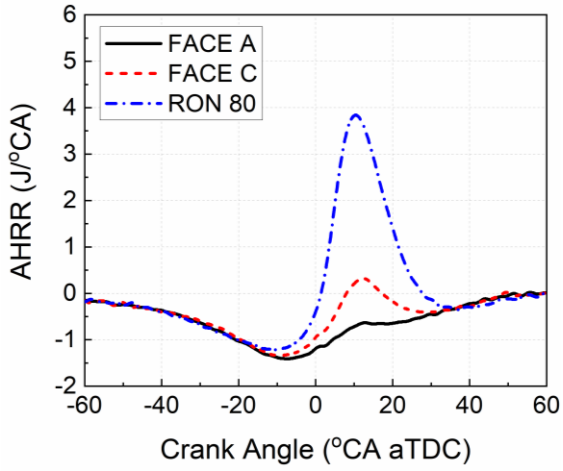

(a) P_{int} = 1.0 bar, CR = 11.0

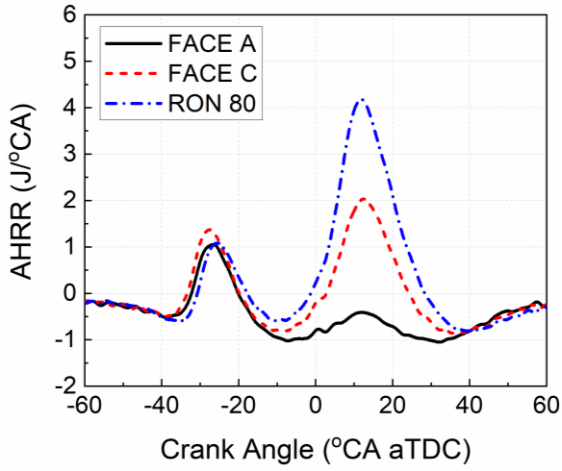

(b) P_{int} = 2.0 bar, CR = 7.0

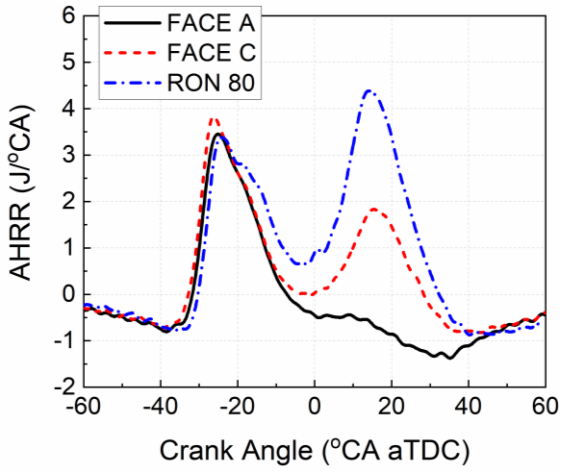

(c) P_{int} = 3.0 bar, CR = 5.3

Figure 5-6 Apparent heat release rate as a function of crank angle for higher RON fuels at X_{O2} = 0.21 and ϕ = 0.25.

Figures 5-6 and 5-7 present the apparent heat release rate (AHRR) profiles during ITHR period at ϕ = 0.25 and 0.5, respectively. All the higher RON fuels exhibit single-stage ignition behavior only at P_{int} = 1 bar and ϕ = 0.25 since the charge passes through the active LTHR range (760 – 880 K) at low pressure. For this condition, the low temperature oxidation rarely occurs at in-cylinder pressure range of 6 to 12 bar whereas it

is more vigorous at the range of 10 to 17 bar for the higher intake pressure of 2 bar. From Figure 5-7, it is clearly observed that the higher fuel concentration at ϕ = 0.5 remarkably enhances the overall LTHR.

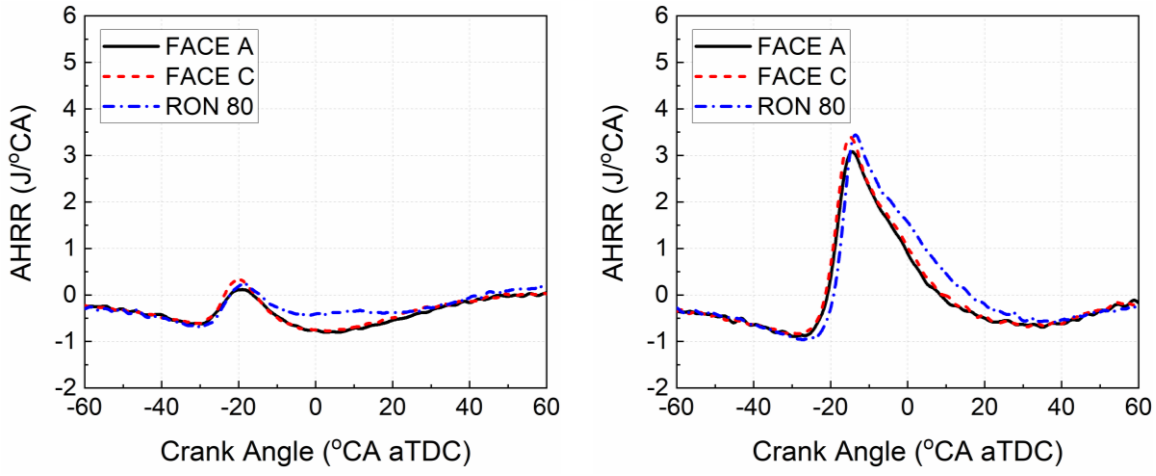

(a) P_{int} = 1.0 bar, CR = 8.5 (b) P_{int} = 2.0 bar, CR = 5.0

Figure 5-7 Apparent heat release rate as a function of crank angle for higher RON fuels at X_{O2} = 0.21 and ϕ = 0.5.

At P_{int} = 1 bar and ϕ = 0.25 from Figure 5-6, the RON 80 fuel shows a distinctive peak indicating the start of HTHR whereas both the FACE gasolines exhibit weak ITHR at CR of 11. This reactivity order is continued despite the presence of LTHR as intake pressure increases. The FACE C gasoline, which has the highest RON among the test fuels, is more reactive than the FACE A gasoline, resulting in earlier onset of ITHR as well as HTHR at any intake pressure, as illustrated in Figures 5-4 and 5-6. It appears that the RON metric itself is not sufficient to represent the autoignition behavior even for the highly paraffinic fuels. More than twice n-alkane content of FACE C gasoline leads to more pronounced LTHR at both equivalence ratios. Through the direct comparison of

AHRR profiles from Figure 5-6 (a) and (b), it can be observed that the stronger LTHR of FACE C gasoline accelerates the intermediate temperature reaction, causing a greater amount ITHR. This finding is also consistent with the experimental results in the previous chapter.

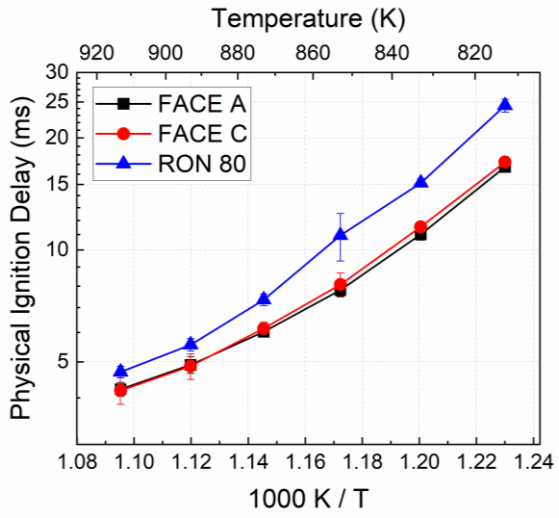

(a) Physical ignition delay

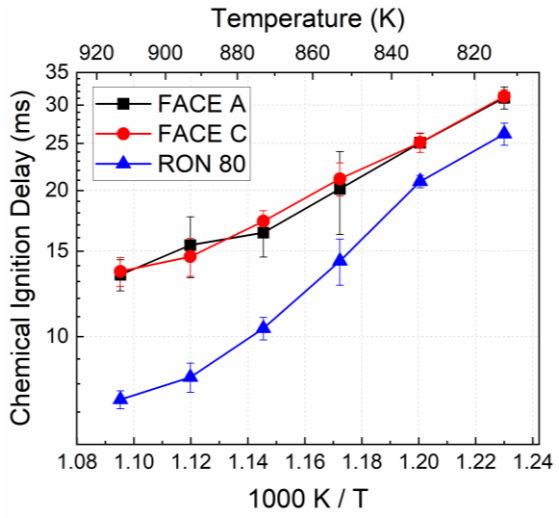

(b) Chemical ignition delay

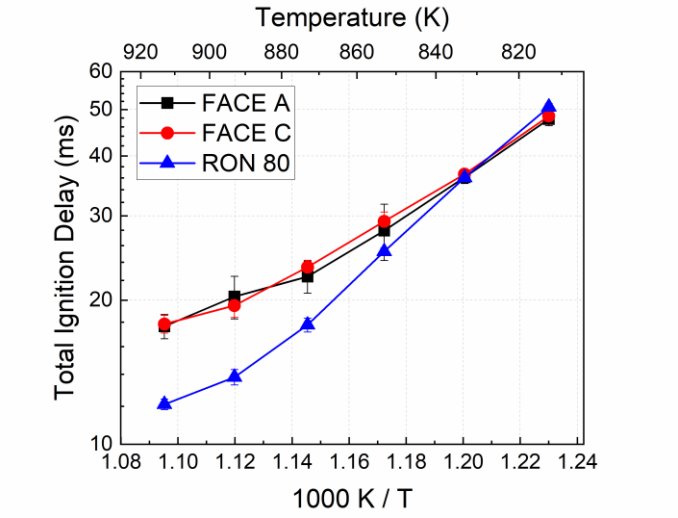

(c) Total ignition delay

Figure 5-8 Physical, chemical, and total ignition delay as a function of ambient temperature for higher RON fuels at X_{O2} = 0.202.

The effects of ambient temperature and oxygen concentration on the physical and chemical ignition behavior of the fuels with similar RON were investigated using the optically accessible constant volume combustion chamber. Figure 5-8 presents the physical, chemical, and total ignition delay times as a function of initial chamber temperature for the higher RON fuels at X_{O2} = 0.202. The overall ignition delay times for the test gasolines are much longer and more sensitive to the ambient air temperature as compared to previous experiments in this same test facility for conventional diesel, biodiesel, and jet fuels, due to lower reactivity of the current test fuels [47, 48, 55, 56, 152].

From Figure 5-8, it is interesting to note that the ignition behavior of RON 80 fuel is distinctively different from that of FACE gasolines in both physical and chemical processes. The RON 80 fuel shows much longer liquid fuel vaporization and quite shorter gas-phase ignition than the higher RON FACE gasolines. The lower volatility of RON 80 fuel, which can be expressed as lower vapor pressure and higher boiling temperature from Table 5-1 and Figure 5-2, increases the physical ignition delay times as shown in Figure 5-8 (a). The lower volatility leads to slower spray evaporation and decelerates the fuel-air mixing [153, 154]. In addition, the higher liquid fuel density of RON 80 fuel further prolongs the physical process. It has been shown that increasing liquid fuel density extends liquid penetration length in spray experiments. The higher liquid fuel density reduces spray jet velocity and plume angle, thereby diminishing the air mixing process [153, 155-159]. The time difference between the physical ignition delay of the test fuels becomes increasingly large as the air temperature decreases, which means that the physical properties are more important at lower temperature. Zhang et al. also found

that the effect of the liquid fuel density on the ignition delay process is more pronounced when reducing the in-cylinder temperature, through computational fluid dynamic (CFD) simulation [134]. Despite the overall longer physical ignition process, the higher gas-phase oxidation reactivity of RON 80 fuel leads to a faster chemical ignition process than for the FACE gasolines, eventually reducing the total ignition delay time.

Both FACE gasolines provide almost identical physical ignition delay time even though the FACE C gasoline has slightly lower vapor pressure, higher boiling temperature, and a bit higher fuel density which can hinder the fuel vaporization. Other physical properties such as viscosity, surface tension, specific heat, and heat of vaporization, which were not explored in this study, also can affect the physical ignition process. However, the greater LTHR of FACE C gasoline, as mentioned earlier, can offset the delay time difference resulting from the liquid fuel evaporation since the physical ignition delay time is measured by the onset of the formation of formaldehyde. Although the prevailing processes affecting the physical ignition delay are related to the fuel physical properties, the low temperature chemistry is also partially included in the physical ignition delay measurement since the formation of formaldehyde is largely affected by LTHR. The chemical ignition delay times for these two fuels are also very similar each other. This finding is consistent with previous shock tube and RCM experimental results of Sarathy et al. and Vuilleumier et al. [136, 141].

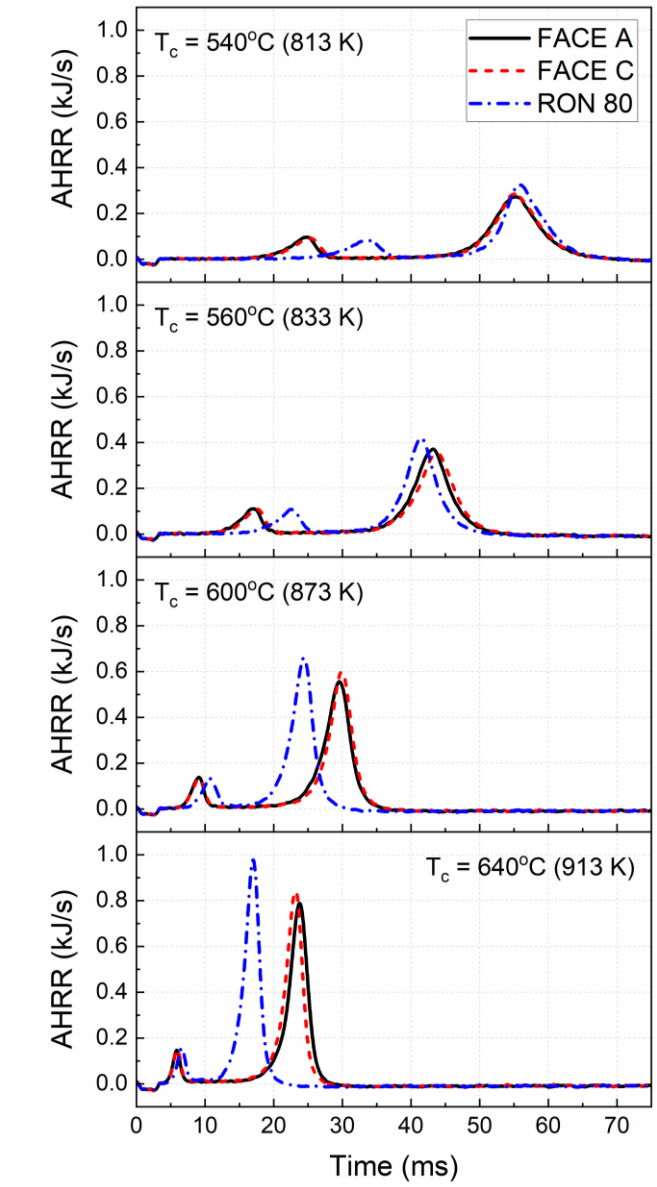

Figure 5-9 Apparent heat release rate for higher RON fuels at T_c = 540, 560, 600, 640ºC and X_{O2} = 0.202.

The AHRRs derived from measured pressure trace data at selected ambient temperature are plotted in Figure 5-9. For all the test fuels, there appears to be a distinct two-stage ignition behavior across the temperature range at initial chamber pressure of 20 bar. The AHRR profiles of alkane-rich FACE A and C gasolines are almost

indistinguishable from each other due to their similar reactivity and physical properties. They also exhibit much longer NTC region than the RON 80 fuel as observed in Figure 5-3. The NTC behavior is dominant in paraffin autoignition chemistry [63]. From the previous chapter, it was found that more LTHR leads to a less pronounced NTC region by producing a greater amount of intermediates and radicals, consequently resulting in early onset of intermediate temperature reaction. This is confirmed in Figure 5-10, where the LTHR intensity is shown as a function of initial ambient air temperature for higher RON fuels. More LTHR contribution of RON 80 fuel to the total amount of heat released decreases the NTC regime at each air temperature. It is also observed that as the air temperature increases, the LTHR intensity for the test fuels linearly decreases, which is consistent with experimental results of Kang et al. [47]. Increasing the initial air temperature reduces the residence time of reactive mixture during the active low temperature oxidation regime (760 – 880 K).

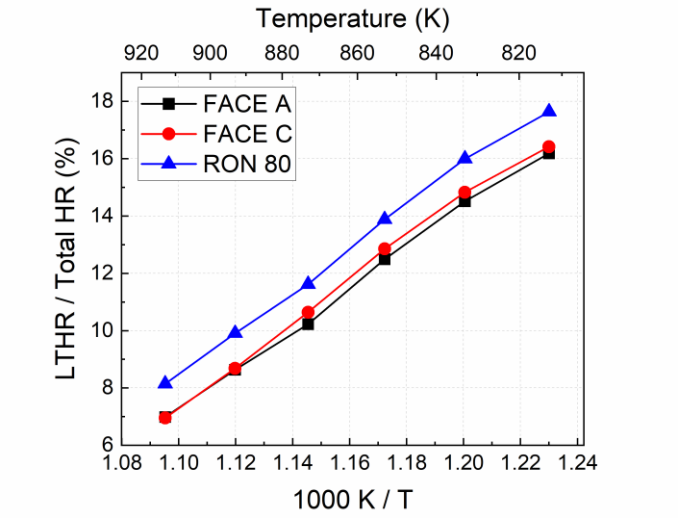

Figure 5-10 LTHR intensity as a function of ambient temperature for higher RON fuels at X_{O_2} = 0.202.

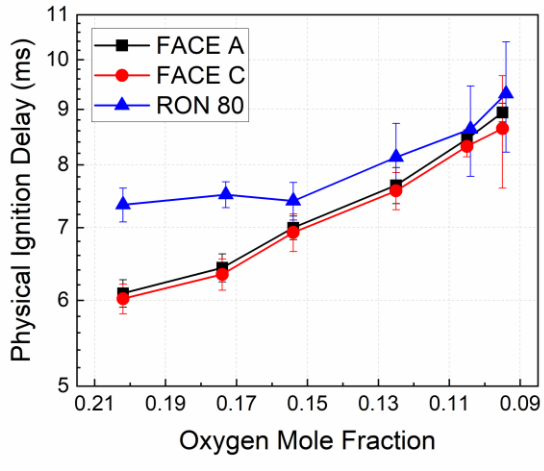

(a) Physical ignition delay

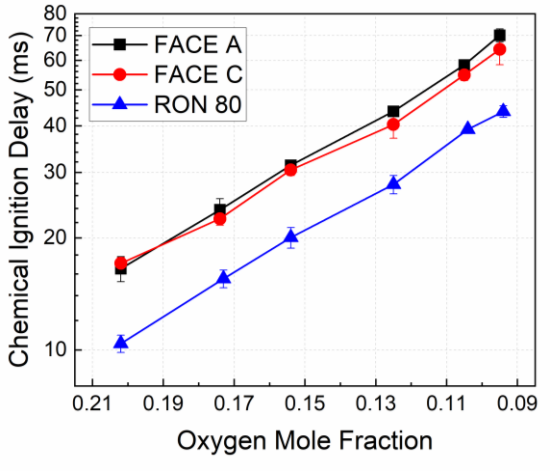

(b) Chemical ignition delay

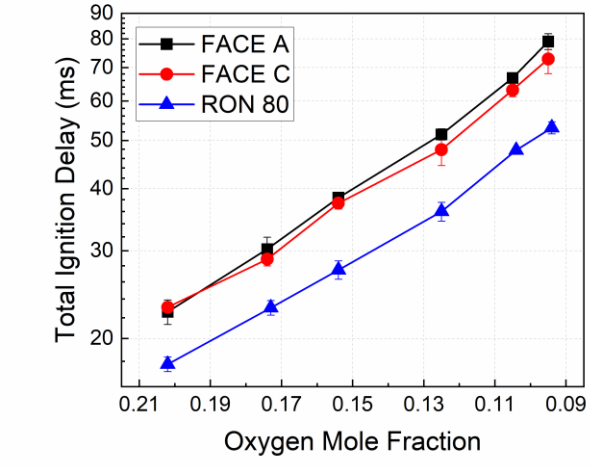

(c) Total ignition delay

Figure 5-11 Physical, chemical, and total ignition delay as a function of ambient oxygen mole fraction for higher RON fuels at T_c = 600ºC.

This part focuses on the effect of ambient oxygen concentration on liquid fuel evaporation and gas-phase ignition through an examination of the physical and chemical ignition processes of the fuels with similar RON. Figure 5-11 presents the physical, chemical, and total ignition delay times as a function of initial oxygen mole fraction for the higher RON fuels at T_c = 600ºC. The oxygen dilution using the simulated EGR

increases both physical and chemical ignition delay times, but the physical process is remarkably less sensitive to the oxygen concentration compared to the chemical process. This indicates that the oxygen dilution rarely affects the physical processes such as atomization, mixing, and evaporation. Mayo et al. and Kang et al. also found similar observation from diesel and jet fuel experiments [47, 56].

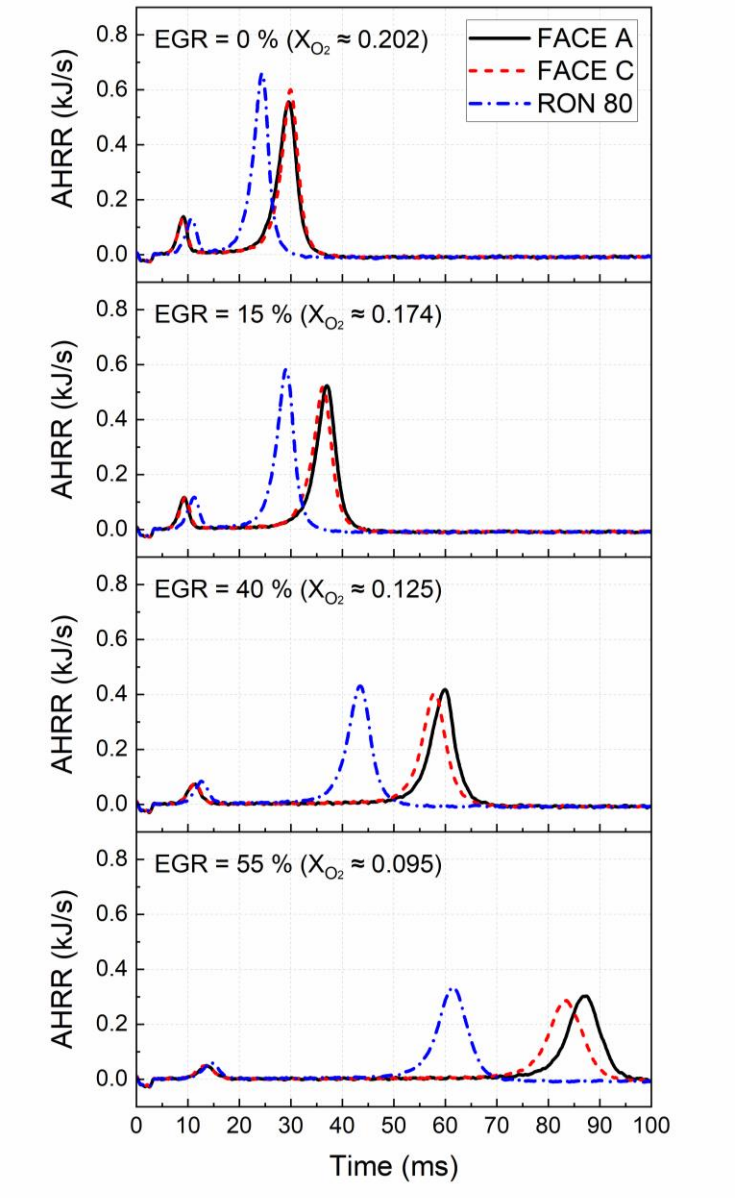

Figure 5-12 Apparent heat release rate for higher RON fuels at X_{O_2} ≈ 0.202, 0.174, 0.125, 0.095 and T_c = 600ºC.

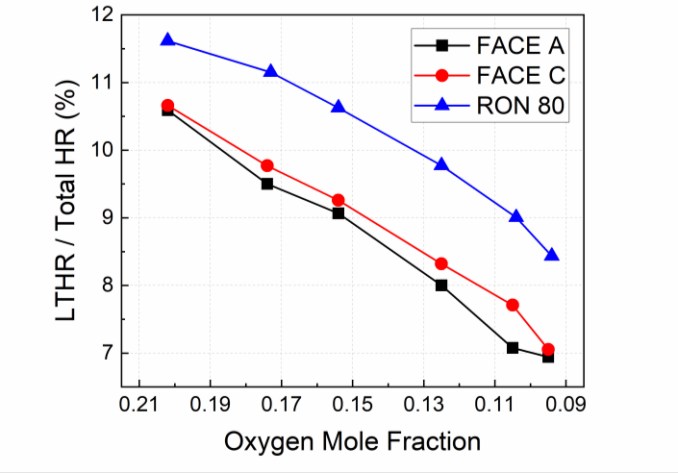

Figure 5-13 LTHR intensity as a function of ambient oxygen mole fraction for higher RON fuels at T_c = 600ºC.

As discussed above for the RON 80 fuel, the lower volatility and higher density lead to a longer physical ignition delay while the higher amount of LTHR results in a shorter chemical ignition delay compared to the FACE gasolines. This trend is not changed under the oxygen diluted conditions. Both the FACE A and C gasolines also show almost identical physical ignition delay times across the test conditions. As the oxygen concentration decreases, however, the gas-phase ignition of FACE A gasoline is more delayed than the FACE C gasoline. This phenomenon can be clearly shown in the AHRR profiles from Figure 5-12. The main heat release event of FACE A gasoline is more retarded than that of FACE C gasoline as the oxygen concentration decreases. As can be seen in Figure 5-13, this is mainly due to the more reduced LTHR intensity of FACE A gasoline which possesses less n-alkane content compared to the FACE C gasoline. This indicates that the fuel with higher amount of n-alkane is less sensitive to the oxygen dilution when the RON and MON are constant. This finding is similar to the greater EGR tolerance of fuels with higher n-alkane content when the DCN is constant [56, 100].

The effect of oxygen dilution on low temperature oxidation has been studied in depth including this author's research works in Chapter 4, which concluded that oxygen dilution significantly suppresses LTHR [26, 103]. Unlike the ambient temperature sweep, the insensitivity of the physical processes and reduced LTHR with the oxygen dilution considerably increases the NTC period as observed in Figure 5-13.

5.3.2 Lower RON Fuels

This section discusses the differences of liquid to gas-phase transition and chemical kinetics of high reactivity gasolines using the motored engine and the constant volume combustion chamber. Figures 5-14 to 5-18 show the autoignition behavior of homogenous mixtures of FACE I, J, RON 70 and 60 fuels at ϕ = 0.25 and 0.5 in the motored engine. From Figure 5-14, where the CO emissions are shown as a function of CR at both naturally aspirated and boosted conditions, the lower RON fuels produce much more CO emissions during pre-ignition than the higher RON fuels, from the above section, due to their higher mass percentage of long chain n-alkanes such as n-heptane and n-octane.

The RON 60 fuel, which is the most reactive fuel among all the test fuels, shows the earliest onset of low and high temperature reactions and final autoignition, as can be seen through the experimental results of CO emissions, maximum in-cylinder gas temperature, and CCR from Figures 5-14, 5-15 and 5-16. At P_{int} = 1 bar from Figure 5-14, one of interesting observations is that the FACE J and RON 70 fuels, which contain considerable aromatic content, begin the low temperature reaction at higher CR than the

FACE I gasoline even though they consist of a higher amount of n-alkanes. This behavior also can be observed for the RON 80 fuel from the CR sweep test in Figure 5-3. The possible reason is that the radical scavenging effect of aromatics, which can reduce the chain-propagation reactions, retard the onset of low temperature reaction.

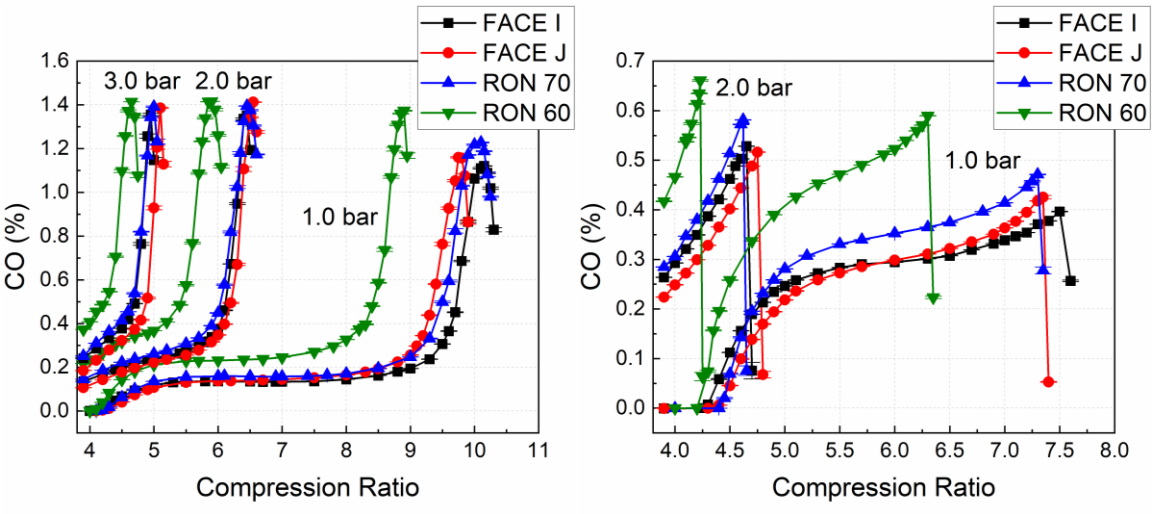

(a) ϕ = 0.25 (b) ϕ = 0.5

Figure 5-14 Carbon monoxide emissions as a function of CR for lower RON fuels at T_{int} = 190ºC and X_{O2} = 0.21.

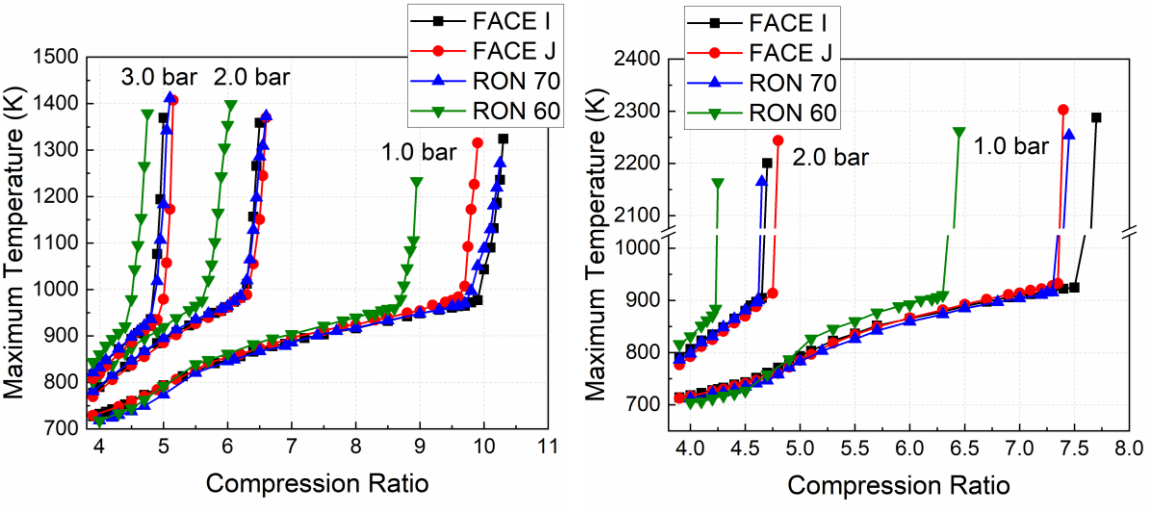

(a) ϕ = 0.25 (b) ϕ = 0.5

Figure 5-15 Maximum in-cylinder bulk temperature as a function of CR for lower RON fuels at T_{int} = 190ºC and X_{O2} = 0.21.

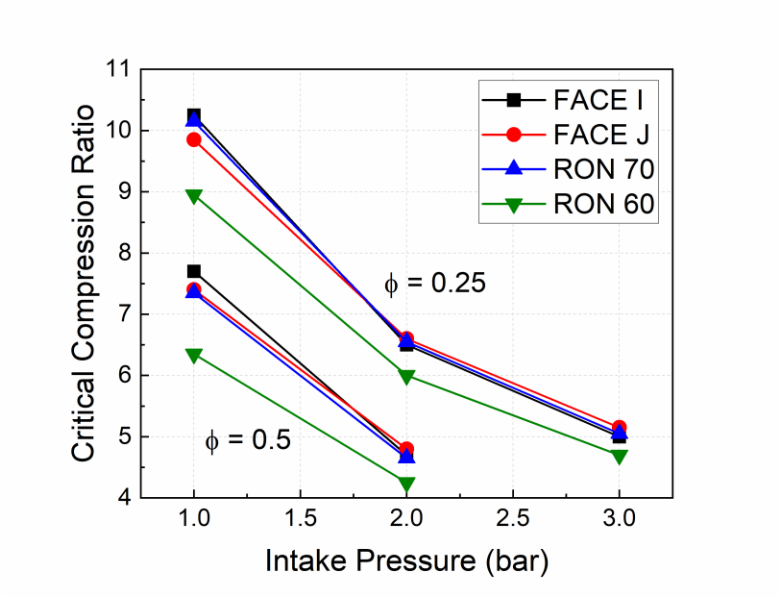

Figure 5-16 Critical compression ratio as a function of intake pressure for lower RON fuels at T_{int} = 190ºC and X_{O2} = 0.21.

It is also interesting to note that the fuel reactivity trend is reversed as the intake pressure increases. The FACE I gasoline, which has almost zero octane sensitivity, becomes more reactive at higher intake pressure than the FACE J and RON 70 fuels which represent mild octane sensitivity. The earlier hot ignition timing and lower CCR of the FACE I gasoline at boosted pressure can be observed in Figure 5-15 and 5-16. Szybist et al. found that a fuel with lower octane sensitivity was the most knock resistant at low load whereas a fuel with higher octane sensitivity was the most knock resistant at high load [67]. Zhang et al. and Vallinayagam et al. also observed that increasing octane sensitivity enhanced fuel reactivity and reduced ignition delay at conditions similar to the MON test [73, 134]. Figures 5-17 and 5-18, where the AHRR is shown as a function of crank angle during ITHR period at both equivalence ratios, explain the reason for this phenomenon. As the intake pressure increases, the LTHR of FACE I gasoline more rapidly increases compared to the higher octane sensitivity fuels, leading to early start of

ITHR, even though the FACE I gasoline contains least amount of n-alkanes. The FACE J gasoline, which contains the highest aromatic content, is most reactive at atmospheric intake pressure and becomes least reactive at the boosted conditions due to the suppression of low temperature reaction by aromatics.

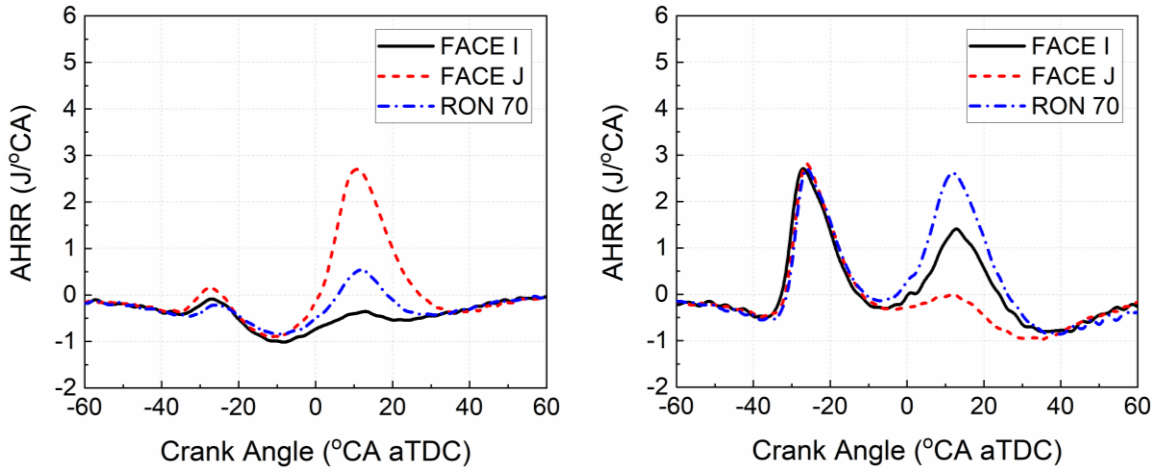

(a) P_{int} = 1.0 bar, CR = 9.6

(b) P_{int} = 2.0 bar, CR = 6.2

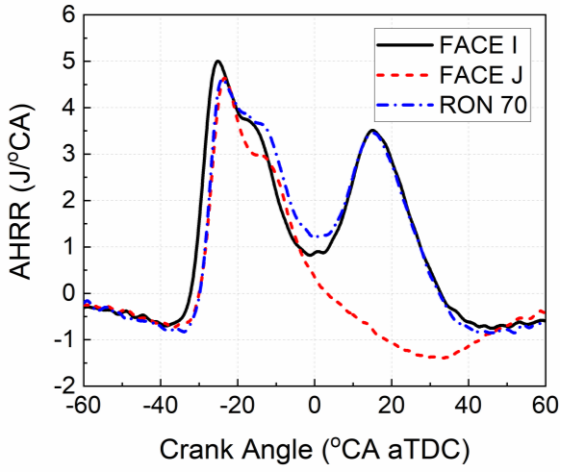

(c) P_{int} = 3.0 bar, CR = 4.8

Figure 5-17 Apparent heat release rate as a function of crank angle for lower RON fuels at X_{O2} = 0.21 and ϕ = 0.25.

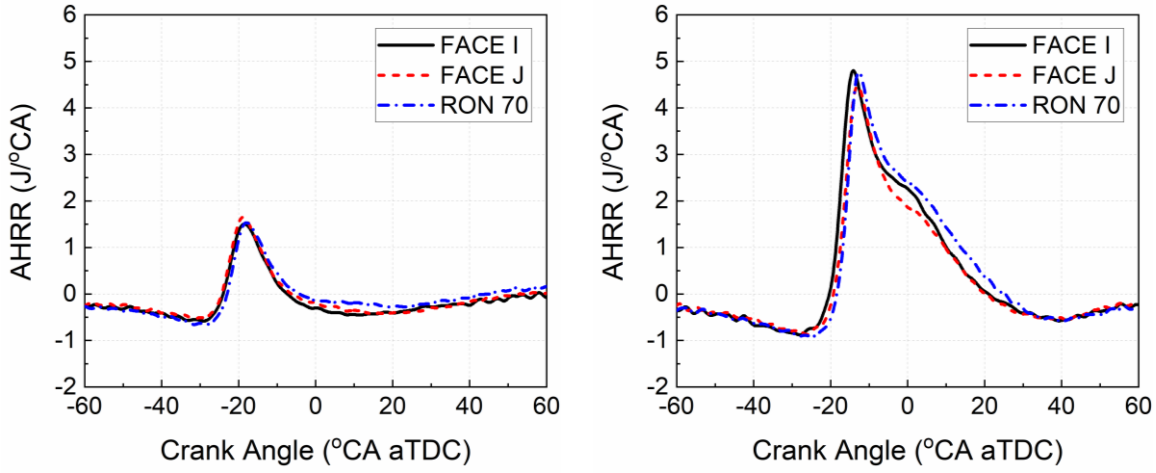

(a) P_{int} = 1.0 bar, CR = 7.3 (b) P_{int} = 2.0 bar, CR = 4.6

Figure 5-18 Apparent heat release rate as a function of crank angle for lower RON fuels at X_{O_2} = 0.21 and ϕ = 0.5.

The physical, chemical, and total ignition delay as a function of initial chamber temperature for the lower RON fuels are plotted in Figure 5-19. Consistent with the results from the higher RON fuels, the physical property effects on ignition process are more important at lower temperature.

The higher aromatic content increases the liquid fuel density and the final boiling temperature as observed in Table 5-1 and Figure 5-2. Therefore, the FACE J and RON 70 fuels, which consist of more than 20 vol. % of aromatics, produce longer physical ignition delay than the FACE I and RON 60 fuels with lower aromatic content, as a result of an extend atomization and evaporation process.

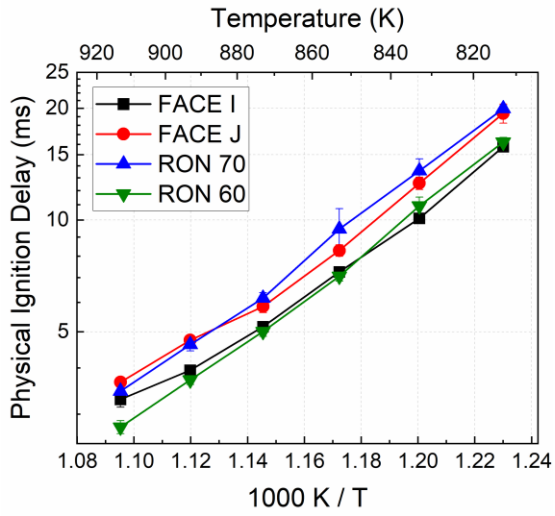

(a) Physical ignition delay

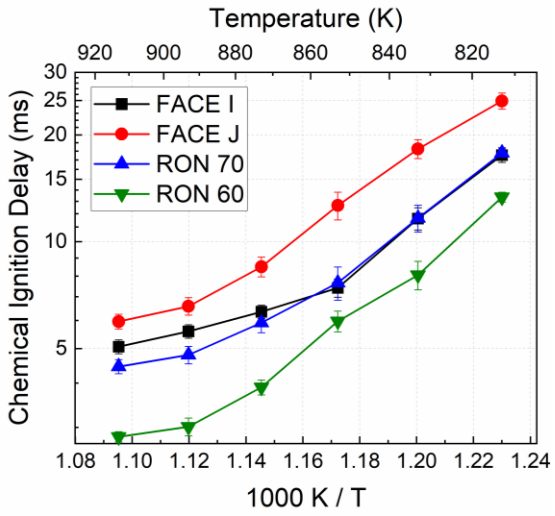

(b) Chemical ignition delay

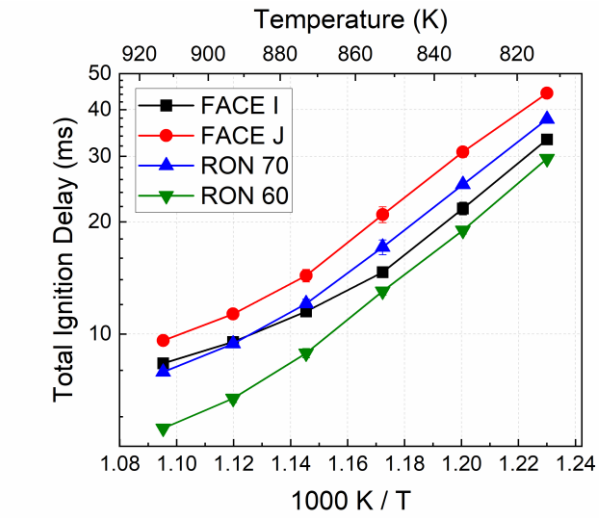

(c) Total ignition delay

Figure 5-19 Physical, chemical, and total ignition delay as a function of ambient temperature for lower RON fuels at X_{O2} = 0.202.

The Arrhenius plots of chemical ignition delay for all the lower RON fuels reveal the NTC behavior despite the narrow temperature range (813 – 913 K) explored in this study. The almost zero aromatic content of FACE I gasoline leads to very distinct NTC behavior at lower ambient air temperature compared to the other test fuels. Thus, the

chemical ignition process of FACE I gasoline becomes less sensitive to the ambient temperature above 853 K. The RON 60 gasoline, the highest reactivity fuel, has the shortest chemical ignition delay time whereas the highest aromatic content FACE J gasoline shows the slowest gas-phase ignition at the current temperature conditions at P_c = 20 bar.

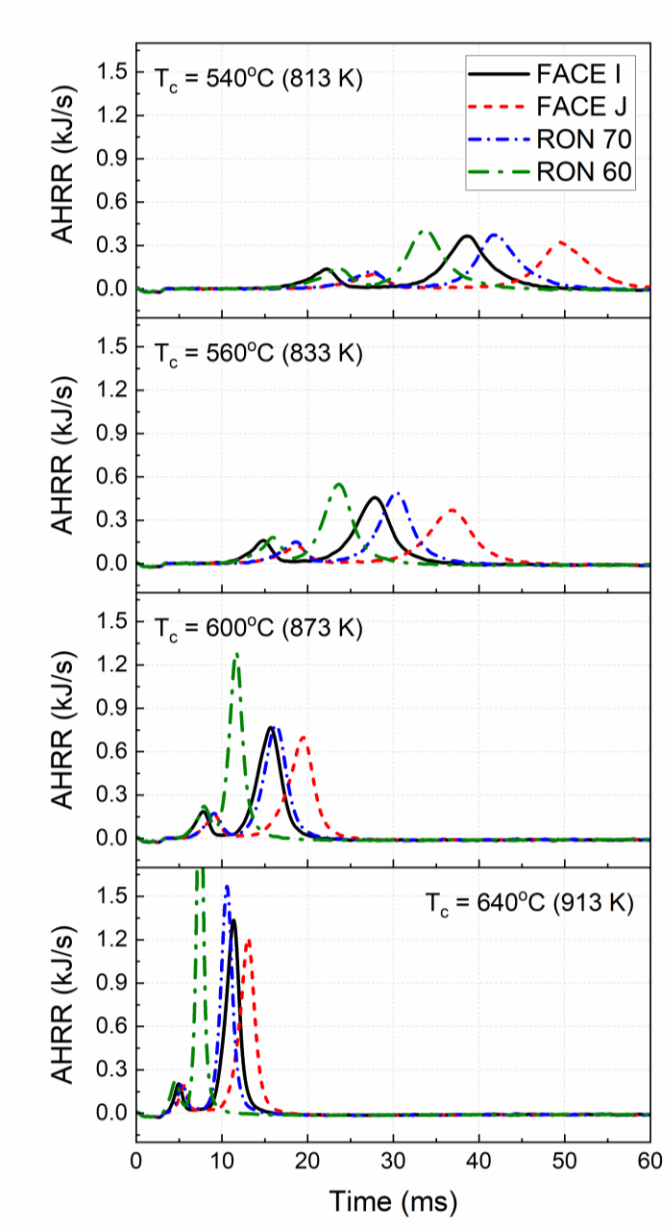

Figure 5-20 Apparent heat release rate for lower RON fuels at T_c = 540, 560, 600, 640ºC and X_{O2} = 0.202.

Figure 5-20 presents the AHRR at selected ambient air temperature for the lower RON fuels. It is observed that both the low and main heat release events are significantly advanced as the temperature increases. However, the alkane-rich FACE I gasoline shows a slower pace of main heat release advancement compared to the high aromatic content fuels, resulting in the reversed ignition delay trend as can be seen in Figure 5-19. Figure 5-21 shows the LTHR contribution to the total heat release as a function of ambient air temperature. This LTHR result can explain the reversed ignition delay trend of the fuels with similar RON. The LTHR of FACE I gasoline more rapidly decreases with increasing the temperature than the FACE J and RON 70 fuels. This leads to a relatively longer NTC period and consequently results in later combustion phasing for FACE I gasoline. In conclusion, the LTHR of lower octane sensitivity fuel more rapidly increases with initial chamber pressure and decreases with initial chamber temperature than that of higher octane sensitivity fuel.

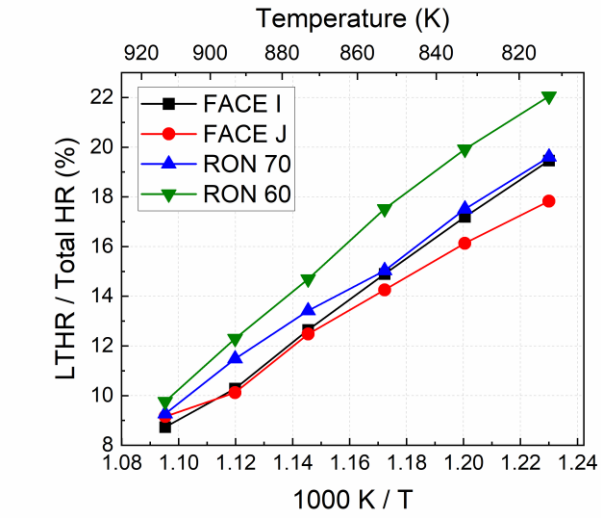

Figure 5-21 LTHR intensity as a function of ambient temperature for lower RON fuels at X_{O2} = 0.202.

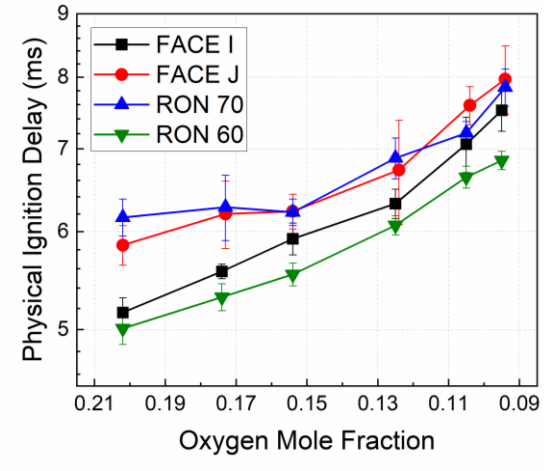

(a) Physical ignition delay

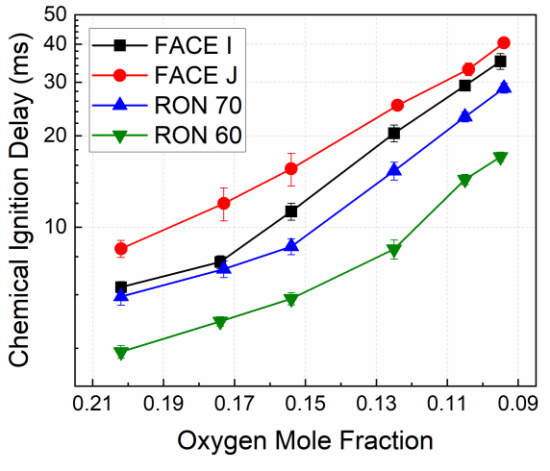

(b) Chemical ignition delay

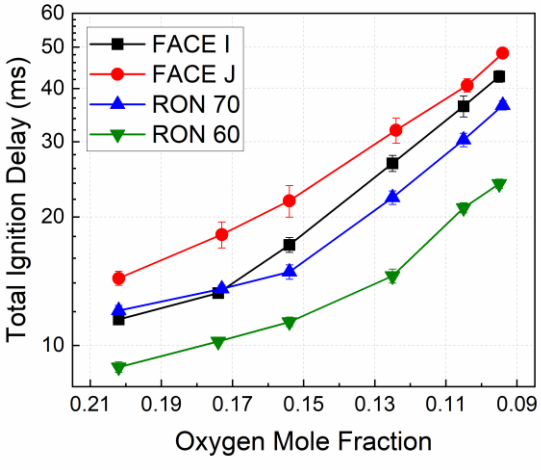

(c) Total ignition delay

Figure 5-22 Physical, chemical, and total ignition delay as a function of ambient oxygen mole fraction for lower RON fuels at T_c = 600ºC.

Figure 5-22 shows the physical, chemical, and total ignition delay times as a function of ambient oxygen mole fraction for the lower RON fuels at T_c = 600ºC. Consistent with the results from the tests of higher RON fuels, the oxygen dilution does not significantly affect the physical ignition delay. For the chemical process, the FACE I gasoline still shows different behavior from the other high aromatic content fuels during

the oxygen concentration sweep. The changes in ambient oxygen levels have a much greater effect on the chemical ignition delay of the low aromatic content fuel, suggesting that the fuel with high aromatic content can tolerate reduced oxygen condition.

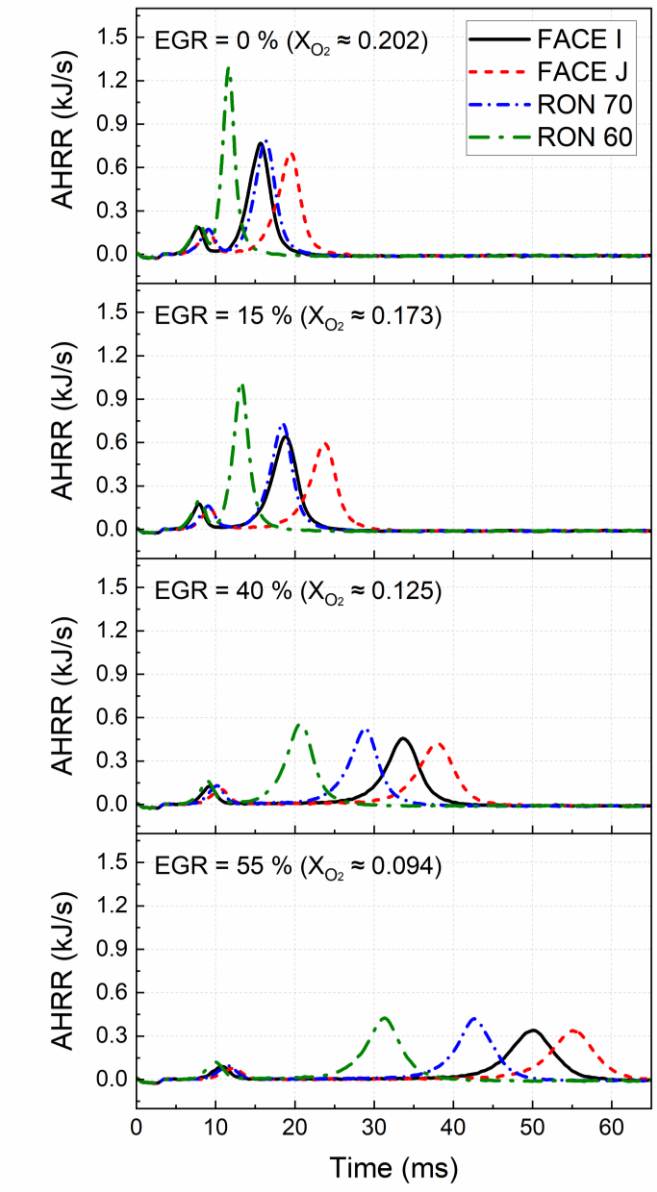

Figure 5-23 Apparent heat release rate for lower RON fuels at X_{O2} ≈ 0.202, 0.174, 0.125, 0.095 and T_c = 600ºC.

Figure 5-23 presents the AHRR results for each lower RON fuel with various simulated EGR conditions. The main heat release rate phasing of FACE I gasoline is almost identical with that of RON 70 fuel under the standard 20.2 vol. % oxygen condition. However, the phasing of FACE I gasoline is more retarded as less ambient oxygen is available. The comparison of LTHR intensity during oxygen concentration sweep is shown in Figure 5-24. The RON 70 fuel exhibits much higher LTHR intensity than the FACE I gasoline, but there is no visible difference in the trend between these two fuels. From Chapters 3 and 4, it was concluded that the oxygen dilution enormously influences the ITHR behavior as well as the LTHR characteristics. The amount of ITHR for lower octane sensitivity fuel more steeply decreases than for higher octane sensitivity fuel with the addition of simulated EGR, leading to greater dependence of gas-phase ignition on oxygen dilution for the FACE I gasoline.

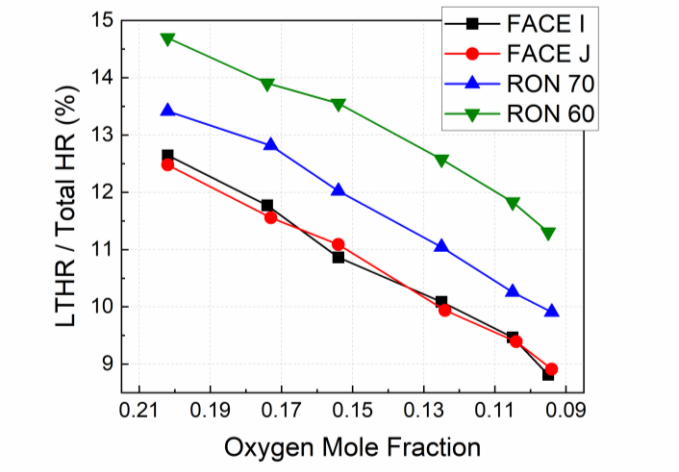

Figure 5-24 LTHR intensity as a function of ambient oxygen mole fraction for lower RON fuels at T_c = 600ºC.

5.4 Conclusion

In order to investigate impacts of fuel physical properties and chemical composition on GCI, FACE A, C, I, and J gasolines and three naphtha blends with RON from 60 to 80 were tested in an HCCI engine and a constant volume combustion chamber through sweeps of pressure, temperature, and oxygen concentration. This study provides a fundamental investigation of autoignition behavior and physical and chemical ignition delay through the comparison of fuels with similar octane number under the condition at which low temperature reactivity is active. Significant findings are as follow:

Physical property effects

- Higher aromatic content leads to lower volatility and higher density, resulting in slower liquid fuel vaporization process. These physical properties become increasingly important as the ambient air temperature decreases.
- Decreasing the air temperature from 640 K to 540 K significantly increases the physical ignition delay time by more than 300% whereas the oxygen dilution from 0.202 to 0.095 rarely increases the physical ignition delay time by less than 47%.
- Both the FACE A and C gasolines show almost identical physical ignition delay during the temperature and oxygen mole fraction sweeps.

Chemical composition effects

- For the same RON, the fuels with higher amount of aromatics, the FACE J and RON 70 fuels, are more resistant to autoignition than the alkane-rich FACE I gasolines at boosted intake pressure.

- For the same RON, the fuels with higher amount of aromatics, the FACE J and RON 70 fuels, are less sensitive to the oxygen dilution.
- For the same RON, the alkane-rich fuel, the FACE I gasoline, is less sensitive to the temperature due to pronounced NTC behavior.
- For the same RON and octane sensitivity, the fuel with higher amount of n-alkane, the FACE C gasoline, is less sensitive to the oxygen dilution than the FACE A gasoline. Both the FACE A and C gasolines show similar ignition behavior during the ambient temperature sweep, but the gas-phase ignition of FACE A gasoline is more delayed than the FACE C gasoline as the ambient oxygen concentration decreases due to more reduced LTHR intensity.
- The FACE I gasoline is much more reactive than the higher octane sensitivity FACE J gasoline at the conditions where low temperature reaction is active.

Chapter 6

Conclusions and Recommendations

6.1 Summary of Dissertation

This dissertation investigated the effects of chemical composition on autoignition behavior in a motored engine and a constant volume combustion chamber. A total of eleven full boiling range gasolines with different octane number and sensitivity have been tested at various pressures, temperatures, and oxygen concentrations. Summaries of these studies are presented as follows.

In Chapter 3, influence of ITHR on autoignition reactivity of single-stage ignition fuels with varying octane sensitivity was investigated in a motored engine. Four full boiling range gasolines with RON of 92 and octane sensitivity range of 0.5 to 11.3 were tested through sweeps of intake temperature, intake oxygen mole fraction, and fuel loading. This study provided a new understanding of ITHR behavior depending on octane sensitivity and its effects on autoignition reactivity of single-stage ignition fuels under various engine operating conditions. Combustion phasing comparisons of the fuels showed that the relative reactivity of lower octane sensitivity fuel increased at lower intake temperature and lower EGR ratio conditions, whereas the relative reactivity of higher octane

sensitivity fuel increased at higher intake temperature and higher EGR ratio conditions. For all of the single-stage ignition fuels that were tested, the amount of ITHR increased in the range of 2% to 7% of total heat release as the intake temperature and the intake oxygen mole fraction increased. These ITHR trends, depending on octane sensitivity, were almost identical with the trends of combustion phasing, showing that ITHR significantly affects fuel autoignition reactivity and determines octane sensitivity. In addition, the strong dependence of ITHR on equivalence ratio enhanced the ϕ-sensitivity. For the similar combustion phasing, the S11.3 and the S8.7 which were the higher octane sensitivity fuels exhibited faster rise rates of ITHR intensity than the S0.5 and the S4.8 respectively, leading to more advanced hot-ignition phasing with increasing equivalence ratio.

In Chapter 4, effects of octane number, pressure, and EGR on low and intermediate temperature heat release of two-stage ignition fuels were explored in the motored engine. Three high reactivity gasoline-like fuels with RON range of 60 to 80 were investigated through CR sweeps to characterize low and intermediate temperature oxidation behavior under various engine operating conditions. This study provided a new understanding of the correlation between LTHR and ITHR as well as the individual effects of pressure and oxygen mole fraction on ITHR. The experimental results showed that LTHR significantly enhanced ITHR, eventually advancing the autoignition timing. As the intake oxygen mole fraction decreased from 0.21 to 0.14, the LTHR and the ITHR of RON 60 were suppressed by 30% and 38%, respectively. The intake boosting from atmospheric pressure to 1.4 bar absolute increased the LTHR by 49% even at a constant fuel loading. For all the test fuels, the average ITHR per crank angle also increased with

the intake pressure, showing concise and strong intermediate temperature reaction. However, the magnitude of ITHR for the lower RON fuel, which exhibited a great amount of ITHR, became saturated as the intake pressure increased.

Finally, in Chapter 5, effects of physical properties and chemical composition on autoignition behavior of FACE A, C, I, and J gasolines and three naphtha blends with RON range of 60 to 80 were investigated in the motored engine and a constant volume combustion chamber. This study provided a fundamental investigation of autoignition behavior and physical and chemical ignition delay through sweeps of pressure, temperature, and oxygen concentration under the condition at which low temperature reactivity was active. With regard to physical properties, higher aromatic content led to lower volatility and higher density, resulting in slower liquid fuel evaporation process. Decreasing the air temperature from 640 K to 540 K significantly increased the physical ignition delay time by more than 300% whereas the oxygen dilution from 0.202 to 0.095 rarely increased the physical ignition delay time by less than 47%. This concluded that the physical ignition delay was very sensitive to the ambient air temperature whereas the oxygen dilution rarely affected the physical ignition delay. With regard to chemical properties at the same RON, the higher aromatic content fuels, the FACE J and RON 70 fuels, were more resistant to autoignition at boosted pressure and less sensitive to the oxygen dilution whereas the alkane-rich fuel, FACE I gasolines, was less sensitive to the temperature due to pronounced NTC behavior. For the same RON and octane sensitivity, the fuel with higher amount of n-alkane, the FACE C gasoline, was less sensitive to the oxygen dilution than the FACE A gasoline. Both the FACE A and C gasolines showed similar ignition behavior during the ambient temperature sweep, but the gas-phase

ignition of FACE A gasoline was more delayed than the FACE C gasoline as the ambient oxygen concentration decreased due to more reduced LTHR intensity.

6.2 Recommendations for Future Work

This work has been focused on one aspect of GCI combustion control, i.e., fuel autoignition kinetics. Another aspect of the control technique is fuel stratification using injection strategies. The fuel stratification can provide fast control of combustion phasing in GCI engines [160]. The number of direct injections, the injection timing, and the fuel-fraction split ratio between injections significantly affect the fuel stratification, eventually controlling the main combustion event. Therefore, it would be worthwhile to investigate the effect of fuel stratification on autoignition behavior and combustion performance of various reactivity fuels.

Another potential topic is to extend the current study to consider the effect of charge cooling on autoignition reactivity. The modified CFR engine with an upstream, pre-vaporized fuel injection system used in this study is an optimum experimental device for studying autoignition characteristics driven by chemical kinetic of fuels over a wide range of pressures, temperatures, and oxygen mole fractions. However, heat of vaporization (HoV) charge cooling has a significant effect on autoignition behavior especially for high ethanol content fuels [161, 162]. This charge cooling effect is important for engines with a direct fuel injection system. In order to study both the chemical and charge cooling effects, it is recommended to apply an additional port fuel or direct injection system to the engine.

Appendix

A. Detailed Hydrocarbon Analysis (DHA) of Test Fuels

Table A-1 DHA for RON 60 (> 0.1 mol%)

Group	Component	Wgt%	Vol%	Mol%
Paraffin	n-Butane	1.452	1.78	2.396
	n-Pentane	4.884	5.535	6.495
	n-Hexane	8.506	9.153	9.469
	n-Heptane	8.759	9.091	8.387
	n-Octane	7.023	7.094	5.898
	n-Nonane	0.394	0.39	0.295
I-Paraffins	i-Pentane	3.088	3.536	4.106
	2,2-Dimethylbutane	0.227	0.248	0.252
	2,3-Dimethylbutane	0.643	0.69	0.716
	2-Methylpentane	4.818	5.235	5.364
	3-Methylpentane	3.047	3.254	3.392
	2,4-Dimethylpentane	0.555	0.586	0.532
	3,3-Dimethylpentane	0.185	0.19	0.177
	2-Methylhexane	4.73	4.946	4.528
	3-Methylhexane	3.569	3.686	3.417
	2,2-Dimethylhexane	0.195	0.199	0.164
	2,5-Dimethylhexane	0.565	0.578	0.475
	2,4-Dimethylhexane	0.683	0.692	0.574
	3,3-Dimethylhexane	0.208	0.208	0.175
	2,3-Dimethylhexane	0.387	0.386	0.325
	2-Methylheptane	3.478	3.537	2.921
	4-Methylheptane	1.177	1.185	0.989

	3-Methylheptane	2.734	2.749	2.296
	3-Ethylhexane	1.091	1.085	0.917
	2,4-Dimethylheptane	0.48	0.479	0.359
	2,6-Dimethylheptane	0.929	0.93	0.695
	2,5-Dimethylheptane	1.097	1.089	0.821
	4-Methyloctane	0.599	0.59	0.448
	2-Methyloctane	0.667	0.663	0.499
	3-Methyloctane	0.612	0.603	0.458
Mono-Aromatics	Benzene	0.893	0.721	1.097
	Toluene	4.708	3.853	4.902
	Ethylbenzene	0.461	0.377	0.417
	m-Xylene	3.531	2.899	3.191
	p-Xylene	1.55	1.277	1.401
	o-Xylene	0.872	0.703	0.788
Mono-Naphthenes	Cyclopentane	0.297	0.283	0.406
	Methylcyclopentane	2.205	2.091	2.514
	Cyclohexane	2.639	2.405	3.008
	1t,3-Dimethylcyclopentane	0.449	0.426	0.439
	1c,3-Dimethylcyclopentane	0.43	0.409	0.42
	1t,2-Dimethylcyclopentane	0.875	0.826	0.855
	Methylcyclohexane	6.101	5.627	5.961
	1,1,3-Trimethylcyclopentane	0.269	0.255	0.23
	Ethylcyclopentane	0.19	0.176	0.186
	1c,2t,4-Trimethylcyclopentane	0.273	0.254	0.233
	1t,2c,3-Trimethylcyclopentane	0.21	0.194	0.18
	1,3-dimethyl-t-cyclohexane	1.636	1.507	1.399
	Ethylcyclohexane	1.206	1.091	1.031
	1c,2t,4t-Trimethylcyclohexane	0.155	0.141	0.118
Iso-Olefins	3-Heptene, 4-methyl-	0.56	0.52	0.479

Table A-2 DHA for RON 70 (> 0.1 mol%)

Group	Component	Wgt%	Vol%	Mol%
Paraffin	n-Butane	0.578	0.712	0.923
	n-Pentane	6.526	7.436	8.401
	n-Hexane	6.596	7.137	7.109
	n-Heptane	6.148	6.417	5.699
	n-Octane	4.452	4.522	3.62
	n-Nonane	0.333	0.331	0.241
	n-Decane	0.217	0.212	0.142
I-Paraffins	i-Pentane	7.236	8.333	9.315
	2,2-Dimethylbutane	1.304	1.433	1.405
	2,3-Dimethylbutane	0.736	0.794	0.794
	2-Methylpentane	4.063	4.438	4.378
	3-Methylpentane	2.51	2.696	2.705
	2,4-Dimethylpentane	0.554	0.587	0.513
	3,3-Dimethylpentane	0.136	0.14	0.126
	2-Methylhexane	3.454	3.632	3.201
	3-Methylhexane	2.521	2.618	2.337
	2,2,4-Trimethylpentane	1.358	1.401	1.104
	2,2-Dimethylhexane	0.136	0.14	0.111
	2,5-Dimethylhexane	0.571	0.588	0.464
	2,4-Dimethylhexane	0.617	0.629	0.502
	3,3-Dimethylhexane	0.139	0.14	0.113
	2,3,4-Trimethylpentane	0.557	0.552	0.453
	2,3-Dimethylhexane	0.416	0.416	0.338
	2-Methylheptane	2.262	2.312	1.839
	4-Methylheptane	0.857	0.868	0.697
	3-Methylheptane	1.873	1.893	1.523
	3-Ethylhexane	0.729	0.729	0.593
	2,2,5-Trimethylhexane	0.3	0.302	0.217
	2,4-Dimethylheptane	0.309	0.31	0.224
	2,6-Dimethylheptane	0.577	0.581	0.418
	2,5-Dimethylheptane	0.71	0.709	0.514
	4-Methyloctane	0.375	0.372	0.272
	2-Methyloctane	0.424	0.424	0.307
	3-Methyloctane	0.39	0.386	0.282
Mono-Aromatics	Benzene	0.653	0.53	0.776
	Toluene	9.976	8.21	10.055
	Ethylbenzene	0.287	0.236	0.251
	m-Xylene	2.251	1.858	1.969

	p-Xylene	0.821	0.68	0.718
	o-Xylene	0.7	0.568	0.613
	n-Propylbenzene	0.18	0.149	0.139
	1-Methyl-3-ethylbenzene	0.47	0.388	0.363
	1-Methyl-4-ethylbenzene	0.217	0.18	0.168
	1,3,5-Trimethylbenzene	0.266	0.219	0.205
	1-Methyl-2-ethylbenzene	0.197	0.16	0.152
	1,2,4-Trimethylbenzene	0.837	0.682	0.647
	1,2,3-Trimethylbenzene	0.191	0.153	0.148
Mono-Naphthenes	Cyclopentane	2.848	2.726	3.771
	Methylcyclopentane	1.656	1.579	1.828
	Cyclohexane	2.616	2.398	2.887
	1t,3-Dimethylcyclopentane	0.321	0.305	0.303
	1c,3-Dimethylcyclopentane	0.305	0.293	0.289
	1t,2-Dimethylcyclopentane	0.621	0.59	0.588
	Methylcyclohexane	4.26	3.951	4.03
	1,1,3-Trimethylcyclopentane	0.183	0.175	0.152
	Ethylcyclopentane	0.134	0.125	0.127
	1c,2t,4-Trimethylcyclopentane	0.184	0.172	0.152
	1t,2c,3-Trimethylcyclopentane	0.141	0.131	0.117
	1,3-dimethyl-t-cyclohexane	1.022	0.947	0.846
	1c,4-Dimethylcyclohexane	0.316	0.288	0.262
	Ethylcyclohexane	0.76	0.692	0.629
n-Olefins	Hexene-1	2.619	2.756	2.89
Iso-Olefins	3-Heptene, 4-methyl-	0.369	0.344	0.306

Table A-3 DHA for RON 80 (> 0.1 mol%)

Group	Component	Wgt%	Vol%	Mol%
Paraffin	n-Butane	0.608	0.758	0.954
	n-Pentane	5.665	6.523	7.16
	n-Hexane	4.455	4.872	4.714
	n-Heptane	4.043	4.264	3.679
	n-Octane	2.613	2.683	2.086
	n-Nonane	0.369	0.371	0.262
	n-Decane	0.424	0.419	0.272
I-Paraffins	i-Pentane	10.104	11.76	12.771
	2,2-Dimethylbutane	2.29	2.544	2.423
	2,3-Dimethylbutane	0.745	0.812	0.788
	2-Methylpentane	2.876	3.176	3.044
	3-Methylpentane	1.759	1.909	1.861
	2,4-Dimethylpentane	0.542	0.581	0.494
	2-Methylhexane	2.291	2.435	2.085
	3-Methylhexane	1.6	1.679	1.456
	2,2,4-Trimethylpentane	2.634	2.745	2.103
	2,2,3-Trimethylpentane	0.202	0.204	0.161
	2,5-Dimethylhexane	0.597	0.62	0.476
	2,4-Dimethylhexane	0.586	0.604	0.468
	2,3,4-Trimethylpentane	1.069	1.072	0.853
	2,3-Dimethylhexane	0.42	0.425	0.335
	2-Methylheptane	1.331	1.375	1.062
	4-Methylheptane	0.488	0.499	0.39
	3-Methylheptane	1.106	1.131	0.883
	3-Ethylhexane	0.437	0.442	0.349
	2,2,5-Trimethylhexane	0.479	0.488	0.34
	2,4-Dimethylheptane	0.185	0.188	0.131
	2,6-Dimethylheptane	0.339	0.345	0.241
	2,5-Dimethylheptane	0.433	0.436	0.308
	4-Methyloctane	0.24	0.241	0.171
	2-Methyloctane	0.277	0.28	0.197
	3-Methyloctane	0.264	0.264	0.187
Mono-Aromatics	Benzene	0.379	0.311	0.443
	Toluene	15.208	12.649	15.052
	Ethylbenzene	0.17	0.142	0.146
	m-Xylene	1.305	1.089	1.121
	p-Xylene	0.477	0.4	0.41
	o-Xylene	0.605	0.496	0.52

	n-Propylbenzene	0.351	0.293	0.266
	1-Methyl-3-ethylbenzene	0.918	0.766	0.697
	1-Methyl-4-ethylbenzene	0.427	0.358	0.324
	1,3,5-Trimethylbenzene	0.519	0.433	0.394
	1-Methyl-2-ethylbenzene	0.385	0.316	0.292
	1,2,4-Trimethylbenzene	1.636	1.347	1.241
	1,2,3-Trimethylbenzene	0.379	0.306	0.288
	1-Methyl-3-n-propylbenzene	0.218	0.183	0.148
Naphthalenes	2-Methylnaphthalene	0.198	0.14	0.126
Mono-Naphthenes	Cyclopentane	5.271	5.099	6.853
	Methylcyclopentane	1.013	0.976	1.098
	Cyclohexane	2.551	2.363	2.764
	1t,3-Dimethylcyclopentane	0.193	0.186	0.179
	1c,3-Dimethylcyclopentane	0.183	0.177	0.17
	1t,2-Dimethylcyclopentane	0.379	0.364	0.352
	Methylcyclohexane	2.553	2.393	2.371
	1,3-dimethyl-t-cyclohexane	0.604	0.565	0.491
	Ethylcyclohexane	0.45	0.414	0.366
n-Olefins	Hexene-1	5.181	5.511	5.615

Bibliography

[1] "International Energy Outlook 2019," *U.S. Energy Information Administration (EIA)*, 2019.

[2] "Outlook for Energy: A perspective to 2040," *ExxonMobil*, 2019.

[3] "Transport IPCC WGIII Fifth Assessment Report," *IPCC*, 2014.

[4] H. Ritchie and M. Roser, "CO_2 and Greenhouse Gas Emissions," *https://ourworldindata.org*, 2020.

[5] "The death of the internal combustion engine," ed: The Economist, 2017.

[6] G. Kalghatgi, "Is it really the end of internal combustion engines and petroleum in transport?," *Applied Energy*, vol. 225, pp. 965-974, 2018, doi: 10.1016/j.apenergy.2018.05.076.

[7] "World Energy Council. Global transport scenarios 2050," *World Energy Council*, 2011.

[8] "World Oil Outlook," *OPEC*, 2019.

[9] G. Kalghatgi and B. Johansson, "Gasoline compression ignition approach to efficient, clean and affordable future engines," *Proceedings of the Institution of Mechanical Engineers, Part D: Journal of Automobile Engineering*, vol. 232, no. 1, pp. 118-138, 2017, doi: 10.1177/0954407017694275.

[10] Z. Lu *et al.*, "Well-to-Wheels Analysis of the Greenhouse Gas Emissions and Energy Use of Vehicles with Gasoline Compression Ignition Engines on Low Octane Gasoline-Like Fuel," *SAE International Journal of Fuels and Lubricants*, vol. 9, no. 3, pp. 527-545, 2016, doi: 10.4271/2016-01-2208.

[11] J. P. Szybist, A. L. Boehman, D. C. Haworth, and H. Koga, "Premixed ignition behavior of alternative diesel fuel-relevant compounds in a motored engine experiment," *Combustion and Flame,* vol. 149, no. 1-2, pp. 112-128, 2007, doi: 10.1016/j.combustflame.2006.12.011.

[12] Y. Yang and A. L. Boehman, "Experimental study of cyclohexane and methylcyclohexane oxidation at low to intermediate temperature in a motored engine," *Proceedings of the Combustion Institute,* vol. 32, no. 1, pp. 419-426, 2009, doi: 10.1016/j.proci.2008.06.162.

[13] Y. Zhang, Y. Yang, and A. L. Boehman, "Premixed ignition behavior of C9 fatty acid esters: A motored engine study," *Combustion and Flame,* vol. 156, no. 6, pp. 1202-1213, 2009, doi: 10.1016/j.combustflame.2009.01.024.

[14] D. Kang, S. V. Bohac, A. L. Boehman, S. Cheng, Y. Yang, and M. J. Brear, "Autoignition studies of C5 isomers in a motored engine," *Proceedings of the Combustion Institute,* vol. 36, no. 3, pp. 3597-3604, 2017, doi: 10.1016/j.proci.2016.09.012.

[15] V. Kalaskar, D. Kang, and A. L. Boehman, "Impact of Fuel Composition and Intake Pressure on Lean Autoignition of Surrogate Gasoline Fuels in a CFR Engine," *Energy & Fuels,* vol. 31, no. 10, pp. 11315-11327, 2017, doi: 10.1021/acs.energyfuels.7b01157.

[16] J. Choi, "Recycled Water Injection in a Turbocharged Gasoline Engine and Detailed Effects of Water on Auto-Ignition," Ph.D. Dissertation, The University of Michigan, 2019.

[17] J. B. Heywood, *Internal Combustion Engine Fundamentals*. McGraw-Hill, 1988.

[18] "JANAF Thermochemical Tables," *United States National Bureau of Standards,* NSRDS-NBS 37, 1971.

[19] W. K. C. Jonathan W. Fox, and John B. Heywood, "A Model for Predicting Residual Gas Fraction in Spark-Ignition Engines," *SAE Technical Paper,* 1993.

[20] Y. Zhang, "Low Temperature Oxidation of Biodiesel Surrogates in a Motored Engine and the Oxidation Behavior of Soot Generated from the Combustion of a Biodiesel Surrogate in a Diffusion Flame," Ph.D. Dissertation, The Pennsylvania State University, 2010.

[21] E. A. Ortiz-Soto, G. A. Lavoie, J. B. Martz, M. S. Wooldridge, and D. N. Assanis, "Enhanced heat release analysis for advanced multi-mode combustion engine experiments," *Applied Energy,* vol. 136, pp. 465-479, 2014, doi: 10.1016/j.apenergy.2014.09.038.

[22] E. A. Ortiz-Soto, "Combustion Modeling of Spark Assisted Compression Ignition for Experimental Analysis and Engine System Simulations," Ph.D. Dissertation, The University of Michigan, 2013.

[23] J. Chang *et al.*, "New Heat Transfer Correlation for an HCCI Engine Derived from Measurements of Instantaneous Surface Heat Flux," *SAE Technical Paper,* 2004-01-2996, 2004.

[24] I. Truedsson, M. Tuner, B. Johansson, and W. Cannella, "Pressure Sensitivity of HCCI Auto-Ignition Temperature for Primary Reference Fuels," *SAE International Journal of Engines,* vol. 5, no. 3, pp. 1089-1108, 2012, doi: 10.4271/2012-01-1128.

[25] J. E. Dec and M. Sjöberg, "Isolating the Effects of Fuel Chemistry on Combustion Phasing in an HCCI Engine and the Potential of Fuel Stratification for Ignition Control," *SAE Technical Paper,* 2004-01-0557, 2004.

[26] M. Sjöberg, J. E. Dec, and W. Hwang, "Thermodynamic and Chemical Effects of EGR and Its Constituents on HCCI Autoignition," *SAE Technical Paper,* 2007-01-0207, 2007.

[27] M. Sjöberg and J. E. Dec, "Comparing late-cycle autoignition stability for single- and two-stage ignition fuels in HCCI engines," *Proceedings of the Combustion Institute,* vol. 31, no. 2, pp. 2895-2902, 2007, doi: 10.1016/j.proci.2006.08.010.

[28] W. Hwang, J. Dec, and M. Sjöberg, "Spectroscopic and chemical-kinetic analysis of the phases of HCCI autoignition and combustion for single- and two-stage ignition fuels," *Combustion and Flame,* vol. 154, no. 3, pp. 387-409, 2008, doi: 10.1016/j.combustflame.2008.03.019.

[29] Y. Yang, J. E. Dec, N. Dronniou, and M. Sjöberg, "Tailoring HCCI heat-release rates with partial fuel stratification: Comparison of two-stage and single-stage-ignition fuels," *Proceedings of the Combustion Institute,* vol. 33, no. 2, pp. 3047-3055, 2011, doi: 10.1016/j.proci.2010.06.114.

[30] J. E. Dec, Y. Yang, and N. Dronniou, "Boosted HCCI - Controlling Pressure-Rise Rates for Performance Improvements using Partial Fuel Stratification with Conventional Gasoline," *SAE International Journal of Engines,* vol. 4, no. 1, pp. 1169-1189, 2011, doi: 10.4271/2011-01-0897.

[31] J. E. Dec, Y. Yang, J. Dernotte, and C. Ji, "Effects of Gasoline Reactivity and Ethanol Content on Boosted, Premixed and Partially Stratified Low-Temperature Gasoline Combustion (LTGC)," *SAE International Journal of Engines,* vol. 8, no. 3, pp. 935-955, 2015, doi: 10.4271/2015-01-0813.

[32] D. Lopez Pintor, J. Dec, and G. Gentz, "Φ-Sensitivity for LTGC Engines: Understanding the Fundamentals and Tailoring Fuel Blends to Maximize This Property," *SAE Technical Paper,* 2019-01-0961, 2019.

[33] D. Vuilleumier *et al.*, "Intermediate temperature heat release in an HCCI engine fueled by ethanol/n-heptane mixtures: An experimental and modeling study," *Combustion and Flame,* vol. 161, no. 3, pp. 680-695, 2014, doi: 10.1016/j.combustflame.2013.10.008.

[34] Y. Yang, J. E. Dec, N. Dronniou, M. Sjöberg, and W. Cannella, "Partial Fuel Stratification to Control HCCI Heat Release Rates: Fuel Composition and Other Factors Affecting Pre-Ignition Reactions of Two-Stage Ignition Fuels," *SAE International Journal of Engines,* vol. 4, no. 1, pp. 1903-1920, 2011, doi: 10.4271/2011-01-1359.

[35] Y. Yang, J. E. Dec, N. Dronniou, and W. Cannella, "Boosted HCCI Combustion Using Low-Octane Gasoline with Fully Premixed and Partially Stratified Charges," *SAE International Journal of Engines,* vol. 5, no. 3, pp. 1075-1088, 2012, doi: 10.4271/2012-01-1120.

[36] M. Mehl, W. Pitz, M. Sarathy, Y. Yang, and J. E. Dec, "Detailed Kinetic Modeling of Conventional Gasoline at Highly Boosted Conditions and the Associated Intermediate Temperature Heat Release," *SAE Technical Paper,* 2012-01-1109, 2012.

[37] I. Truedsson, W. Cannella, B. Johansson, and M. Tuner, "Engine Speed Effect on Auto-Ignition Temperature and Low Temperature Reactions in HCCI Combustion for Primary Reference Fuels," *SAE Technical Paper,* 2014-01-2666, 2014.

[38] H. Persson, A. Hultqvist, B. Johansson, and A. Remón, "Investigation of the Early Flame Development in Spark Assisted HCCI Combustion Using High Speed Chemiluminescence Imaging," *SAE Technical Paper,* 2007-01-0212, 2007.

[39] T. Katrašnik, F. Trenc, and S. R. Oprešnik, "A New Criterion to Determine the Start of Combustion in Diesel Engines," *Journal of Engineering for Gas Turbines and Power,* vol. 128, no. 4, pp. 928-933, 2005, doi: 10.1115/1.2179471.

[40] H. J. Curran, P. Gaffuri, W. J. Pitz, C. K. Westbrook, and W. R. Leppard, "Autoignition chemistry in a motored engine: An experimental and kinetic modeling study," *Symposium (International) on Combustion,* vol. 26, no. 2, pp. 2669-2677, 1996, doi: 10.1016/S0082-0784(96)80102-0.

[41] Y. Zhang and A. L. Boehman, "Experimental study of the autoignition of C8H16O2 ethyl and methyl esters in a motored engine," *Combustion and Flame,* vol. 157, no. 3, pp. 546-555, 2010, doi: 10.1016/j.combustflame.2009.09.003.

[42] Y. Zhang and A. L. Boehman, "Oxidation of 1-butanol and a mixture of n-heptane/1-butanol in a motored engine," *Combustion and Flame,* vol. 157, no. 10, pp. 1816-1824, 2010, doi: 10.1016/j.combustflame.2010.04.017.

[43] Y. Zhang and A. L. Boehman, "Autoignition of binary fuel blends of n-heptane and C7 esters in a motored engine," *Combustion and Flame,* vol. 159, no. 4, pp. 1619-1630, 2012, doi: 10.1016/j.combustflame.2011.11.019.

[44] Y. Yang, A. L. Boehman, and J. M. Simmie, "Effects of molecular structure on oxidation reactivity of cyclic hydrocarbons: Experimental observations and conformational analysis," *Combustion and Flame,* vol. 157, no. 12, pp. 2369-2379, 2010, doi: 10.1016/j.combustflame.2010.04.015.

[45] D. Kang, S. Kirby, J. Agudelo, M. Lapuerta, K. Al-Qurashi, and A. L. Boehman, "Combined Impact of Branching and Unsaturation on the Autoignition of Binary Blends in a Motored Engine," *Energy & Fuels,* vol. 28, no. 11, pp. 7203-7215, 2014, doi: 10.1021/ef501629p.

[46] D. Kang *et al.*, "Impact of branched structures on cycloalkane ignition in a motored engine: Detailed product and conformational analyses," *Combustion and Flame,* vol. 162, no. 4, pp. 877-892, 2015, doi: 10.1016/j.combustflame.2014.09.009.

[47] D. Kang, V. Kalaskar, D. Kim, J. Martz, A. Violi, and A. Boehman, "Experimental study of autoignition characteristics of Jet-A surrogates and their validation in a motored engine and a constant-volume combustion chamber," *Fuel*, vol. 184, pp. 565-580, 2016, doi: 10.1016/j.fuel.2016.07.009.

[48] D. Kang, D. Kim, V. Kalaskar, A. Violi, and A. L. Boehman, "Experimental characterization of jet fuels under engine relevant conditions – Part 1: Effect of chemical composition on autoignition of conventional and alternative jet fuels," *Fuel*, vol. 239, pp. 1388-1404, 2019, doi: 10.1016/j.fuel.2018.10.005.

[49] D. Kang, D. Kim, K. H. Yoo, A. Violi, and A. Boehman, "The effect of molecular structures of alkylbenzenes on ignition characteristics of binary n-heptane blends," *Proceedings of the Combustion Institute,* vol. 37, no. 4, pp. 4681-4689, 2019, doi: 10.1016/j.proci.2018.06.128.

[50] J. R. Agudelo, M. Lapuerta, O. Moyer, and A. L. Boehman, "Autoignition of Alcohol/C7-Esters/n-Heptane Blends in a Motored Engine under HCCI Conditions," *Energy & Fuels,* vol. 31, no. 3, pp. 2985-2995, 2017, doi: 10.1021/acs.energyfuels.7b00059.

[51] H. Liu, K. H. Yoo, A. L. Boehman, and Z. Zheng, "Experimental Study of Autoignition Characteristics of the Ethanol Effect on Biodiesel/n-Heptane Blend

in a Motored Engine and a Constant-Volume Combustion Chamber," *Energy & Fuels,* vol. 32, no. 2, pp. 1884-1892, 2018, doi: 10.1021/acs.energyfuels.7b03726.

[52] S. Wu, D. Kang, H. Zhang, R. Xiao, and A. L. Boehman, "The oxidation characteristics of furan derivatives and binary TPGME blends under engine relevant conditions," *Proceedings of the Combustion Institute,* vol. 37, no. 4, pp. 4635-4643, 2019, doi: 10.1016/j.proci.2018.08.060.

[53] X. Meng, E. Hu, K. H. Yoo, A. L. Boehman, and Z. Huang, "Experimental and Numerical Study on Autoignition Characteristics of the Polyoxymethylene Dimethyl Ether/Diesel Blends," *Energy & Fuels,* vol. 33, no. 3, pp. 2538-2546, 2019, doi: 10.1021/acs.energyfuels.8b04469.

[54] "ASTM D7668-14a. Standard Test Method for Determination of Derived Cetane Number (DCN) of Diesel Fuel Oils—Ignition Delay and Combustion Delay Using a Constant Volume Combustion Chamber Method," ASTM International, 2014, doi: 10.1520/d7668-14a.

[55] M. P. Mayo, "Effects of Air Temperature and Oxygen Dilution on the Ignition Behavior of Liquid Fuels in an Optical Spray Chamber," Master, The Pennsylvania State University, 2014.

[56] M. P. Mayo and A. L. Boehman, "Ignition Behavior of Biodiesel and Diesel under Reduced Oxygen Atmospheres," *Energy & Fuels,* vol. 29, no. 10, pp. 6793-6803, 2015, doi: 10.1021/acs.energyfuels.5b01439.

[57] M. Müller, "General Air Fuel Ratio and EGR Definitions and their Calculation from Emissions," *SAE Technical Paper,* 2010-01-1285, 2010.

[58] A. Hultqvist, M. C. B. Johansson, A. Franke, M. Richter, and M. Aldén, "A Study of the Homogeneous Charge Compression Ignition Combustion Process by Chemiluminescence Imaging," *SAE Technical Ppaer,* 1999-01-3680, 1999.

[59] N. Docquier and S. Candel, "Combustion control and sensors: a review," *Progress in Energy and Combustion Science,* vol. 28, no. 2, 2002, doi: 10.1016/S0360-1285(01)00009-0.

[60] B. Kim, M. Kaneko, Y. Ikeda, and T. Nakajima, "Detailed spectral analysis of the process of HCCI combustion," *Proceedings of the Combustion Institute,* vol. 29, pp. 671–677, 2002, doi: 10.1016/S1540-7489(02)80086-4.

[61] R. S. Sheinson and F. W. Williams, "Chemiluminescence Spectra from Cool and Blue Flames: Electronically Excited Formaldehyde," *Combustion and Flame,* vol. 21, no. 2, pp. 221-230, 1973, doi: 10.1016/S0010-2180(73)80026-4.

[62] M. Pöschl and T. Sattelmayer, "Influence of temperature inhomogeneities on knocking combustion," *Combustion and Flame,* vol. 153, no. 4, pp. 562-573, 2008, doi: 10.1016/j.combustflame.2007.11.009.

[63] W. R. Leppard, "The Chemical Origin of Fuel Octane Sensitivity," *SAE Technical Paper,* 902137, 1990.

[64] C. K. Westbrook, M. Mehl, W. J. Pitz, and M. Sjöberg, "Chemical kinetics of octane sensitivity in a spark-ignition engine," *Combustion and Flame,* vol. 175, pp. 2-15, 2017, doi: 10.1016/j.combustflame.2016.05.022.

[65] A. D. B. Yates, A. Swarts, and C. L. Viljoen, "Correlating Auto-Ignition Delays And Knock-Limited Spark-Advance Data For Different Types Of Fuel," *SAE Technical Paper,* 2005-01-2083, 2005.

[66] A. Amer *et al.*, "Fuel Effects on Knock in a Highly Boosted Direct Injection Spark Ignition Engine," *SAE International Journal of Fuels and Lubricants,* vol. 5, no. 3, pp. 1048-1065, 2012, doi: 10.4271/2012-01-1634.

[67] J. P. Szybist and D. A. Splitter, "Pressure and temperature effects on fuels with varying octane sensitivity at high load in SI engines," *Combustion and Flame,* vol. 177, pp. 49-66, 2017, doi: 10.1016/j.combustflame.2016.12.002.

[68] J. P. Szybist and D. A. Splitter, "Understanding chemistry-specific fuel differences at a constant RON in a boosted SI engine," *Fuel,* vol. 217, pp. 370-381, 2018, doi: 10.1016/j.fuel.2017.12.100.

[69] T. Han, "Strategies to Improve Efficiency and Emissions in Spark Ignition Engines," Ph.D. Dissertation, The University of Michigan, 2019.

[70] A. K. Voice, P. Kumar, and Y. Zhang, "Effect of Fuel Reactivity on Ignitability and Combustion Phasing in a Heavy-Duty Engine Simulation for Mixing-Controlled and Partially Premixed Combustion," *Journal of Engineering for Gas Turbines and Power,* vol. 140, no. 4, 2017, doi: 10.1115/1.4038015.

[71] K. Cho, Y. Zhang, and D. Cleary, "Investigation of Fuel Effects on Combustion Characteristics of Partially Premixed Compression Ignition (PPCI) Combustion Mode at Part-Load Operations," *SAE International Journal of Engines,* vol. 11, no. 6, pp. 1371-1383, 2018, doi: 10.4271/2018-01-0897.

[72] Hao Shi, Y. An, and B. Johansson, "Study of Fuel Octane Sensitivity Effects on Gasoline Partially Premixed Combustion Using Optical Diagnostics," *SAE Technical Paper,* no. 2019-24-0025, 2019, doi: 10.4271/2019-24-0025.

[73] R. Vallinayagam *et al.*, "The Physical and Chemical Effects of Fuel on Gasoline Compression Ignition," *SAE Technical Paper* 2019-01-1150, 2019, doi: 10.4271/2019-01-1150.

[74] J. E. Dec, W. Hwang, and M. Sjöberg, "An Investigation of Thermal Stratification in HCCI Engines Using Chemiluminescence Imaging," *SAE Technical Paper*, no. 2006-01-1518, 2006.

[75] C. K.Westbrook, "Chemical kinetics of hydrocarbon ignition in practical combustion systems," *Proceedings of the Combustion Institute*, vol. 28, no. 2, pp. 1563-1577, 2000, doi: 10.1016/S0082-0784(00)80554-8.

[76] J. E. Dec and Y. Yang, "Boosted HCCI for High Power without Engine Knock and with Ultra-Low NOx Emissions - using Conventional Gasoline," *SAE International Journal of Engines*, vol. 3, no. 1, pp. 750-767, 2010, doi: 10.4271/2010-01-1086.

[77] M. Sjöberg and J. E. Dec, "Smoothing HCCI Heat-Release Rates Using Partial Fuel Stratification with Two-Stage Ignition Fuels," *SAE Technical Paper*, no. 2006-01-0629, 2006.

[78] G. M. Chupka, E. Christensen, L. Fouts, T. L. Alleman, M. A. Ratcliff, and R. L. McCormick, "Heat of Vaporization Measurements for Ethanol Blends Up To 50 Volume Percent in Several Hydrocarbon Blendstocks and Implications for Knock in SI Engines," *SAE International Journal of Fuels and Lubricants*, vol. 8, no. 2, pp. 251-263, 2015, doi: 10.4271/2015-01-0763.

[79] G. T. Kalghatgi, "Fuel Anti-Knock Quality - Part I. Engine Studies," *SAE Technical Paper*, 2001.

[80] G. Kalghatgi, P. Risberg, and H.-E. Ångstrom, "A Method of Defining Ignition Quality of Fuels in HCCI Engines," *SAE Technical Paper*, 2003-01-1816, 2003.

[81] M. Sjöberg and W. Zeng, "Combined Effects of Fuel and Dilution Type on Efficiency Gains of Lean Well-Mixed DISI Engine Operation with Enhanced Ignition and Intake Heating for Enabling Mixed-Mode Combustion," *SAE International Journal of Engines*, vol. 9, no. 2, pp. 750-767, 2016, doi: 10.4271/2016-01-0689.

[82] P. Risberg, G. Kalghatgi, and H.-E. Ångstrom, "The Influence of EGR on Auto-ignition Quality of Gasoline-like Fuels in HCCI Engines," *SAE Technical Paper*, no. 2004-01-2952, 2004.

[83] H. Liu, M. Yao, B. Zhang, and Z. Zheng, "Influence of Fuel and Operating Conditions on Combustion Characteristics of a Homogeneous Charge

Compression Ignition Engine," *Energy & Fuels,* vol. 23, pp. 1422-1430, 2009, doi: 10.1021/ef800950c.

[84] E. Singh, J. Badra, M. Mehl, and S. M. Sarathy, "Chemical Kinetic Insights into the Octane Number and Octane Sensitivity of Gasoline Surrogate Mixtures," *Energy & Fuels,* vol. 31, no. 2, pp. 1945-1960, 2017, doi: 10.1021/acs.energyfuels.6b02659.

[85] G. K. a. H.-E. Å. Per Risberg, "Auto-ignition Quality of Gasoline-Like Fuels in HCCI Engines," *SAE Technical Paper,* no. 2003-01-3215, 2003.

[86] F. Zhao, D. N. Assanis, T. N. Asmus, J. E. Dec, J. A. Eng, and P. M. Najt, *Homogeneous Charge Compression Ignition (HCCI) Engines: Key Research and Development Issues*. SAE International, 2003.

[87] J. E. Dec, "Advanced compression-ignition engines—understanding the in-cylinder processes," *Proceedings of the Combustion Institute,* vol. 32, no. 2, pp. 2727-2742, 2009, doi: 10.1016/j.proci.2008.08.008.

[88] J. E. Dec, "Advanced Compression-Ignition Combustion for High Efficiency and Ultra-Low NOXand Soot," *Encyclopedia of Automotive Engineering,* pp. 1-40, 2014, doi: 10.1002/9781118354179.auto121.

[89] J. Chang, G. Kalghatgi, A. Amer, and Y. Viollet, "Enabling High Efficiency Direct Injection Engine with Naphtha Fuel through Partially Premixed Charge Compression Ignition Combustion," *SAE Technical Paper,* 2012-01-0677, 2012, doi: 10.4271/2012-01-0677.

[90] J. Chang, G. Kalghatgi, A. Amer, P. Adomeit, H. Rohs, and B. Heuser, "Vehicle Demonstration of Naphtha Fuel Achieving Both High Efficiency and Drivability with EURO6 Engine-Out NOx Emission," *SAE International Journal of Engines,* vol. 6, no. 1, pp. 101-119, 2013, doi: 10.4271/2013-01-0267.

[91] C. A. J. Leermakers, P. C. Bakker, L. M. T. Somers, L. P. H. de Goey, and B. H. Johansson, "Commercial Naphtha Blends for Partially Premixed Combustion," *SAE International Journal of Fuels and Lubricants,* vol. 6, no. 1, pp. 199-216, 2013, doi: 10.4271/2013-01-1681.

[92] Y. Viollet, J. Chang, and G. Kalghatgi, "Compression Ratio and Derived Cetane Number Effects on Gasoline Compression Ignition Engine Running with Naphtha Fuels," *SAE International Journal of Fuels and Lubricants,* vol. 7, no. 2, pp. 412-426, 2014, doi: 10.4271/2014-01-1301.

[93] V. Manente, C.-G. Zander, B. Johansson, P. Tunestal, and W. Cannella, "An Advanced Internal Combustion Engine Concept for Low Emissions and High

Efficiency from Idle to Max Load Using Gasoline Partially Premixed Combustion," *SAE Technical Paper,* 2010-01-2198, 2010.

[94] V. Manente, B. Johansson, and W. Cannella, "Gasoline partially premixed combustion, the future of internal combustion engines?," *International Journal of Engine Research,* vol. 12, no. 3, pp. 194-208, 2011, doi: 10.1177/1468087411402441.

[95] G. K. Leif Hildingsson, Nigel Tait, Bengt Johansson and Andrew Harrison, "Fuel Octane Effects in the Partially Premixed Combustion Regime in Compression Ignition Engines," *SAE Technical Paper,* 2009.

[96] C. P. Kolodziej, M. Sellnau, K. Cho, and D. Cleary, "Operation of a Gasoline Direct Injection Compression Ignition Engine on Naphtha and E10 Gasoline Fuels," *SAE International Journal of Engines*, vol. 9, no. 2, pp. 979-1001, 2016, doi: 10.4271/2016-01-0759.

[97] K. Cho, E. Latimer, M. Lorey, D. J. Cleary, and M. Sellnau, "Gasoline Fuels Assessment for Delphi's Second Generation Gasoline Direct-Injection Compression Ignition (GDCI) Multi-Cylinder Engine," *SAE International Journal of Engines,* vol. 10, no. 4, pp. 1430-1442, 2017, doi: 10.4271/2017-01-0743.

[98] S. Tanaka, F. Ayala, J. C. Keck, and J. B. Heywood, "Two-stage ignition in HCCI combustion and HCCI control by fuels and additives," *Combustion and Flame,* vol. 132, no. 1-2, pp. 219–239, 2003, doi: 10.1016/S0010-2180(02)00457-1.

[99] G. Shibata, K. Oyama, T. Urushihara, and T. Nakano, "Correlation of Low Temperature Heat Release with Fuel Composition and HCCI Engine Combustion," *SAE Technical Paper,* 2005-01-0138, 2005.

[100] G. K. Lilik and A. L. Boehman, "Effects of Fuel Composition on Critical Equivalence Ratio for Autoignition," *Energy & Fuels,* vol. 27, no. 3, pp. 1601-1612, 2013, doi: 10.1021/ef3016014.

[101] M. Yao, Z. Zheng, B. Zhang, and Z. Chen, "The Effect of PRF Fuel Octane Number on HCCI Operation," *SAE Technical Paper,* 2004-01-2992, 2004.

[102] J. P. Szybist and B. G. Bunting, "Cetane Number and Engine Speed Effects on Diesel HCCI Performance and Emissions," *SAE Technical Paper,* 2005-01-3723, 2005.

[103] M. Sjöberg and J. E. Dec, "EGR and Intake Boost for Managing HCCI Low-Temperature Heat Release over Wide Ranges of Engine Speed," *SAE Technical Paper,* 2007-01-0051, 2007.

[104] V. Hosseini, W. S. Neill, and W. L. Chippior, "Influence of Engine Speed on HCCI Combustion Characteristics using Dual-Stage Autoignition Fuels," *SAE Technical Paper*, 2009-01-1107, 2009.

[105] M. Wang, H. Lee, and J. Molburg, "Allocation of Energy Use in Petroleum Refineries to Petroleum Products," *The International Journal of Life Cycle Assessment*, vol. 9, no. 1, pp. 34-44, 2004, doi: 10.1007/BF02978534.

[106] G. Kalghatgi, C. Gosling, and M. J. Wier, "The outlook for transport fuels: Part 1," *Petroleum Technology Quarterly*, Q1, 2016.

[107] G. T. Kalghatgi, "Auto-Ignition Quality of Practical Fuels and Implications for Fuel Requirements of Future SI and HCCI Engines," *SAE Technical Paper*, 2005-01-0239, 2005.

[108] I. Glassman and R. A. Yetter, *Combustion*, 4th ed. Academic Press, 2008.

[109] C. K.Westbrook and F. L.Dryer, "Chemical kinetic modeling of hydrocarbon combustion," *Progress in Energy and Combustion Science*, vol. 10, no. 1, pp. 1-57, 1984, doi: 10.1016/0360-1285(84)90118-7.

[110] W. R. Leppard, "A Comparison of Olefin and Paraffin Autoignition chemistries: A Motored-Engine Study," *SAE Technical Paper*, 892081, 1989.

[111] W. R. Leppard, "The Autoignition Chemistries of Primary Reference Fuels, Olef in/Paraff in Binary Mixtures, and Non-Linear Octane Blending," *SAE Technical Paper*, 922325, 1992.

[112] Y. Yang, A. L. Boehman, and J. M. Simmie, "Uniqueness in the low temperature oxidation of cycloalkanes," *Combustion and Flame*, vol. 157, no. 12, pp. 2357-2368, 2010, doi: 10.1016/j.combustflame.2010.06.005.

[113] Y. Yang and A. L. Boehman, "Oxidation chemistry of cyclic hydrocarbons in a motored engine: Methylcyclopentane, tetralin, and decalin," *Combustion and Flame*, vol. 157, no. 3, pp. 495-505, 2010, doi: 10.1016/j.combustflame.2009.08.011.

[114] A. Ahmed, G. Goteng, V. S. B. Shankar, K. Al-Qurashi, W. L. Roberts, and S. M. Sarathy, "A computational methodology for formulating gasoline surrogate fuels with accurate physical and chemical kinetic properties," *Fuel*, vol. 143, pp. 290-300, 2015, doi: 10.1016/j.fuel.2014.11.022.

[115] V. S. B. Shankar *et al.*, "Oxidation of Alkane Rich Gasoline Fuels and their Surrogates in a Motored Engine," *7th European Combustion Meeting*, 2015.

[116] G. Särner, M. Richter, M. Aldén, L. Hildingsson, A. Hultqvist, and B. Johansson, "Simultaneous PLIF Measurements for Visualization of Formaldehyde- and Fuel-Distributions in a DI HCCI Engine," *SAE Technical Paper,* 2005-01-3869, 2005.

[117] G. K. Lilik, "Advanced Diesel Combustion of High Cetane Number Fuels and the Impacts on the Combustion Process," Ph.D. Dissertation, The Pennsylvania State University, 2012.

[118] H. Wei, F. Liu, J. Pan, L. Zhou, Z. Hu, and M. Pan, "On pre-ignition heat release of fuels with various octane sensitivities under compression ignition conditions," *Applied Thermal Engineering,* vol. 159, 2019, doi: 10.1016/j.applthermaleng.2019.113953.

[119] E. J. Silke, W. J. Pitz, C. K. Westbrook, M. Sjöberg, and J. E. Dec, "Understanding the Chemical Effects of Increased Boost Pressure under HCCI Conditions," *SAE Technical Paper,* 2008-01-0019, 2008.

[120] W. J. Pitz *et al.*, "Development of an Experimental Database and Chemical Kinetic Models for Surrogate Gasoline Fuels," *SAE Technical Paper,* 2007-01-0175, 2007.

[121] R. H. Thring, "Homogeneous-Charge Compression-Ignition (HCCI) Engines," *SAE Technical Ppaer,* 892068, 1989.

[122] K. Epping, S. Aceves, R. Bechtold, and J. Dec, "The Potential of HCCI Combustion for High Efficiency and Low Emissions," *SAE Technical Ppaer,* 2002-01-1923, 2002.

[123] R. D. Reitz and G. Duraisamy, "Review of high efficiency and clean reactivity controlled compression ignition (RCCI) combustion in internal combustion engines," *Progress in Energy and Combustion Science,* vol. 46, pp. 12-71, 2015, doi: 10.1016/j.pecs.2014.05.003.

[124] Y. Zhang, A. Voice, T. Tzanetakis, M. Traver, and D. Cleary, "An Evaluation of Combustion and Emissions Performance With Low Cetane Naphtha Fuels in a Multicylinder Heavy-Duty Diesel Engine," *Journal of Engineering for Gas Turbines and Power,* vol. 138, no. 10, 2016, doi: 10.1115/1.4032879.

[125] Y. Zhang, P. Kumar, M. Traver, and D. Cleary, "Conventional and Low Temperature Combustion Using Naphtha Fuels in a Multi-Cylinder Heavy-Duty Diesel Engine," *SAE International Journal of Engines,* vol. 9, no. 2, pp. 1021-1035, 2016, doi: 10.4271/2016-01-0764.

[126] Y. Zhang *et al.*, "Mixing-Controlled Combustion of Conventional and Higher Reactivity Gasolines in a Multi-Cylinder Heavy-Duty Compression Ignition Engine," *SAE Technical Paper,* 2017, doi: 10.4271/2017-01-0696.

[127] G. T. Kalghatgi, P. Risberg, and H.-E. Ångström, "Advantages of Fuels with High Resistance to Auto-ignition in Late-injection, Low-temperature, Compression Ignition Combustion," *SAE Technical Paper,* 2006-01-3385, 2006.

[128] G. T. Kalghatgi, P. Risberg, and H.-E. Ångström, "Partially Pre-Mixed Auto-Ignition of Gasoline to Attain Low Smoke and Low NOx at High Load in a Compression Ignition Engine and Comparison with a Diesel Fuel," *SAE Technical Paper,* 2007-01-0006, 2007.

[129] G. Kalghatgi, L. Hildingsson, and B. Johansson, "Low NOx and Low Smoke Operation of a Diesel Engine Using Gasolinelike Fuels," *Journal of Engineering for Gas Turbines and Power,* vol. 132, no. 9, 2010, doi: 10.1115/1.4000602.

[130] K. Cho *et al.*, "Understanding Fuel Stratification Effects on Partially Premixed Compression Ignition (PPCI) Combustion and Emissions Behaviors," presented at the SAE Technical Paper Series, 2019.

[131] M. Sellnau, M. Foster, W. Moore, J. Sinnamon, K. Hoyer, and W. Klemm, "Pathway to 50% Brake Thermal Efficiency Using Gasoline Direct Injection Compression Ignition," presented at the SAE Technical Paper Series, 2019.

[132] J. Badra, Y. Viollet, A. Elwardany, H. G. Im, and J. Chang, "Physical and chemical effects of low octane gasoline fuels on compression ignition combustion," *Applied Energy,* vol. 183, pp. 1197-1208, 2016, doi: 10.1016/j.apenergy.2016.09.060.

[133] N. Naser, M. Jaasim, N. Atef, S. H. Chung, H. G. Im, and S. M. Sarathy, "On the effects of fuel properties and injection timing in partially premixed compression ignition of low octane fuels," *Fuel,* vol. 207, pp. 373-388, 2017, doi: 10.1016/j.fuel.2017.06.048.

[134] Y. Zhang, A. Voice, Y. Pei, M. Traver, and D. Cleary, "A Computational Investigation of Fuel Chemical and Physical Properties Effects on Gasoline Compression Ignition in a Heavy-Duty Diesel Engine," *Journal of Energy Resources Technology,* vol. 140, no. 10, 2018, doi: 10.1115/1.4040010.

[135] W. Cannella, M. Foster, G. Gunter, and W. Leppard, "FACE Gasolines and Blends with Ethanol: Detailed Characterization of Physical and Chemical Properties," *Coordinating Research Council, INC.,* 2014.

[136] S. M. Sarathy *et al.*, "Ignition of alkane-rich FACE gasoline fuels and their surrogate mixtures," *Proceedings of the Combustion Institute,* vol. 35, no. 1, pp. 249-257, 2015, doi: 10.1016/j.proci.2014.05.122.

[137] T. Javed, E. F. Nasir, E.-t. Es-sebbar, and A. Farooq, "A comparative study of the oxidation characteristics of two gasoline fuels and an n-heptane/iso-octane surrogate mixture," *Fuel,* vol. 140, pp. 201-208, 2015, doi: 10.1016/j.fuel.2014.09.095.

[138] S. M. Sarathy *et al.*, "Compositional effects on the ignition of FACE gasolines," *Combustion and Flame,* vol. 169, pp. 171-193, 2016, doi: 10.1016/j.combustflame.2016.04.010.

[139] T. Javed *et al.*, "Ignition studies of two low-octane gasolines," *Combustion and Flame,* vol. 185, pp. 152-159, 2017, doi: 10.1016/j.combustflame.2017.07.006.

[140] A. G. Abdul Jameel *et al.*, "A minimalist functional group (MFG) approach for surrogate fuel formulation," *Combustion and Flame,* vol. 192, pp. 250-271, 2018, doi: 10.1016/j.combustflame.2018.01.036.

[141] D. Vuilleumier *et al.*, "The Influence of Intake Pressure and Ethanol Addition to Gasoline on Single- and Dual-Stage Autoignition in an HCCI Engine," *Energy & Fuels,* vol. 32, no. 9, pp. 9822-9837, 2018, doi: 10.1021/acs.energyfuels.8b00887.

[142] D. Kang *et al.*, "Auto-ignition study of FACE gasoline and its surrogates at advanced IC engine conditions," *Proceedings of the Combustion Institute,* vol. 37, no. 4, pp. 4699-4707, 2019, doi: 10.1016/j.proci.2018.08.053.

[143] B. Chen, C. Togbé, Z. Wang, P. Dagaut, and S. M. Sarathy, "Jet-stirred reactor oxidation of alkane-rich FACE gasoline fuels," *Proceedings of the Combustion Institute,* vol. 36, no. 1, pp. 517-524, 2017, doi: 10.1016/j.proci.2016.05.040.

[144] B. Chen, C. Togbé, H. Selim, P. Dagaut, and S. M. Sarathy, "Quantities of Interest in Jet Stirred Reactor Oxidation of a High-Octane Gasoline," *Energy & Fuels,* vol. 31, no. 5, pp. 5543-5553, 2017, doi: 10.1021/acs.energyfuels.6b03193.

[145] B. Chen *et al.*, "Exploring gasoline oxidation chemistry in jet stirred reactors," *Fuel,* vol. 236, pp. 1282-1292, 2019, doi: 10.1016/j.fuel.2018.09.055.

[146] V. S. Bhavani Shankar *et al.*, "Primary Reference Fuels (PRFs) as Surrogates for Low Sensitivity Gasoline Fuels," *SAE Technical Paper,* 2016-01-0748, 2016, doi: 10.4271/2016-01-0748.

[147] M. U. Waqas, N. Atef, E. Singh, J.-B. Masurier, M. Sarathy, and B. Johansson, "Blending Behavior of Ethanol with PRF 84 and FACE A Gasoline in HCCI Combustion Mmode," *SAE Technical Paper,* 2017-24-0082, 2017.

[148] A. Elwardany, J. Badra, J. Sim, M. Khurshid, M. Sarathy, and H. Im, "Modeling of Heating and Evaporation of FACE I Gasoline Fuel and its Surrogates," *SAE Technical Paper,* 2016-01-0878, 2016.

[149] A. G. A. Jameel, "A Functional Group Approach for Predicting Fuel Properties," Ph.D. Dissertation, King Abdullah University of Science and Technology, 2019.

[150] M. Mehl, H. J. Curran, W. J. Pitz, and C. K. Westbrook, "Chemical kinetic modeling of component mixtures relevant to gasoline," *4th European Combustion Meeting*, 2009.

[151] C. K. Westbrook, W. J. Pitz, and W. R. Lepp, "The Autoignition Chemistry of Paraffinic Fuels and Pro-Knock and Anti-Knock Additives: A Detailed Chemical Kinetic Study," *SAE Technical Paper*, 912314, 1991.

[152] D. Kang, D. Kim, V. Kalaskar, A. Boehman, and A. Violi, "Experimental characterization of jet fuels under engine relevant conditions – Part 2: Insights on optimization approach for surrogate formulation," *Fuel*, vol. 239, pp. 1405-1416, 2019, doi: 10.1016/j.fuel.2018.10.006.

[153] D. Kim, J. Martz, and A. Violi, "Effects of fuel physical properties on direct injection spray and ignition behavior," *Fuel*, vol. 180, pp. 481-496, 2016, doi: 10.1016/j.fuel.2016.03.085.

[154] W. De Ojeda, T. Bulicz, X. Han, M. Zheng, and F. Cornforth, "Impact of Fuel Properties on Diesel Low Temperature Combustion," *SAE International Journal of Engines*, vol. 4, no. 1, pp. 188-201, 2011, doi: 10.4271/2011-01-0329.

[155] J. D. Naber and D. L. Siebers, "Effects of Gas Density and Vaporization on Penetration and Dispersion of Diesel Sprays," *SAE Technical Paper*, 960034, 1996.

[156] B. S. Higgins, C. J. Mueller, and D. L. Siebers, "Measurements of Fuel Effects on Liquid-Phase Penetration in DI Sprays," *SAE Technical Paper*, 1999-01-0519, 1999.

[157] C. L. Genzale, L. M. Pickett, and S. Kook, "Liquid Penetration of Diesel and Biodiesel Sprays at Late-Cycle Post-Injection Conditions," *SAE Technical Paper*, 2010-01-0610, 2010.

[158] S. Kook and L. M. Pickett, "Liquid length and vapor penetration of conventional, Fischer–Tropsch, coal-derived, and surrogate fuel sprays at high-temperature and high-pressure ambient conditions," *Fuel*, vol. 93, pp. 539-548, 2012, doi: 10.1016/j.fuel.2011.10.004.

[159] M. A. Groendyk and D. Rothamer, "Effects of Fuel Physical Properties on Auto-Ignition Characteristics in a Heavy Duty Compression Ignition Engine," *SAE International Journal of Fuels and Lubricants*, vol. 8, no. 1, pp. 200-213, 2015, doi: 10.4271/2015-01-0952.

[160] G. Gentz, J. Dernotte, C. Ji, D. Lopez Pintor, and J. Dec, "Combustion-Timing Control of Low-Temperature Gasoline Combustion (LTGC) Engines by Using Double Direct-Injections to Control Kinetic Rates," *SAE Technical Paper* 2019-01-1156, 2019, doi: 10.4271/2019-01-1156.

[161] R. A. Stein *et al.*, "Effect of Heat of Vaporization, Chemical Octane, and Sensitivity on Knock Limit for Ethanol - Gasoline Blends," *SAE International Journal of Fuels and Lubricants*, vol. 5, no. 2, pp. 823-843, 2012, doi: 10.4271/2012-01-1277.

[162] C. P. Kolodziej and T. Wallner, "Combustion characteristics of various fuels during research octane number testing on an instrumented CFR F1/F2 engine," *Combustion Engines*, vol. 171, no. 4, pp. 164-169, 2017, doi: 10.19206/CE-2017-427.